THERMOMECHANICAL BEHAVIOR OF FUNCTIONALLY GRADED MATERIALS

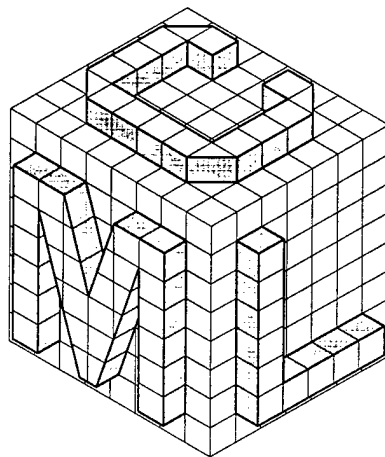Final Report for AFOSR Grant F49620-95-1-0342

CML Report 98-01
August 1998

J. N. Reddy
Computational Mechanics Laboratory
Department of Mechanical Engineering
Texas A & M University
College Station, TX 77843–3123

REPORT DOCUMENTATION PAGE

1. AGENCY USE ONLY *(Leave blank)*	2. REPORT DATE	3.	ᴅᴀᴛᴇs COVERED	
	August 1998	Final Technical Report	1 May 95 to 31 Jul 98	

4. TITLE AND SUBTITLE	5. FUNDING NUMBERS
Thermomechanical Behavior of Functionally Graded Materials	F49620-95-1-0342

6. AUTHOR(S)

J. N. Reddy

7. PERFORMING ORGANIZATION NAME(S) AND ADDRESS(ES)	8. PERFORMING ORGANIZATION REPORT NUMBER
Computational Mechanics Laboratory Department of Mechanical Engineering Texas A&M University College Station, TX 77843-3123	

9. SPONSORING/MONITORING AGENCY NAME(S) AND ADDRESS(ES)	10. SPONSORING/MONITORING AGENCY REPORT NUMBER
AFOSR/NA 110 Duncan Avenue, Suite B115 Bolling AFB, DC 20332-8050	F49620-95-1-0342

11. SUPPLEMENTARY NOTES

12a. DISTRIBUTION AVAILABILITY STATEMENT	12b. DISTRIBUTION CODE
Approved for Public Release; Distribution Unlimited.	

13. ABSTRACT *(Maximum 200 words)*

The research involved developing theoretical formulations and finite element anayses of the thermomechanical, transient response of functionally graded cylinders and plates. Nonlinearities (geometric and material), thermomechanical coupling (between elastic deformation and heat transfer), and power-law distribution of the two-constitutent material variation through the thickness were accounted for in the formulations. The first-oder shear deformation plate theory is used for the kinematics of the plate problem. Numerical results of the deflections, temperature distributions, and stress distributions in the cylinder and plates are calculated. Parametric studies with respect to varying volume fraction of the metal in metal-ceramic plates is conducted. The effect of the temperature field imposed on FGM plates is discussed. It is found that the response of the plates with material properties between that of the ceramic and metal is not intermediate to that of the ceramic and metal plates. The important issue of brittle-ductile mixtures is also addressed in the closing stages of the research, although it requires further study. Yield stresses of the ceramic-metal mixture are obtained using the mixture theory. Yielding within the mixture is assumed to occur when the partial stresses in the metallic component satisfy the classical J2 criterion. Further study of inelasticity and fracture of functionally graded materials must be undertaken. Also, extension of the present work to functionally graded shell structures is recommended.

14. SUBJECT TERMS			15. NUMBER OF PAGES
			78
			16. PRICE CODE

17. SECURITY CLASSIFICATION OF REPORT	18. SECURITY CLASSIFICATION OF THIS PAGE	19. SECURITY CLASSIFICATION OF ABSTRACT	20. LIMITATION OF ABSTRACT
Unclassified	Unclassified	Unclassified	UL

FINAL REPORT

THERMOMECHANICAL BEHAVIOR OF FUNCTIONALLY GRADED MATERIALS

AFOSR Grant F49620-95-1-0342

J. N. Reddy

Department of Mechanical Engineering
Texas A & M University
College Station, Texas 77843-3123 USA

Report Submitted to

August 1998

THERMOMECHANICAL BEHAVIOR OF FUNCTIONALLY GRADED MATERIALS

RESEARCH OBJECTIVES

The objective of the present research is aimed at developing mechanics formulations, mathematical models and computational models for functionally graded materials. Specifically, the nonlinear coupled thermomechanical response of these materials under static, dynamic, and thermal loading environments are studied. The work includes parametric studies performed by varying volume fraction distributions and material combinations. Key issues such as effective yielding in brittle ductile mixtures are also addressed. As part of the research, a finite element program for solving fully coupled nonlinear transient thermoelastic and thermoinelastic equations for functionally graded solids is developed. Specific studies include analysis of the transient thermomechanical response of structural elements such as bars and plates made of functionally graded materials.

REPORTS SUBMITTED

- J. N. Reddy, "Thermomechanical Behavior of Functionally Graded Materials", Proposal, CML Report 94-01, 1994.

- G. N. Praveen, C. D. Chin and J. N. Reddy, "A Pseudo-dynamic Thermoelastic Analysis of a Functionally Gradient Ceramic Cylinder", CML Report 96-01, March 1996.

- G. N. Praveen, C. D. Chin, and J. N. Reddy, "Nonlinear Transient Thermoelastic Analysis of Functionally Gradient Ceramic-Metal Plates", CML Report, 96-02, September 1996.

- C. D. Chin, and J. N. Reddy, "A Parametric Study of Thermomechanical Behavior of Functionally Graded Materials", CML Report 97-01, July 1997.

- G. N. Praveen, and J. N. Reddy, "Thermomechanical Behavior of Functionally Graded Materials - Final Report", CML report 98-01, August 1998.

REFEREED PUBLICATIONS

1. G. N. Praveen and J. N. Reddy, "Nonlinear Transient Analysis of Functionally Graded Ceramic-Metal Plates," *Journal of Solids and Structures,* Vol. 35, No. 33, pp. 4457–4476, 1998.

2. J. N. Reddy and C. D. Chin, "Thermomechanical Analysis of Functionally Graded Cylinders and Plates," *J. Thermal Stresses,* to appear.

3. S. W. Gong, K. Y. Lam, and J. N. Reddy, "Analysis of Impact on Laminated Cylindrical Shells Made of Functionally Gradient Materials," *Acta Mechanica,* to appear.

4. J. N. Reddy, C. M. Wang, and S. Kitipornchai, "Axisymmetric bending of functionally graded circular and annular plates," *European Journal of Mechanics,* to appear.

CONFERENCE PUBLICATIONS/PRESENTATIONS

1. G. N. Praveen and J. N. Reddy, "On the Nonlinear Transient Thermomechanical Response of Functionally Gradient Plates Subjected to Surface Heating," *McNU'97*, Northwestern University, Evanston, IL, 29 June–July 2, 1997.

2. G. N. Praveen and J. N. Reddy, "Nonlinear Transient Thermoelastic Analysis of Functionally Graded Ceramic-Metal Plates," *IMECE'97* (1997 International Mechanical Engineering Congress & Exposition), Dallas, November 16–21, 1997.

3. G. N. Praveen and J. N. Reddy, "Thermoelastic Analysis of Functionally Graded Cylinders and Plates," *12th Engineering Mechanics Conference*, San Diego, CA, May 17-20, 1998.

SEMINAR PRESENTATIONS

1. J. N. Reddy, "Thermomechanical Behavior of Functionally Graded Materials," *Seminar*, The Centre for Computational Mechanics, Mechanical and Production Engineering, National University of Singapore, June 3, 1997.

2. J. N. Reddy, "Thermomechanical Behavior of Functionally Graded Materials," *Seminar*, Department of Mechanical Engineering, Indian Institute of Science, August 11, 1998.

SESSIONS ORGANIZED

1. J. N. Reddy and C. Brinson, "Functionally Graded and Shape Memory Materials," a three–session symposium organized at the *1997 International Mechanical Engineering Congress and Exposition (IMECE'97)*, November 16–21, 1997, Dallas, Texas.

2. J. N. Reddy, "Constitutive and Computational Models of Shape Memory and Functionally Graded Materials," a two–session symposium organized at the *Engineering Mechanics Specialty Meeting of ASCE*, University of California, San Diego, May 17–20, 1998.

THESES COMPLETED

1. C.-D. Chin, "A Parametric Study of Thermomechanical Behavior of Functionally Gradient Materials," M.S. Thesis, Texas A&M University, October 1996.

STUDENTS SUPPORTED

1. C.-D. Chin, M. S. Student, Mechanical Engineering

2. G. N. Praveen, Ph. D. Student, Mechanical Engineering

3. Govindarajan Rengarajan, Ph. D. Student, Mechanical Engineering

Thermomechanical Behavior of Functionally Graded Materials

Abstract

This report begins with a detailed introduction to the concept of functionally graded materials, highlighting their technological importance. Section 1 contains a detailed review of literature in the area of functionally graded materials, while placing in perspective, the present research. The various applications of FGMs is outlined and the key issues relating to the present research on FGMs are discussed. Specific issues that were addressed in the present research and the problems solved during the course of the present work are explained. In section 2, the detailed analysis of the pseudo-dynamic thermoelastic response of functionally graded ceramic cylinders is described. In this section, we present the finite element formulation of the one dimensional, axisymmetric heat transfer equation and the thermoelastic radial boundary value problem. A two-step solution of the governing equations of thermoelasticity is presented. Thermoelastic coupling is considered by taking into effect the temperature dependence of the constitutive equations. Nonlinearities due to the temperature dependence of the material properties of the constituent ceramic and metal, are considered. A parametric study with respect to varying volume fraction of the metal, is conducted. Temperature and radial/hoop stress distributions arising due to rapid heating of the inner surface of the functionally gradient cylinder are presented.

In section 3, the nonlinear transient thermoelastic analysis of functionally graded plates is presented. The response of functionally graded ceramic-metal plates is investigated using a finite element that accounts for the transverse shear strains, rotary inertia and large rotations in the von Kármán sense. The static and dynamic response of the functionally graded material (fgm) plates are investigated by varying the volume fraction of the ceramic and metal using a simple power law distribution. Numerical results for the deflection and stresses are presented. The effect of the temperature field imposed on the fgm plate is discussed. It is demonstrated that the response of the plates with material properties between that of the ceramic and metal is not intermediate to that of the ceramic and metal plates.

The important issue of yielding of brittle-ductile mixtures is addressed in the section 4. Ceramics and metals exhibit contrasting material behavior in that metals undergo yielding under sufficiently large loads, while ceramics are mostly brittle. In materials that are mixtures of ceramics and metals, the ceramic embrittles the mixture and the metal imparts ductility to the mixture. In the present work, we obtain the yield stresses of ceramic-metal mixtures with recourse to mixture theory. A comparison with a one-dimensional model is also shown. Yielding within the mixture is assumed to occur when the partial stresses in the metallic component satisfy the classical J_2 criterion.

The research conducted as part of the present effort adds significantly to the body of literature present, in several key research areas in functionally graded materials. In particular, significant results are obtained in the areas of thermomechanical modeling including nonlinear and transient effects. Yield point estimates of the mixture materials help in understanding inelastic behavior of functionally graded media. The detailed studies have been performed to study the effects of including nonlinearities induced by thermomechanical coupling and temperature dependence of material properties, and their importance has been highlighted.

Contents

1 Functionally Graded Materials

1.1 Introduction

Functionally gradient materials (FGM) are a class of composites that have a gradual variation of material properties from one surface to another. These novel materials were proposed by the Japanese in 1984 [1, 2] and are projected as thermal barrier materials for applications in space planes, space structures and nuclear reactors, to name only a few. As conceived and manufactured today, these materials are isotropic and nonhomogeneous. In general, all the multi–phase materials, in which the material properties are varied gradually in a predetermined manner, fall into the category of functionally gradient materials [2]. In fact, the functionally gradient material characteristics are represented in sea shells, bones, etc, and perhaps a better understanding of the highly complex form of materials in nature will help us in synthesizing new materials (the science of so called "biomimetics" [3]).

The gradation in properties of the material reduces thermal stresses, residual stresses, and stress concentration factors [4]. If two dissimilar materials are bonded together, there is a very high chance that debonding will occur at some extreme loading conditions, be it static, dynamic, or thermal loads. Cracks are likely to initiate at interfaces and grow into the weaker material section. Another problem is the presence of residual stresses due to the difference in coefficients of thermal expansion between the materials. These problems can be resolved by gradually varying the volume fraction of the constituents rather than abruptly changing them over an interface. The gradual variation results in a very efficient material tailored to suit our needs. Figure 1 illustrates the compositional variation from one surface to another.

A metal-ceramic fgm

High temperature side	Ceramic rich	Heat resistant Good anti-oxidant properties Low thermal conductivity
Low temperature side	Metal rich	Mechanical toughness, strength High thermal conductivity High fracture toughness
In between	Ceramic + Metal	Effective thermal stress relaxation throughout

In what follows, we will present a brief review of literature and summarize the developments.

1.2 Review of Literature

A large amount of published literature is in Japanese. However, the second international symposium on functionally gradient materials was held in San Francisco recently [5] and this symposium has thrown light on current trends in manufacturing, design, and analysis

with functionally gradient materials. The review will be presented in the following order: applications of FGM, design and optimization, fabrication techniques, and mathematical modeling.

1.2.1 Applications of FGM

As mentioned earlier, the functionally graded materials are projected as thermal barrier materials [2]. High–temperature applications such as space planes [6], space structures, nuclear reactors, insulations for cooling structures [7], and on a different length scale altogether, the VLSI chips [8], etc. are potential targets for the use of functionally gradient materials. However, on a broader spectrum, these materials are viewed as nanocomposites [9] with applications in such diverse fields as electronics, optics, biology, and so on.

Interestingly, the graded material concept goes hand in hand with the science of biomimetics [3]. Most of nature's material forms are nonhomogeneous with functionally graded material structure. It would not be too much to hope for, in the near future, materials whose constitution can be sufficiently controlled to meet our functional requirements. Another application of the functionally gradient materials is the use in the interfaces between two dissimilar homogeneous materials so as to relieve stresses and reduce stress intensity factors [4].

The functionally graded materials have potential applications in piezoelectricity too. A class of piezoelectric composites have piezoelectrically active materials in the form of fibers or particles embedded in a medium that may or may not be piezoelectric. These composites attract interest due to their enhanced electromechanical properties over the individual constituents [10]. Functionally grading the volume fraction of the constituents such that the thermoelectromechanical properties are enhanced will lead to a functionally graded piezoelectric material.

In recent years, sonar and medical ultrasonic imaging devices have been enhanced by the use of piezoelectric composites [11, 12, 13]. One of the major problems associated with the homogeneous piezoelectric materials is the impedance matching for maximum energy transfer. By combining piezoelectric ceramics and polymers with passive phase materials, the efficiency of converting electrical energy to mechanical energy is improved beyond that of conventional piezoelectric materials. In addition, it has been demonstrated that an increase in bandwidth can be achieved by tailoring the volume fraction of variuos constituents [12, 13]. Currently considered piezoelectric composites include multilayer piezoelectrics (alternating layers of piezoelectric ceramics and metal electrodes), combinations of piezoelectric ceramics and polymers based on different connectivity schemes [11]. While it does not appear that functionally graded materials have been either suggested or used for this purpose, it is likely that additional enhancements to bandwidth and electromechanical coupling can be made by using functionally gradient materials.

1.2.2 Design and Optimization

Usually, a designer is faced with the task of designing a system for optimal performance under certain given conditions and constraints, and at best he has the choice of the material to use. In fiber reinforced composite laminates, he has the additional flexibility of orienting

the fibers in a lamina to suit his design requirements. With the advent of FGM, he can go a step further and use the so called "inverse design" concept. Basically, the material composition and the volume fraction gradation is determined from an analysis based on the reduction of thermal stresses, residual stresses etc. The material is then fabricated using the profile distribution obtained from the analysis.

The profiles for the material property variation that have been studied so far have been represented by polynomials, exponential functions, or homogeneous layers. Jin and Noda [14] use an exponential profile variation and determine certain parameters associated with the exponential function by minimizing the thermal stress intensity factors. Fakui [15] considered the effects of volume fraction of the powder and the centrifugal force in centrifugal casting on the cubic polynomial function profile. Matsuzaki et al. [7] optimized numerically the thickness and compositional distribution of the FGM with respect to the heat transfer in cooling systems. Williamson et al. [16] and Drake et al. [17] discuss the optimum microstructural characteristics with respect to the residual stresses.

1.2.3 Fabrication Techniques

Several techniques for fabricating functionally gradient materials are available and the developments are presented in reference [5]. Prominent techniques are centrifugal casting [15], successive coating using vapor deposition [18], physical vapor deposition (PVD) by sputtering [19] and chemical vapor deposition (CVD) [20], automatic powder spraying and stacking (APSS) [21], combustion synthesis [22], sintering [23] and many more (see reference [5]). Evaluation of fabricated materials for strength and toughness, and the characterization of the material properties has also been done.

1.2.4 Mathematical Modeling

In the study of FGM, the modeling involves the characterization of the constitution of the material, and the theoretical and computational analysis (for instance, thermomechanical analysis) of the functionally graded solids (solids made of functionally gradient materials).

1.2.5 Constitutive Relations

Generally speaking, there are two ways to model the material property gradation in solids: (i) assume a profile for volume fraction variation – this could be thought of as a "macroscopic" approach , and (ii) a micromechanics approach to study the nonhomogeneous media.

In the section on design and optimization mention was made of the different compositional profiles that are currently being used. Polynomial representations include quadratic variations [24, 25] and cubic variations [16, 26, 27]. Exponential functions have been used in references [28, 29]. Piecewise homogeneous layer representations have been used in references [30, 31].

At the microstructural level, the functionally graded material is characterized by a transition from a dispersive phase to an alternative structure with a networking structure in between [32]. The micromechanics of a random inhomogeneous media has been a subject of some intensive study in the last decade [33]. However, such studies, until recently, have mainly concentrated on inclusions or inhomogeneities of different shapes in a homogeneous

3

substrate ("statistical homogeneity" is assumed). In general, the micromechanics study of a nonhomogeneous media can be classified into three approaches: (i) the variational approach [34, 35] that provides an upper and lower bound for effective moduli of nonhomogeneous materials, (ii) the Eshelby–type inclusion theories [32, 36, 37] (mean–field theories, self–consistent schemes, and generalized self–consistent schemes), and (iii) percolation theory [38] and multiple scattering theory [39].

Among these references, Zhai et al. [32] and Nan et al. [39] directly address the constitutive relations of functionally graded materials. Pindera and Freed [40], Pindera et al. [41], and Aboudi et al. [42] use the unit–cell approach to analyze the functionally graded materials. Recently, a special issue on functionally gradient materials has been released by International Journal of Composites Engineering [43], wherein the papers are primarily based on micromechanics.

1.2.6 Analytical Studies

The focus of analytical studies on solids made of functionally graded materials has been mainly in three areas, viz., the study of interface cracks, the thermomechanical response, and the elasto–plastic analysis.

Interface Cracks

If the interface region between two dissimilar homogeneous materials is made of a functionally gradient material, the stress intensity factor reduces significantly [4]. Presence of cracks in a nonhomogeneous medium has been a subject of intensive study, for example see references [4, 14, 28, 29, 44, 45, 46, 47]. The studies involve solutions to mixed boundary value problems, wherein transform methods are utilized to reduce the problem to an integral equation form, which is then solved numerically. The material property gradation in the interface is usually represented by an exponential function as it leads to analytically tractable expressions.

Erdogan and group [4, 28, 45, 46] have studied the problem of a plane crack in a nonhomogeneous medium. An interesting result of their study is that Poisson's ration has no significant effect on the stress intensity factor, and hence, it is usually held constant [28]. They have also observed that the crack tip stress and displacement oscillations in bonded dissimilar materials disappear if the interface is graded [45], and that square root singularity is maintained at the crack tip (crack in the interface zone made of functionally gradient material).

Noda and group [14, 29, 47] have studied the steady–state and transient heat conduction problem of a functionally graded solid (solid made of functionally gradient material) with a crack. Their conclusions are that elastic modulus of ceramics should be greater than the modulus of metals, heat conductivity and thermal expansion coefficients in ceramic should be less than metals, and variation in thermal coefficient of expansion from ceramic to metal should be less dramatic than the variation of elastic modulus and heat conductivity.

Thermomechanical Problems

The principal applications of functionally graded materials are in high–temperature environments. Severe requirements are placed on these materials – maximum temperature

of 2100K and and a temperature difference between the surfaces of around 1000K over a span of a centimeter. Quite naturally, the study of the material response under such intense high–temperature loadings is essential.

Studies carried out so far have mainly concentrated on the uncoupled thermomechanical problem (with the exception of [49]). Jin and Noda [14] have used the minimization of thermal stress intensity factor for a crack in a metal/ceramic functionally gradient material as a criterion for optimizing material property variation. They have studied both the steady–state [29] and the transient [47] heat conduction problems, but have neglected the thermomechanical coupling.

Numerous other people have studied the thermal response of a functionally graded solid [24, 27, 30, 29, 47, 48, 49]. It has generally been observed that grading the material properties reduces thermal stresses and residual stresses. Tanaka et al. [50, 51] have designed FGM property profiles using sensitivity and optimization methods based on the criterion of reduction of thermal stresses. Fuchiyama et al. [24] have shown that it is important to consider the temperature dependence on material properties. The crack initiates just after cooling on the high–temperature side (eg., ceramic), and the crack exhibits an accelerated growth into the material, followed by a deceleration before it stops. Zhang et al. [49] have compared the solutions of linear uncoupled, linear coupled, and nonlinear coupled equations and show that the effect of thermomechanical coupling is significant and it is necessary to consider the coupling to predict realistic stress distribution. It is interesting to note that they have studied the thermal shock problem and have stressed the importance of considering the thermomechanical coupling, while in reference [47] the coupling effect has been considered insignificant and ignored.

Elasto–Plastic Analysis

In a ceramic/metal composite, cracking develops in the ceramic and plastic deformations develop in the metal region. Williamson et al. [16, 17] have done elastic–plastic finite element analyses of a functionally graded $Ni–Al_2O_3$ disk and rod specimens and observed that plasticity effects must be included to realistically model the stress reduction. An interesting result of their study is that including the effects of plasticity offers stress relaxation in non–graded specimens, but not as much in graded specimens. Teraki et al. [48] have done a theoretical and numerical elastic–plastic analysis of ceramic/metal FGM under cyclic thermal load. They have observed "thermal ratcheting", i.e., the plastic strains increase with every cycle.

Analysis with Functionally Graded Piezoelectric Materials

Tani and Liu [25] have studied the SH wave propagation in a functionally graded piezoelectric plate. Their analysis indicate that the displacement waves are confined to a small portion of the plate, and the rest of the plate carry negligible waves. This result shows a glimpse of the usefulness of functionally grading the piezoelectric materials.

1.2.7 Computational Studies

Williamson et al. [16, 17] have used ABAQUS to study the plastic response of axisymmetric functionally graded specimens under simulated cooling. Kawasaki and Watanabe [52] have

used NASTRAN to study the thermal stress field in disk shaped functionally gradient materials. Fuchiyamo et al. [24] have used an 8-node quadrilateral axisymmetric element to study the transient thermal stresses and stress intensity factors.

1.3 Summary of Developments

As discussed in the section on review, the key issues related to the functionally gradient materials are: applications of FGM, design and optimization, fabrication techniques, experimental evaluation and characterization, and mathematical modeling. This is illustrated pictorially in Figure 2.

One of the issues of principal concern is the mathematical modeling of functionally gradient materials. This involves the study of the constitutive relations of the material and the analysis of solids made of FGM under various loading conditions. Box I summarizes the developments in the modeling of the constitutive behavior, and Box II summarizes the analytical studies done so far.

<div align="center">

Box I

Constitutive Relations

</div>

1. Assumed Variation of Material Properties
   - Polynomial profiles (e.g., $E = a_0 + a_1 z + a_2 z^2$)
   - Exponential profiles (e.g., $E = E_0 e^{\beta x}$)
   - Piecewise homogeneous layers ($E_i, \nu_i, \rho_i, k_i; i =$ layer number)

2. Micromechanics Approach
   - Variational methods
     - Upper and lower bounds of effective elastic moduli
   - Eshelby–type inclusion theories
     - Mean–field schemes
     - Self–consistent schemes
     - Generalized self–consistent schemes
   - Percolation, multiple scattering theories

1.4 Present Research

The primary focus of the present research is in the area of mathematical modeling. While no research was done in the areas of fabrication, and experimental evaluation and characterization, the results available in the literature on these areas were used extensively both for comparison and guidance. The present research falls into the following categories.

Box II
Analytical Studies

1. Interface Cracks
   - Cracks in Graded Interface Region
     - Mixed boundary value problem
   - Thermal loading environments
   - Optimize material property variation
     - Criteria : reduction in thermal stresses, residual

2. Thermomechanical Problems
   - Study of thermal stresses
   - Residual stresses, surface cracks
     during cooling
   - Uncoupled and coupled thermoelastic equations
   - Linear and nonlinear thermoelastic equation
   - Steady–state and transient responses
   - Loadings : Constant surface heating, thermal shocks
   - Effect of material property variation
     on thermal stresses, etc.

3. Elastic–Plastic Analysis
   - Plastic deformation in the metal rich region
   - Thermomechanical fatigue
   - Finite element studies

1.4.1 Modeling of the Constitutive Behavior

Box I summarizes the developments in the modeling of the constitutive relations in the functionally graded materials. The more common approach consists of representing material property variations by continuously differentiable functions whose coefficients are optimized considering the reduction of thermal stresses, etc. In general, materials with these property variations have been proven to be manufacturable with either existing or new fabrication techniques. However, a generalized representation has been lacking. Deeming this type of representation of material properties as macroscopic can present a few problems. For instance, a few property variations are difficult to represent by these continuously differentiable function representations. This is illustrated through Figure 3, where the variations can be assumed to be that of the volume fraction of any one constituent of the functionally graded material.

On the other hand, the piecewise homogeneous representation introduces artificial interfaces. Therefore, in order to model a large class of variations, either continuous but difficult (see Figure 3) or discontinuous at certain planes, it is necessary to adopt a layerwise polynomial representation. Conceptually and mathematically, this is similar to the layerwise theories for composite laminates [53, 54], though simpler due to the isotropic nature of the functionally graded materials. The present approach can be naturally extendable to orthotropic situations.

The varying properties of the medium are represented by a set of mathematical or numerical layers. The functionally graded material is discretized through the thickness into as many layers as required. For instance, Figure 4 shows the possible numerical layer divisions for the complex property variations shown in Figure 3. The variation within each layer can be represented by linear, quadratic, or higher–order polynomials, if necessary. This type of representation encompasses a large class of variations including discrete layer representations and piezoelectric layers.

1.4.2 Thermomechanical Response

The importance of studying the thermomechanical response of the functionally gradient material systems was mentioned earlier. However, we will briefly outline these reasons again:

1. Applications in high–temperature environments

2. Steep gradient of temperature through the thickness

3. Very high thermal stresses and thermal stress intensity factors

4. Onset of surface cracks with cooling

5. Variation of properties such as thermal conductivity, coefficients of thermal expansion, etc.

In order to obtain an accurate thermal response of the functionally graded material system, it is necessary to model the system using full, nonlinear, coupled thermoelastic equations. However, in literature, the main focus has been the linear, uncoupled equations.

Zhang et al. [49], and Amin and Sierakowski [55] discuss the importance of thermomechanical coupling, particularly in the presence of transient loading conditions such as thermal shocks etc.

The present work contains a detailed study on the coupled nonlinear coupled thermoelastic response of the solids (rods, plates, and shells) made of functionally graded materials. While analytical solutions have been obtained for simple cases, the general problem is solved numerically. A general finite element model is developed to obtain the thermomechanical response. The steady–state and transient conditions were also considered. The thermal response is characterized for several loading conditions and material property variations.

1.4.3 Inelastic Analysis

The study of the inelastic response assumes importance since metals usually form an integral part of the functionally graded materials. It is necessary to understand the stress relaxation that occurs in the functionally gradient material in order to design the material property variation appropriately. The focus of the present research is on:

1. Elastic–plastic analysis of FGM specimens

2. The effect of thermomechanical coupling in the inelastic regime (for e.g., see Allen [56]).

1.4.4 Inverse Design/Optimization

All of the above objectives quite naturally lead us to the design aspect of the functionally graded materials. We have at our hand the ability to tailor the material properties according to our needs. The thermomechanical response of the system both in the elastic and inelastic regime will influence the material property variation in the solid.

1.5 Summary of Present Research

The present research aims at developing mechanics formulations, mathematical models and computational models for functionally graded materials. Specifically, the nonlinear coupled thermomechanical response of these materials under static, dynamic, and thermal loading environments are studied. The following is an outline of the various important issues in the present research.

1. Mechanics formulations, mathematical models, and computational formulations

2. A finite element program for solving fully coupled nonlinear thermoelastic and thermoinelastic equations

3. Design of FGM property variations using the thermomechanical response; parametric study for optimum profile variations; quantify the results for use by designers and manufacturers

4. Study the response of structural elements (rods, plates, and shells) made of functionally graded materials under static, dynamic, and thermal loading environments using the finite element program.

References

[1] Yamanouchi, M., Koizumi, M., Hirai, T., and Shiota, I., (Editors), *FGM '90*, Proceedings of the First International Symposium on Functionally Gradient Materials, Japan, 1990.

[2] Koizumi, M., "The Concept of FGM", *Ceramic Transactions, Functionally Gradient Materials*, Vol. 34, 1993, pp. 3–10.

[3] Jones, W.F., and Whitney, J.M., (Editors), *Advances in Experimental Mechanics and Biomimetics*, Proceedings of the Winter Annual Meeting of the ASME, California, 1992.

[4] Erdogan, F., and Ozturk, M., "Diffusion Problems in Bonded Nonhomogeneous Materials With an Interface Cut", *Int. J. Engg. Sci.*, Vol. 30, 1992, pp. 1507–1523.

[5] Holt, J.B., Koizumi, M., Hirai, T., and Munir, Z.A., (Editors), *Ceramic Transactions, Functionally Gradient Materials*, Proceedings of the Second International Symposium on Functionally Gradient Materials, Vol. 34, California, 1992.

[6] Suemitsu, T., et al., "Carbon/Carbon Composites for Combustors of Space Planes", *Ceramic Transactions, Functionally Gradient Materials*, Vol. 34, 1993, pp. 315–322.

[7] Matsuzaki, Y., et al., "Analysis–Assisted Fabrication of TiAl–Based Thermal Barrier FGM and Its Performance in a Supersonic Hot Gas Flow", *Ceramic Transactions, Functionally Gradient Materials*, Vol. 34, 1993, pp. 323–330.

[8] Abramov, I.I., and Kharitonov, V.V., "Numerical Analysis of Functionally Integrated VLSIC Elements Taking into Account Thermal Effects, I. Model", *J. Engg. Phy*, Vol. 54, 1988, pp. 227–231.

[9] Hirai, T., "Functionally Gradient Materials and Nanocomposites", *Ceramic Transactions, Functionally Gradient Materials*, Vol. 34, 1993, pp. 11–20.

[10] Dunn, M.L., and Taya, M., "Micromechanics Predictions of the Effective Electroelastic Moduli of Piezoelectric Composites", *Int. J. Sol. Struct.*, Vol. 30, 1993, pp. 161–175.

[11] Thomann, H., "Piezoelectric Composites", in *Advanced Structural and Functional Materials*, W.G.J. Bunk (Ed.), 1991, pp. 119–219.

[12] Smith, W.A., "Modeling 1–3 Composite Piezoelectrics: Thickness Mode Oscillations", *IEEE Trans. on Ultrasonics, Ferroelectrics, and Frequency Control*, Vol. 38, 1991, pp. 40–47.

[13] Smith, W.A., "Modeling 1–3 Composite Piezoelectrics: Hydrostatic Response", *IEEE Trans. on Ultrasonics, Ferroelectrics, and Frequency Control*, Vol. 40, 1993, pp. 41–49.

[14] Jin,Z., and Noda, N., "Minimization of Thermal Stress Intensity Factors for a Crack in Metal–Ceramic Mixture", *Ceramic Transactions, Functionally Gradient Materials*, Vol. 34, 1993, pp. 47–54.

[15] Fakui, Y., "Fundamental Investigation of Functionally Gradient Material Manufacturing System Using Centrifugal Force", *JSME Int. Journal, Series III*, Vol. 34, 1991, pp. 144–148.

[16] Williamson, R.L., Rabin, B.H., and Drake, J.T., "Finite Element Analysis of Thermal residual Stresses at Graded Ceramic–Metal Interfaces, Part I. Model Description and Geometric Effects", *J. Appl. Phys.*, Vol. 74, 1993, pp. 1310–1320.

[17] Drake, J.T., Williamson, R.L., and Rabin, B.H., "Finite Element Analysis of Thermal Residual Stresses at Graded Ceramic–Metal Interfaces, Part II. Interface Optimization for residual Stress reduction", *J. Appl. Phys.*, Vol. 74, 1993, pp. 1321–1326.

[18] Hirai, T., and Sasaki, M., "Vapor-Deposited Functionally Gradient Materials", *JSME Int. Journal.*, Vol. 34, 1991, pp. 123–129.

[19] Robson, M.T., Blue, C.A., Warrier, S.G., and Liu, R.Y., "Sputter deposition of SiC Coating on Silicon Wafers", *Scripta Mettalurgica et Materialia*, Vol. 27, 1992, pp. 565–570.

[20] Fujii, K., Imai, H., Nomura, S., and Shindo, M., "FGM of Silicon Carbide and Carbon as Advanced Oxidation Resistant Graphite", *J. of Nuclear Materials*, Vol. 187, 1992, pp. 204–208.

[21] Sata, N., "Characteristic of SiC-TiB$_2$ Composites as the Surface Layer of SiC-TiB$_2$-Cu Functionally Gradient Material Produced by Self–Propagating High-Temperature Synthesis", *Ceramic Transactions, Functionally Gradient Materials*, Vol. 34, 1993, pp. 109–115.

[22] Radhakrishnan, R., Bhaduri, S.B., and Wojcicki, S., "Processing of Dense FGMs in the TiB$_2$-Cu System", *Ceramic Transactions, Functionally Gradient Materials*, Vol. 34, 1993, pp. 117–123.

[23] Kawai, C., Wakamatsu, S., Sakagami, S., and Nomura, T., "Fabrication of Continuous Fiber Reinforced SiC Matrix Composites with Gradient Compositions", *Ceramic Transactions, Functionally Gradient Materials*, Vol. 34, 1993, pp. 133–139.

[24] Fuchiyama, T., Noda, N., Tsuji, T., and Obata, Y., "Analysis of Thermal Stress and Stress Intensity Factor of Functionally Gradient Materials", *Ceramic Transactions, Functionally Gradient Materials*, Vol. 34, 1993, pp. 425–432.

[25] Tani, J., and Liu, G.R., "SH Surface Waves in Functionally Gradient Piezoelectric Plates", *JSME Int. Journal, Series A*, Vol. 36, 1993, pp. 152–155.

[26] Fakui, Y., and Yamanaka, N., "Elastic Analysis for Thick-Walled Tubes of Functionally Graded Material Subjected to Internal Pressure", *JSME Int. Journal, Series I*, Vol. 35, 1992, pp. 379–385.

[27] Fakui, Y., Yamanaka, Y., and Wakashima, K., "The Stress and Strains in a Thick-Walled Tube of Functionally Graded Material Under Uniform Thermal Loading", *JSME Int. Journal, Series A*, Vol. 36, 1993, pp. 156–162.

[28] Delale, F., and Erdogan, F., "The Crack Problem for a Nonhomogeneous Plane", *J. Appl. Mech.*, Vol. 50, 1983, pp. 609–614.

[29] Noda, N., and Jin, Z.H., "Thermal Stress Intensity Factors for a Crack in a Strip of Functionally Gradient Material", *Int. J. Sol. Struct.*, Vol. 30, 1993, pp. 1039–1056.

[30] Araki, N., Makino, A., Ishiguro, T., and Mihara, J., "An Analytical Solution of Temperature Response in Multilayered Material for Transient Mathod", *Int. J. Thermophysics*, Vol. 13, 1992, pp. 515–538.

[31] Ishiguro, T., Makino, A., Araki, N., and Noda, N., "Transient Temperature Response in Functionally Gradient Materials", *Int. J. Thermophysics*, Vol. 14, 1993, pp. 101–121.

[32] Zhai, P.C., Jiang, C.R., and Zhang, Q.J., "Application of Three–Phase Micromechanical Theories To Ceramic/Metal Functionally Gradient Materials", *Ceramic Transactions, Functionally Gradient Materials*, Vol. 34, 1993, pp. 449–456.

[33] Christensen, R.M., *Mechanics of Composite Materials*, John Wiley and Sons, New York, 1979.

[34] Willis, J.R., "The Overall Elastic response of Composite Materials", *J. Appl. Mech.*, Vol. 50, 1983, pp. 1202–1209.

[35] Hashin, Z., and Shtrikman, S., "On Some Variational Principles in Anisotropic and Nonhomogeneous Elasticity", *J. Mech. Phys. Solids*, Vol. 10, 1962, pp. 335–342.

[36] Eshelby, J.D., "The Determination of the Elastic Field of an Ellipsoid Inclusion, and Related Problems", *Proc. Royal Soc. London*, Vol. 241, 1957, pp. 376–396.

[37] Ju, J.W., and Chen, T.M., "Micromechanics and Effective Moduli of Elastic Composites with Randomly Dispersed Inhomogeneities", *Macroscopic Behavior of Heterogeneous Materials from the Microstructure*, Proceedings of the Winter Annual Meeting of the ASME, 1992, pp. 95–108.

[38] Torquato, S., "Connection Between Morphology and Effective properties of Heterogeneous Materials", *Macroscopic Behavior of Heterogeneous Materials from the Microstructure*, Proceedings of the Winter Annual Meeting of the ASME, 1992, pp. 53–65.

[39] Nan, C.W., Yuan, R.Z., and Zhang, L.M., "The Physics of Metal/Ceramic Functionally Gradient Materials", *Ceramic Transactions, Functionally Gradient Materials*, Vol. 34, 1993, pp. 75–82.

[40] Pindera, M.J., and Freed, A.D., "The Effect of Matrix Microstructure on the Evolution of residual Stresses in Titanium–Aluminide Composites", *Constitutive Behavior of High–Temperature Composites*, Majumdar, B.S., Newaz, G.M., and Mall, S., (Editors), 1992, pp. 37–52.

[41] Pindera, M.J., Salzar, R.S., and Williams, T.O., "An Evaluation of a New Approach for the Thermoplastic Response of Metal–Matrix Composites", *Comp. Engg.*, Vol. 3, 1993, pp. 1185–1201.

12

[42] Aboudi, J., Pindera, M.J., and Arnold, S.M., "Thermoelastic Response of Metal–Matrix Composites with Large Diameter Fibers Subjected to Thermal Gradients", *NASA TM-106344*, 1993.

[43] Pindera, M.J., Arnold, S.M., Aboudi, J., and Hui, D., (Editors), *Use of Composites in Functionally Gradient Materials*, Composites Engineering Special Issue, Vol. 4, 1994.

[44] Eischen, J.W., "Fracture of Nonhomogeneous Materials", *Int. J. Fract.*, Vol. 34, 1987, pp. 3–22.

[45] Erdogan, F., and Ozturk, M., "Fracture Mechanics of Debonding in Dissimilar Materials Bonded Through a Functionally Gradient Interface Zone", *Ceramic Transactions, Functionally Gradient Materials*, Vol. 34, 1993, pp. 31–38.

[46] Erdogan, F., and Wu, F., "Analysis of FGM Specimens for Fracture Toughness Testing", *Ceramic Transactions, Functionally Gradient Materials*, Vol. 34, 1993, pp. 39–46.

[47] Jin, Z.H., and Noda, N., "Transient Thermal Stress Intensity Factors for a Crack in a Semi–Infinite Plate of a Functionally Gradient Material", *Int. J. Sol. Struct.*, Vol. 31, 1994, pp. 203–218.

[48] Teraki, J., Hirano, T., and Wakashima, K., "An Elastic–Plastic Analysis of Thermal Stresses in a FGM plate Under Cyclic Thermal Load", *Ceramic Transactions, Functionally Gradient Materials*, Vol. 34, 1993, pp. 67–74.

[49] Zhang, Q.J., Zhang, L.M., and Yuan, R.Z., "A Coupled Thermoelasticity Model of Functionally Gradient Materials Under Sudden High Surface Heating", *Ceramic Transactions, Functionally Gradient Materials*, Vol. 34, 1993, pp. 99–106.

[50] Tanaka, K., et al., "Design of Thermoelastic Materials Using Direct Sensitivity and Optimization Methods. Reduction of Thermal Stresses in Functionally Gradient Materials", *Comp. Meth. Appl. Mech. Engg.*, Vol. 106, 1993, pp. 271–284.

[51] Tanaka, K., et al., "An Improved Solution to Thermoelastic Material Design in Functionally Gradient Materials: Scheme to Reduce Thermal Stresses", *Comp. Meth. Appl. Mech. Engg.*, Vol. 109, 1993, pp. 377–389.

[52] Kawasaki, A., and Watanabe, R., "Fabrication of Disk–Shaped Functionally Gradient Materials by Hot Pressing and Their Thermomechanical Performance", *Ceramic Transactions, Functionally Gradient Materials*, Vol. 34, 1993, pp. 157–164.

[53] Reddy, J.N., "A Generalization of Two–Dimensional Theories of Laminated Composite Plates", *Commun. Appl. Numer. Meth.*, Vol. 3, 1987, pp. 173–180.

[54] Reddy, J.N., "An Evaluation of Equivalent–Single–Layer and Layerwise Theories of Composite Laminates", *Composite Structures*, Vol. 25, 1993, pp. 21–35.

[55] Amin, A.M., and Sierakowski, R.L., "Effect of Thermomechanical Coupling of the Response of Elastic Solids", *AIAA Journal*, Vol. 28, 1990, pp. 1319–1322.

[56] Allen, D.H., "Thermomechanical Coupling in Inelastic Solids", *Appl. Mech. Rev.*, Vol. 44, 1991, pp. 361–373.

(a) at the microstructure level   (b) as a continuous medium
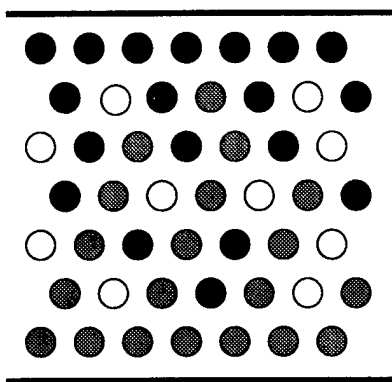
● Material 1 (say, ceramic)
◉ Material 2 (say, metal)
○ Voids

▦ Material 1 (say, ceramic) rich
▢ Material 2 (say, metal) rich
▨ Material 1 + Material 2

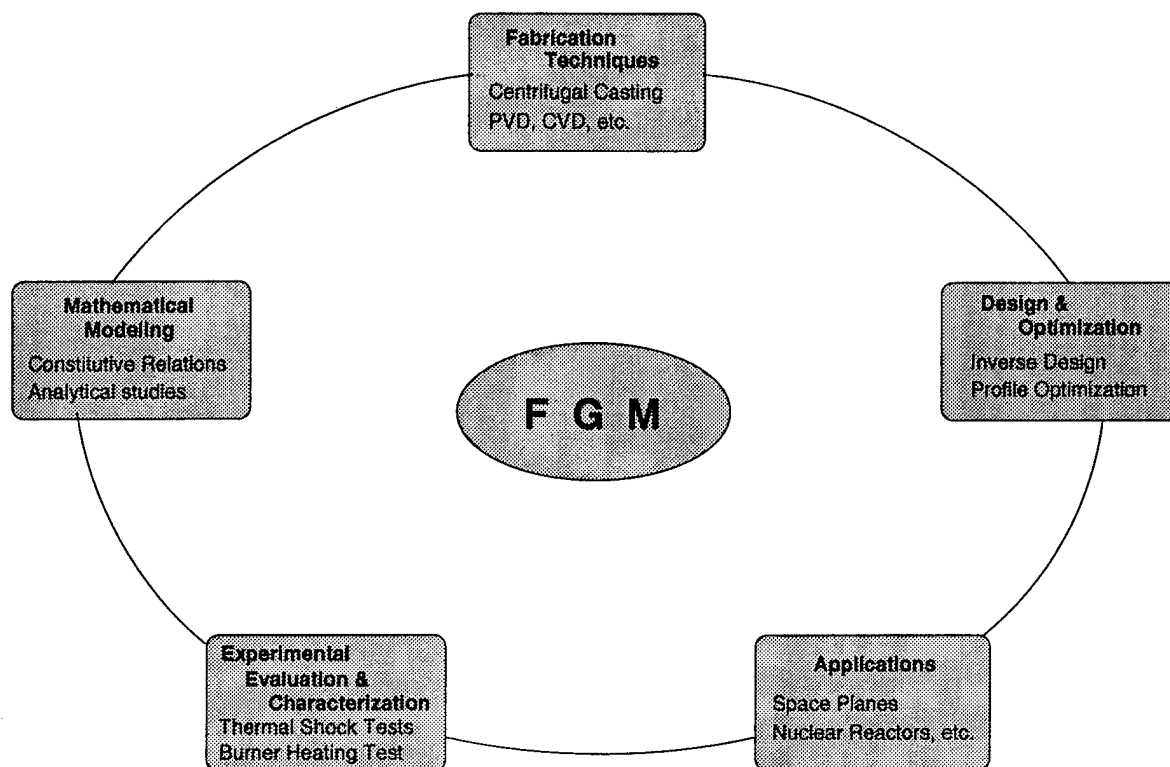Figure 1: Variation of material composition betweeen surfaces.
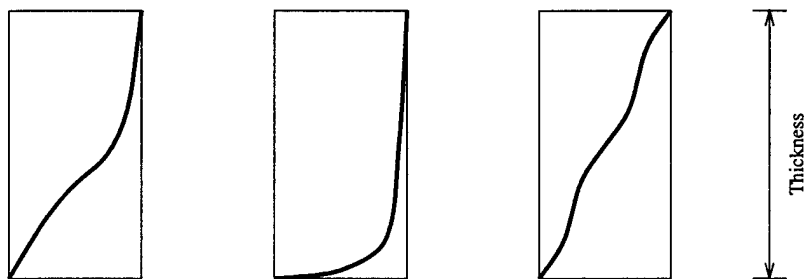
Figure 2: Illustration of issues involved in FGMs.

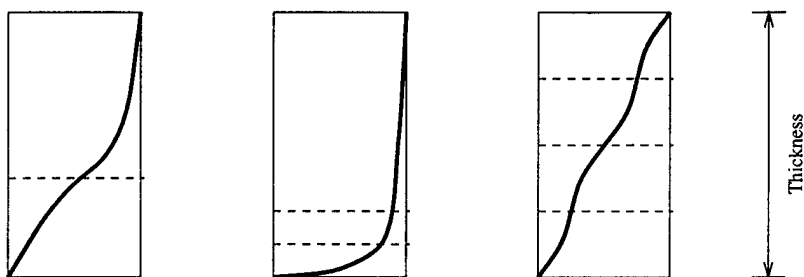Figure 3: Illustration of material property profiles.

Figure 4: Numerical layer divisions corresponding to complex property variations through the thickness.

17

2 Pseudo-dynamic Thermoelastic Analysis of a Functionally Graded Ceramic-Metal Cylinder

2.1 Introduction

The study of response of structures to rapid heating is of importance. Often, structural components are required to sustain high temperature gradients. These temperature gradients may occur over extremely short periods of time, and so the material is exposed to a state of thermal shock. Typical situations where thermal shock occurs are during rentry of space vehicles, where the temperature changes from -100 degrees F to about 2000 degrees F in a few minutes, the Advanced Gas turbine, wherein a severe temperature transient of a change in temperature of 1500 degrees C occurs over a time period of 15s. Plasma facing materials, propulsion system of planes, cutting tools, engine exhaust liners, aerospace skin structures, incinerator linings, thermal barrier coatings of turbine blades, thermal resistant tiles and, directional heat flux materials are all examples where materials have to operate in extremely high temperature transient environments.

Functionally graded materials are a new class of materials which are constructed to operate in high temperature environments. Typically, functionally graded materials are made from a mixture of ceramic and a combination of different metals. These materials are microscopically heterogeneous. Material heterogeneity introduces property gradients. These property gradients have to be appropriately tailored in order to gain advantage of the properties of the individual components. The high temperature resistance is provided by the ceramic. Ceramics are hard, brittle, corrosion resistant and are made by firing clay or other minerals and consist of one or more metals in combination with one or more non-metals, usually including oxygen. The thermal conductivity of ceramics is very small compared to that of metals. This enables the ceramics to withstand higher temperature gradients, for a given heat flux, as compared to metals. Also, the coefficient of thermal expansion for ceramics is small. This results in smaller thermal strains, and hence smaller thermal stresses.

Thermal shock results when there are sudden and large temperature changes, thus causing an uneven stress distribution and an uneven expansion. This could result in fracture. Since ceramics are brittle, mixing the ceramic with ductile metals is advantageous in such situations. The joining of ceramics with metals may be done in two ways. The structural component may be constructed by introducing distinct metal layers into a ceramic structure. This introduces interfaces and results in thermal mismatch. If the property mismatch across interfaces is large, then, this leads to large thermal stresses that are undesirable. Alternatively, a mixture of the ceramic with the metal and ceramic with a continuously varying volume fraction may be manufactured. This eliminates interface problems. The stress distributions are more smooth.

The main application of functionally graded materials are in high temperature environments. As a result, the study of material response to high temperature conditions is very essential. Noda [1] has presented an extensive review that covers a wide range of topics from thermoelastic to thermo-inelastic problems. In this paper, Noda also discusses the importance of temperature dependent properties on thermoelastics problems. He further presented analytical methods to handle transient heat conduction problems and indicates the necessity of an optimization of FGM properties.

Most studies which have been performed so far have mainly concentrated on the uncoupled thermomechanical problems, notable exceptions include Zhang [2] and Amin [3]. Zhang and his coworkers modeled an isotropic ceramic/metal laminated beam subjected to abrupt heating condition, and demonstrated the influence of thermomechanical coupling on the thermal shock response. Amin and Sierakowski [3] discussed the importance of thermomechanical coupling when the materials are subjected to transient thermal loading conditions. In contrast, Jin and Noda [4] considered the coupling effect to be insignificant and ignored it in their study.

In the area of thermoelastic formulations, Tanigawa [5] used a layerwise model to solve a transient heat conduction problem and optimized the material composition to reduce the thermal stress distribution. Tanigawa [6] also compiled a comprehensive review on the thermoelastic analysis of functionally graded materials. In the review, he discussed closed form solutions for some simple geometries. These solutions, however, were restricted to steady-state conditions. Tanaka et al. [7,8] have formulated a method to design FGM property profiles using sensitivity and optimization methods based on the criterion of reduction of thermal stresses.

Most of the studies on thermal shock have been on experimental aspects. Kumakawa and Niion [9] studied the thermal fatigue properties of functionally graded material specimens by estimating the variation of effective thermal conductivity with thermal cycles under high heat flux conditions. Experimentally, they confirmed that there is an optimum compositional distribution to reduce thermal fatigue and concluded that normalized effective thermal conductivity is a useful index for showing thermal fatigue characteristics. Takahashi [10] using laser irradiation and plasma-arc heating methods for the evaluation of thermomechanical behavior of functionally graded materials. Specifically, the laser irradiation method was applied to examine the possible fracture process of thermal barrier coating system in advanced gas turbine environments. The results have shown that ZrO_2-based FGM gives a higher thermal shock/fatigue resistance compared to a conventional ZrO_2 coating materials. Shindo [11] studied numerically the thermal shock fracture of composite materials with temperature dependent properties, and analyzed the thermoelastic behavior of a cracked layered composite and an edge cracked orthotropic strip. Kokini [12] studies the effect of a transient thermal load on an interface crack in a ceramic-to-metal bond and examines the effect of geometry, material properties, constraint conditions and heat conduction across the crack.

The response of graded cylinders to rapid heating has not been considered before. Also, none of the analyses in literature, take into consideration, the dependence of all the material properties, on temperatures. In situations where the service temperatures are high, analyses which consider temperature independent properties may be in considerable error. This paper considers the problem of thermoelastic deformations of a cylinder subjected to rapid heating and also considers the effect of temperature variation of all the appropriate material properties.

2.2   Thermoelastic Finite Element Model of Cylinder

In this section, we present the equations, finite element model and preliminary results for the pseudo-dynamic response of the functionally graded ceramic cylinders under rapid radial heating. The analysis is termed 'pseudo-dynamic' due to the fact that the inertia forces

appearing in the elasticity equations is neglected. The time dependence of the response of the cylinder is limited to the unsteady heat transfer equation alone.

Cylindrical pipes carrying hot gases experience high thermal transients. It is important to study the stress distribution in such situations. The stresses in the cylinder are developed primarily due to rapid changes in temperature. Figure 1. shows the hollow cylinder and the boundary conditions. The shaded annular region is continuously graded in terms of the material properties. In the present problem, the inner surface of the cylinder is subjected to a rapid increase in temperature and the unsteady heat transfer equation is solved. A time marching scheme is adopted in order to solve the parabolic equation. Then, at each time step, the equilibrium equation is solved. Temperature dependence of the constitutive equations is considered. Thus, at each time step, the constitutive equation is updated, with the temperature at that time step, which is obtained by solving the energy equation. As a first approximation, thermomechanical coupling and inertia terms in the equilibrium equation are neglected. The property variation is modeled using simple polynomial fits upto cubic order. Effective properties of the metal-ceramic composite are computed using a simple rule of mixtures, that is a linear function of the volume fraction of the metal. The variation of volume fraction along the radius is expressed in terms of a power law function of the radial coordinate, and is shown in Figure 2.

2.2.1 Heat Transfer in FGM Cylinder

The equation for the axisymmetric heat transfer in a heterogeneous cylinder is obtained from the statement of the conservation of energy. The heat transfer equation in polar coordinates is given by

$$-\frac{1}{r}\left(\frac{\partial T}{\partial r}\frac{\partial(kr)}{\partial r} + kr\frac{\partial^2 T}{\partial r^2}\right) + \rho C_v \frac{\partial T}{\partial t} = 0 \tag{1}$$

where the thermal conductivity k, density ρ and the specific heat C_v, are all functions of temperature and the radial coordinate, r. This equation is non-linear and is solved iteratively. The boundary conditions are such that the outer surface of the cylinder is insulated and the inner surface of the cylinder is subjected to a convection condition. It is assumed that hot gases flow through the cylinder and therefore a convection boundary condition is imposed at the inner surface. The cylinder is assumed to be at room temperature initially. The boundary conditions are written as

$$2\pi kr\frac{\partial T}{\partial r} + 2\pi rh\left(T - T_\infty\right) = 0 \quad : \quad r_{inner}$$

$$2\pi kr\frac{\partial T}{\partial r} = 0 \quad : \quad r_{outer} \tag{2}$$

where h is the heat transfer coefficient at the inner radius of the cylinder, k is the thermal conductivity and T_∞ is the temperature of the hot gases flowing through the hollow cylinder. Next, a semi-discrete finite element model of the equations is developed following the three step procedure in Reddy [13]. We then substitute the time approximation from the alpha-family of approximations, to obtain the fully discretized finite element model of the equations. The discretized system of equations is non-linear and have to be solved iteratively using the

Picard scheme. The non-linearities appearing in the force term are assumed to be known from the previous time-step, and the non-linearities in the stiffness matrix are assumed to be known from the previous iteration, in the Picard scheme. The time-step chosen is evaluated using a simple eigenvalue analysis of the discretized equations. The alpha family of approximations for parabolic time dependent equations and the descretized set of equations in the Picard scheme are as follows:

$$
\begin{aligned}
\{T\}_s &= \{T\}_s + \Delta t \left\{\dot{T}\right\}_{s+\alpha} \\
\{\dot{u}\}_{s+\alpha} &= (1-\alpha)\left\{\dot{T}\right\}_s + \alpha\left\{\dot{T}\right\}_{s+1} \quad for\ 0 \le \alpha \le 1 \\
\alpha &= 0.5\ stable\ Crank-Nicolson\ scheme;\ O\left((\Delta t)^2\right) \quad (3)
\end{aligned}
$$

$$
\begin{aligned}
\left[K\left(\hat{T}^n_{s+1}\right)\right]^n_{s+1} \{T\}^{n+1}_{s+1} &= \left[\bar{K}\right]^n_s \{T\}_s + \left\{\hat{F}\right\}^n_{s,s+1} \\
\hat{K}_{ij} &= \int_{r_a}^{r_b} \rho C_v r \psi_i \psi_j dr + \alpha\Delta t \left(\int_{r_a}^{r_b} k^n_{s+1} r \frac{\partial\psi_i}{\partial r}\frac{\partial\psi_j}{\partial r} dr + H_{ij}\right) \\
\bar{K}_{ij} &= \int_{r_a}^{r_b} \rho C_v r \psi_i \psi_j dr - (1-\alpha)\Delta t \left(\int_{r_a}^{r_b} k_s r \frac{\partial\psi_i}{\partial r}\frac{\partial\psi_j}{\partial r} dr + H_{ij}\right) \\
\left\{\hat{f}_i\right\} &= \Delta t \left(\alpha\{f_i\}_{s+1} + (1-\alpha)\{f_i\}_s\right) \\
T^o_{s+1} &= T^c_s\ c \Rightarrow converged \\
convergence &\Rightarrow \frac{\parallel T^{n+1}_{s+1} - T^n_{s+1} \parallel_2}{\parallel T^{n+1}_{s+1} \parallel_2} \le 10^{-3} \quad (4)
\end{aligned}
$$

where $\left[\hat{K}\right]^n_{s+1}$ is the stiffness matrix at time step $s+1$ and at the n th iteration in the Picard scheme, and $\{T\}^{n+1}_{s+1}$ is the n+1 th iterate to be solved at the same time step. The right hand side of the above equation is the modified force vector that is computed from the solution at the previous timestep and from the n th iterate in the Picard scheme. The term H_{ij} is due to the convection boundary condition and is added to the first diagonal term of the stiffness matrix, corresponding to the first element. ψ_i and ψ_j are the one-dimensional lagrange shape functions in the radial coordinate. In this study, quadratic shape functions are used. The temperature distribution along the radius of the cylinder is obtained by solving the discretized set of equations, using the Picard method. Once, the convergence criterion is met and the temperature is known at a particular time step, the equation corresponding to the conservation of linear momentum is solved, at the same time step. The equation of conservation of linear momentum and its finite element model is presented next.

2.2.2 The Thermoelastic Boundary Value Problem

The large change in temperature across the radius of the cylinder gives rise to radial and hoop stresses of large magnitude. Thus, the stress distribution is driven mainly by the temperature distribution. The stresses in the cylinder are calculated under plane strain conditions. The problem is pseudo-dynamic, i.e., the inertia term in the equilibrium equation is neglected, however, the constitutive equations are assumed to change with time. This is because of the

temperature dependence of the constitutive equation. The equation for the conservation of linear momentum along the radial direction is given by

$$\frac{\partial \sigma_{rr}}{\partial r} + \frac{\sigma_{rr} - \sigma_{\theta\theta}}{r} = 0$$

The constitutive equations for the radial stress σ_{rr}, and the hoop stress $\sigma_{\theta\theta}$, are given by

$$\sigma_{rr} = \lambda \varepsilon_{kk} + 2\mu \varepsilon_{rr} - 3\alpha K \left(T - T_o\right)$$
$$\sigma_{\theta\theta} = \lambda \varepsilon_{kk} + 2\mu \varepsilon_{\theta\theta} - 3\alpha K \left(T - T_o\right) \tag{5}$$

where λ and μ are the Lame coefficients, K is the bulk modulus, α is the coefficient of thermal expansion, and T_o is the thermal strain-free reference temperature, which in the present case is taken to be the room temperature. The radial and hoop strains are given in terms of the radial displacement, u, by

$$\varepsilon_{rr} = \frac{\partial u}{\partial r}$$
$$\varepsilon_{\theta\theta} = \frac{1}{r}\frac{\partial u}{\partial \theta} + \frac{u}{r} \tag{6}$$

The finite element model of the equilibrium equation is obtained following the standard three step procedure as before. This yields the following set of equations:

$$[K]\{u\} = \{F\}$$

The element stiffness matrix and the force vector are given by

$$K_{ij} = \int_{r_a}^{r_b} \frac{\partial(r\psi_i)}{\partial r}\left[(\lambda + 2\mu)\frac{\partial \psi_j}{\partial r} + \frac{\lambda}{r}\psi_j\right] - \int_{r_a}^{r_b} \frac{E}{1+\nu}\psi_i\left(\frac{\partial \psi_j}{\partial r} - \frac{\psi_j}{r}\right) dr \tag{7}$$

$$F_i = P_i + \int_{r_a}^{r_b} \frac{\partial(r\psi_i)}{\partial r}3\alpha K\left(T - T_o\right) dr \tag{8}$$

where P_i is the nodal contribution of the externally applied force, which in the present case is zero. On the outer surface of the cylinder, a stress free boundary condition is imposed. On the inner surface, the radial displacement is constrained to be zero. Once the displacement is obtained at the end of each time step, the radial and hoop stresses are calculated, at the time step of interest, using a simple post processing subroutine. This is done for various distributions of volume fraction. The volume fraction of the ceramic is taken to be one at the inner surface and zero at the outer surface. In the next section, the temperature dependence of the properties of some of the commonly used ceramics and metals are listed. These material properties are then used in the thermoelastic analysis of the FGM cylinder.

2.2.3 Material Properties

Tables 1 and 2 list the material properties of Zirconia and Ti6AlV, as a function of temperature. The material property functions have been obtained from literature. In the context of finite elements, these functions may be expressed in terms of the finite element basis functions, within each element. Since, most of the property variation is not limited to simple lower order polynomials, a higher order Gauss Quadrature rule must be used, in general. All material properties, c, are expressed in the following form

$$c = c_o \left(\frac{c_{-1}}{T} + 1 + c_1 T + c_2 T^2 + c_3 T^3 \right) \tag{9}$$

where c_o is the constant appearing in the cubic fit of the material property with temperature. c_{-1}, c_1, c_2 and, c_3 are the coefficients of T^{-1}, T, T^2 and, T^3, obtained after factoring out c_o from the cubic curve fit of the property. The material properties were expressed in this way, so that the higher order effects of the temperature on the material properties would be readily discernible. For the analysis with constant properties, the material properties were all evaluated at 298.15 degrees K. The values of each of the coefficients appearing in the above equation, is listed for the metal and ceramic, from tables 1 and 2. Also, the material property, c, at any point along the radius of the compositionally graded cylinder is expressed as follows:

$$c = c_{metal} \left(v f_{metal} \right) + c_{ceramic} \left(v f_{ceramic} \right) \tag{10}$$

The expressions for the volume fraction of the metal and ceramic are given in the next section. The material properties of the metal and ceramic bring in the explicit temperature dependence, with the temperature depending on the radial position, and the volume fraction is itself a function of the radial coordinate. Note that this way of expressing the material properties makes the analysis nonlinear, because the properties are dependent on temperature which is one of the field variables that we will solve for. As is common with the procedure for solving nonlinear problems, the material properties will be assumed to be known in terms of the temperature obtained in the previous iteration.

2.3 Results

The pseudo-dynamic, axisymmetric thermoelastic boundary value problem is solved for a cylinder with an inner radius of 0.0127m and an outer radius of 0.0254m. The temperature of the hot gases flowing within the hollow cylinder was assumed to be 2000 degrees K, and the heat transfer coefficient was assumed to be 750 W/m^2K. The initial condition was chosen to be uniform at the room temperature at 298.15 K. The radial displacement at the inner surface of the cylinder was constrained to be zero, while, at the outer surface, a stress free boundary condition was imposed. A simple eigenvalue calculation was made to select a timestep of $5.0 \times 10^{-5}s$. The ceramic chosen was Zirconia, along with Ti-6Al-V as the metallic component of the FGM. The volume fraction distribution is chosen in terms of a simple power law, such that the inner radius has a ceramic volume fraction of unity, and the outer radius has a metallic volume fraction of unity. The value of the convection heat transfer coefficient and T_∞ was chosen so that the temperature at the inner surface

increases to about 900-1000 degrees centigrade, over a period of 15s. This was chosen, so as to compare with the start thermal transient of the pipes carrying hot gases, in the Advanced Gas Turbine. The AGT is a 100-hp engine, designed for automobiles upto 3000 lb. The turbine inlet temperature is about 2500 degrees F [14]. One of the most severe thermal shocks the engine suffers arises during the startup period.

The analysis was conducted for volume fraction distribution chosen to be of simple power law type, i.e., a variation of the form $\left(\frac{r-r_i}{r_o-r_i}\right)^n$, where, n is the exponent. If we set

$$r = r_i + \bar{r}\left(r_o - r_i\right) \tag{11}$$

then, the metal volume fraction distribution may be represented as

$$vf = \bar{r}^n \quad (0 \leq \bar{r} \leq 1) \tag{12}$$

The various values of n chosen were 0, 0.3, 0.5, 0.8, 0.9, 1.0, 1.5, 2.0, 2.5, 3.0, 4.0 and 20. The first of these cases corresponds to a fully metallic cylinder and the value of 20, corresponds to an FGM cylinder with a ceramic volume fraction of about 95%. The problem is solved in two steps, as explained earlier. The heat conduction problem is solved at each time step, followed by the elasticity problem. The constitutive equations are updated at each time step and the radial and hoop stresses are calculated. The analysis was conducted separately for the cases where the material properties were assumed to be constant, and for the case where the material property was assumed to vary with temperature. The density was assumed to be constant, for both the ceramic and the metal. The finite element code was run to simulate the thermoelastic response over a time period of 1s. The domain was discretized using 50 quadratic elements. Results are presented after a convergence study was done. The following interesting observations were made regarding the temperature and stress distribution.

The power law exponent of the volume fraction distribution is a measure of the amount of metal or ceramic in the cylinder. The average volume fraction of the metal and the ceramic may be calculated by a simple integration of the distribution over the domain. Table 3 lists the average volume fraction of the metal and ceramic for different values of the exponent in the power law variation.

In all the cases, it was seen that the maximum temperature occured at the ceramic rich end, i.e., the inner surface of the cylinder that is in contact with hot gases. The maximum temperature attained at the inner surface was the lowest for the case of n = 0 which corresponds to a fully metallic cylinder. This is because, in metallic cylinders, the largest magnitude of heat is conducted away into the cylinder. Figure 3 shows the variation of temperature in the radial direction, for power law exponent equal to 1, upto a time period of 1s, and for material properties varying with temperature. No significant change in the maximum temperature was observed for the case where the average volume fraction of the ceramic was greater than 0.5. Therefore, FGMs with 50% volume content of ceramic are good enough to withstand high temperatures and there is not much to be gained by increasing the ceramic content, if the distribution follows the power law. Figure 4 shows the variation of the maximum temperature at the ceramic end, with the power law exponent. The temperature at the inner surface for the case of constant properties was always found to be greater than

that computed with temperature dependent properties. Thus, calculations and design based on temperature independent properties would yield conservative estimates.

The radial stresses, shown in Figure 5, were found to attain a maximum tensile value at the inner surface. For the case of temperature independent properties, the maximum tensile stress at the inner surface is independent of average volume fraction of ceramic, below 50%. The stress reduces below the level corresponding to $\bar{v}_{ceramic} = 0.5$, as the ceramic content increases.

For the case where the material properties are a function of temperature, the change in the ceramic content did not affect the magnitude of the maximum compressive stress. As the ceramic content increases, the maximum tensile stress at the inner surface reduces. Figure 6 shows the variation of the maximum tensile stress at the ceramic end with variation in the power law exponent. In the case where the properties depend on temperature, the radial tensile stresses increase initially, and then reduce continuously for all values of the power law exponent, beyond that corresponding to an average ceramic volume fraction of 20%. Thus, increasing the average volume fraction reduces the tendency to crack in the tensile mode. For the case of constant material properties, the radial stress reduces only beyond a ceramic volume fraction of 50%. Moreover, the stress calculated is always higher than in the case of temperature dependent properties.

The magnitude of the maximum compressive stress shown in Figure 7 was found to be independent of the average ceramic content, for the case where the material properties were assumed to vary with temperature. For the constant property case, the maximum compressive stress tends to decrease as the ceramic volume fraction increases.

For the hoop stresses, in the case of constant material properties, the maximum tensile stress occurs at a short distance from the ceramic rich region and the point at which this occurs tends to move towards the ceramic rich region, as ceramic content increases. However, the magnitude of the maximum tensile hoop stresses remains invariant to the ceramic composition. Figure 8 shows the variation of hoop stresses in the cylinder, with material properties assumed to depend on temperature. Stresses for $n = 0.3, 1.0, 3$ cases were computed, however, results only for the linear volume fraction distribution are shown. The maximum compressive hoop stress always occurs at the inner surface, which is ceramic rich and decreases in magnitude as the ceramic content increases upto 50%, but remains a constant thereafter (Figure 9). The compressive stress at the inner surface suppresses any tendency for cracks to grow in the tensile mode. In the case of variable material properties, the maximum hoop stress remains almost constant, but the point at which this occurs moves towards the region of maximum compression as the ceramic content increases.

Analysis was also conducted for a time period of 15s, at the end of which, the temperature and stress distributions are much smoother. The stresses increased only by one order of magnitude at the end of 15s, as compared to their magnitudes at the end of 1s. This shows that the material has to sustain high stresses in a very short time after thermal loading commences. For the case of linear distribution of the components, the temperature at the insulated metal rich region reached about 75 degrees C, while the temperature at the ceramic rich region was as high as 900 degrees C. The variation of temperature, with and without temperature dependence of material properties, and the radial stress are shown in Figures 10,11, and 12. It is seen that the average temperature calculated with constant material properties is higher than that computed using temperature dependent properties.

2.4 Closure

The above results give us a rough idea about the type of distribution one should choose in order to control the magnitude of the stresses. This analysis has been a simple one-dimensional analysis conducted in order to gain an understanding into the effects of combining metal and ceramics in various proportions. A fully dynamic analysis taking into consideration, the inertia terms and the thermoelastic coupling, will be investigated by considering an operator split methodology. The operator split method was proposed by Armero and Simo [15], in which the differential operator in the equations is additively split into two parts, one corresponding to an adiabatic elastodynamic phase, followed by a heat conduction phase at fixed configuration. One of the main conclusions, is that an asymptotic response is seen, with increasing values of the ceramic content. This type of response is reached at different values of the average ceramic content, for different field variables. In effect, the analysis provides information about the thermoelastic response of the cylinder for different proportions of the ceramic and metal.

2.5 References

1. Noda, N., "Thermal Stresses in Materials with Temperature-Dependent Properties", *Appl. Mech. Rev.*, **44**, pp. 383-397 (1991).

2. Zhang, Q. J., Zhang, L. M., and Yuan, R. Z., "A Coupled Thermoelasticity Model of Functionally Gradient Materials Under Sudden High Surface Heating", Ceramic Transactions, Functionally Gradient Materials, **34**, pp. 99-106 (1993).

3. Amin, A. M. and Sierakowski, R. L., "Effect of Thermomechanical Coupling of the Response of Elastic Solids", *AIAA Journal*, **28**, pp. 1319-1322 (1990).

4. Jin, Z. H., and Noda, N., "Transient Thermal Stress Intensity Factors for a Crack in a Semi-Infinite Plate of a Functionally Gradient Material", *Int. J. Solids Struct.*, **31**, pp. 203-218 (1994).

5. Tanigawa, Y., "Theoretical Approach of Optimum Design for a Plate of Functionally Gradient Materials Under Thermal Loading", NATO ASI Series E: *Applied Sciences, Thermal Shock and Thermal Fatigue Behavior of Advanced Ceramics*, **241**, pp. 171-180 (1992).

6. Tanigawa, Y., "Some Basic Thermoelastic Problems for Nonhomogeneous Structural Materials", *Appl. Mech. Rev.*, **48**, pp. 377-389 (1995).

7. Tanaka, K., et al., "Design of Thermoelastic Materials Using Direct Sensitivity and Optimization Methods. Reduction of Thermal Stresses in Functionally Gradient Materials", *Comp. Meth. Appl. Mech. Engg.*, **106**, pp. 271-284 (1993).

8. Tanaka, K., et al., "An Improved Solution to Thermoelastic Materials Designed in Functionally Gradient Materials: Scheme to Reduce Thermal Stresses.", *Comp. Meth. Appl. Mech. Engg.*, **106**, pp. 377-389 (1993).

9. Kumakawa, A. and Niion M., "Thermal Fatigue Characteristic of Functionally Gradient Materials for Aerospace Applications", NATO ASI Series E:*Applied Sciences, Thermal Shock and Thermal Fatigue Behavior of Advanced Ceramics*, **241**, pp. 567-578 (1992).

10. Takahashi, H., Ishikawa, T., Okugawa, D. and Hashida, T., "Laser and Plasma-Arc Thermal Shock/Fatigue Fracture Evaluation Procedure for Functionally Gradient Materials", NATO ASI Series E: *Applied Sciences, Thermal Shock and Thermal Fatigue Behavior of Advanced Ceramics*, **241**, pp. 543-554 (1992).

11. Shindo, Y., "Thermal Shock of Cracked Composite Materials with Temperature Dependent Properties", NATO ASI Series E:*Applied Sciences, Thermal Shock and Thermal Fatigue Behavior of Advanced Ceramics*, **241**, pp. 181-192 (1992).

12. Kokini, K., "Transient Thermal Fracture of Ceramic-to-Metal Interfaces", NATO ASI Series E: *Applied Sciences, Thermal Shock and Thermal Fatigue Behavior of Advanced Ceramics*, **241**, pp. 531-542 (1992).

13. Reddy, J. N., "An Introduction to the Finite Element Method", 2 nd Edition, McGraw-Hill, Inc., New-York (1993).

14. Musikant, Solomon., "What Every Engineer Should Know About Ceramics", Marcel Dekker., Inc. NewYork (1991).

15. Armero, F. and Simo, J. C., " A New Unconditionally Stable Fractional Step Method for Nonlinear Coupled Thermomechanical Problems", SUDAM Report No. 91-5, Stanford University, December 1991.
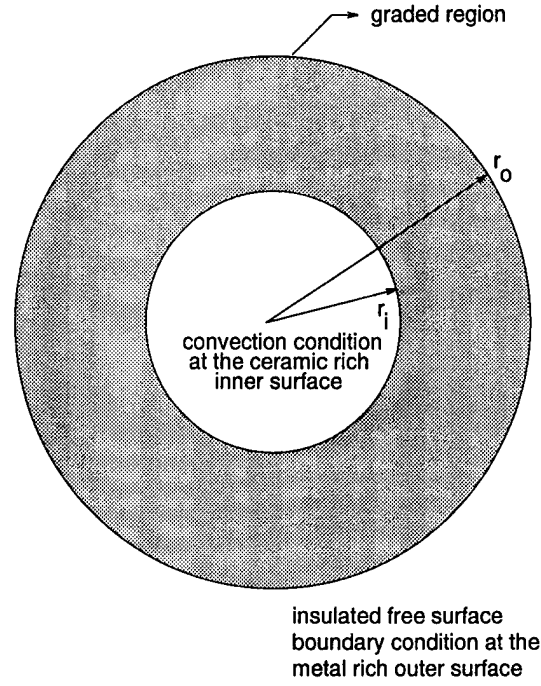
graded region

r_o

r_i

convection condition
at the ceramic rich
inner surface

insulated free surface
boundary condition at the
metal rich outer surface

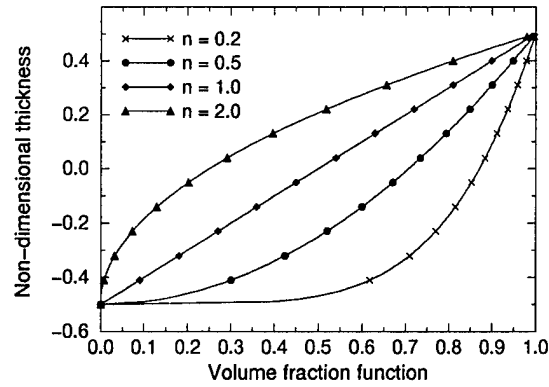Figure 1. Functionally graded cylinder $(r_i = 0.0127m, \ r_o = 0.0254m. \ ZrO_2/Ti - 6Al - V)$.

Figure 2. Volume fraction distribution. $v_{metal} = \left(\frac{r-r_i}{r_o-r_i}\right)^n$, n is the volume fraction exponent with $(0 \leq n \leq 20)$.
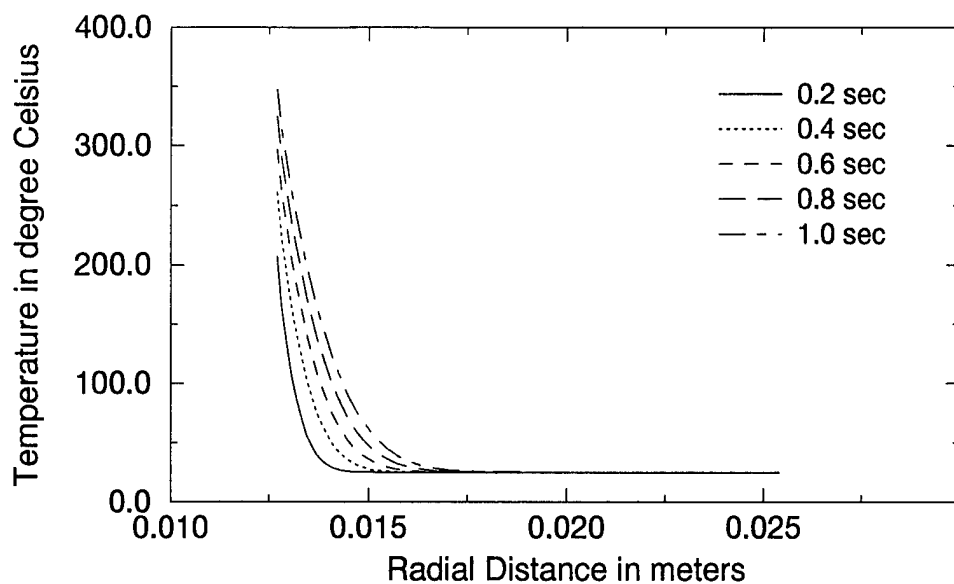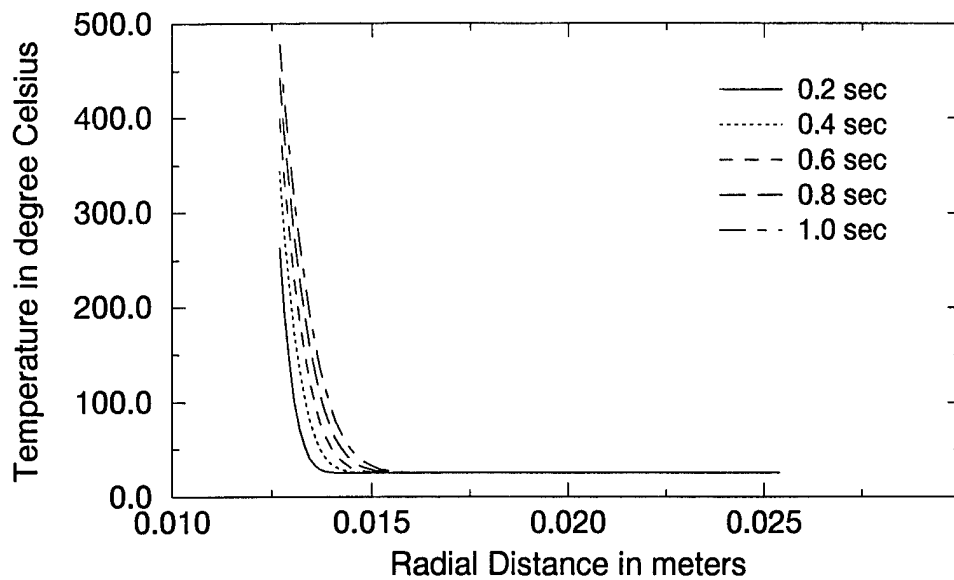
28

Figure 3. Distribution of temperature along the radius of a functionally gradient $ZrO_2/Ti - 6Al - V$ cylinder with metal volume fraction, $vf = \bar{r}^{0.30}$ $(0 \leq \bar{r} \leq 1)$, with temperature dependent material properties, for a time period of 1s.
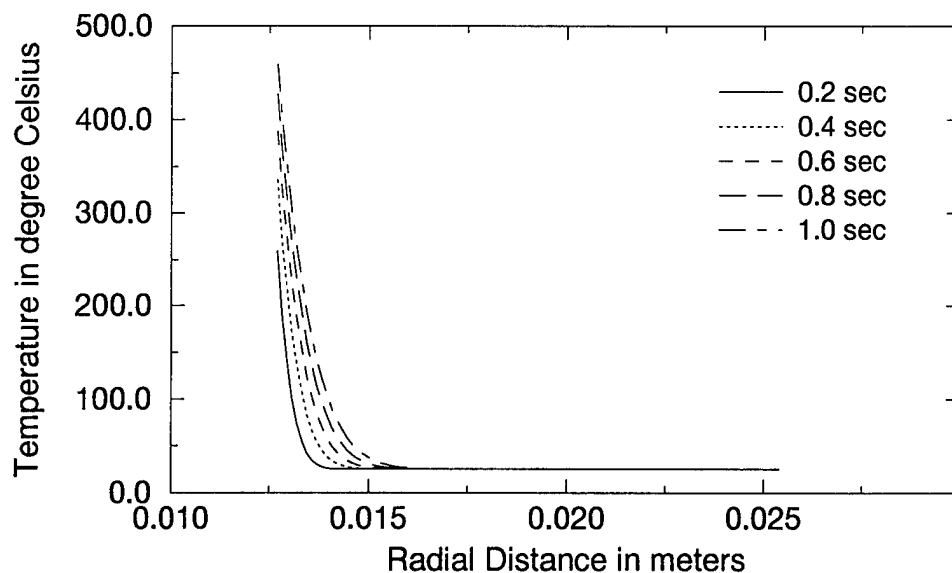
Figure 4. Distribution of temperature along the radius of a functionally gradient $ZrO_2/Ti - 6Al - V$ cylinder with linear metal volume fraction, $vf = \bar{r}^{1.00}$ $(0 \leq \bar{r} \leq 1)$, with temperature dependent material properties, for a time period of 1s.

Figure 5. Distribution of temperature along the radius of a functionally gradient $ZrO_2/Ti-6Al-V$ cylinder with cubic metal volume fraction, $vf = \bar{r}^{3.00}$ $(0 \leq \bar{r} \leq 1)$, with temperature dependent material properties, for a time period of 1s.
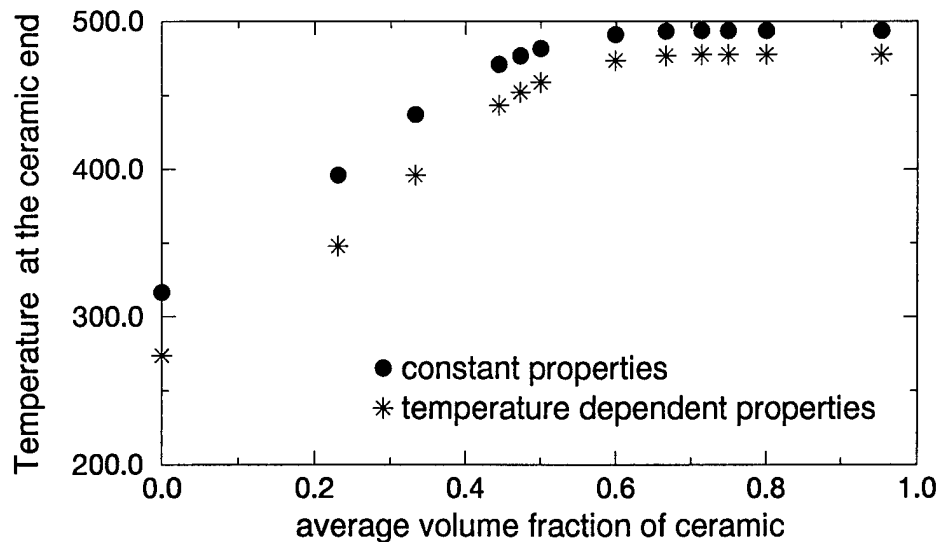

Figure 6. Comparison of the maximum temperature at the ceramic rich end, for a functionally gradient $ZrO_2/Ti-6Al-V$ cylinder, with varying average volume fraction of ceramic, with temperature dependent material properties and constant properties, for a time period of 1s.
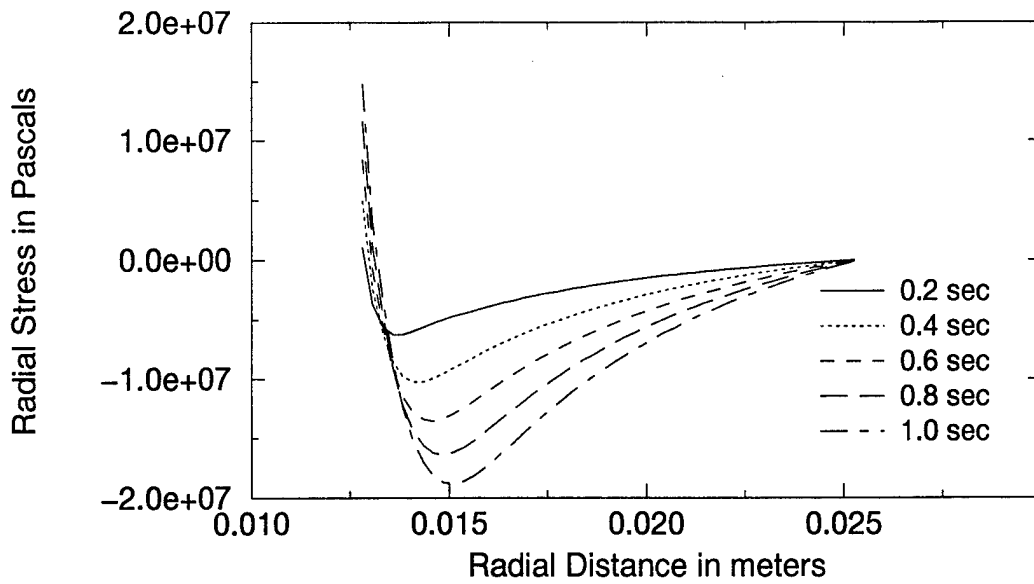
Figure 7. Distribution of radial stresses along the radius of a functionally gradient $ZrO_2/Ti-6Al-V$ cylinder with metal volume fraction, $vf = \bar{r}^{0.30}$ $(0 \le \bar{r} \le 1)$, with temperature dependent material properties, for a time period of 1s.
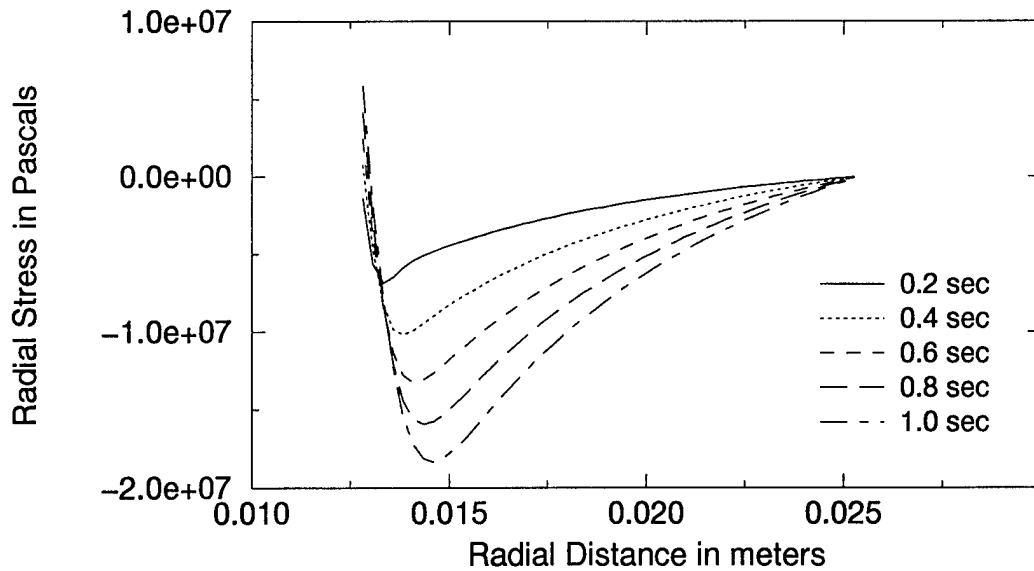

Figure 8. Distribution of radial stresses along the radius of a functionally gradient $ZrO_2/Ti-6Al-V$ cylinder with linear metal volume fraction, $vf = \bar{r}^{1.00}$ $(0 \le \bar{r} \le 1)$, with temperature dependent material properties, for a time period of 1s.
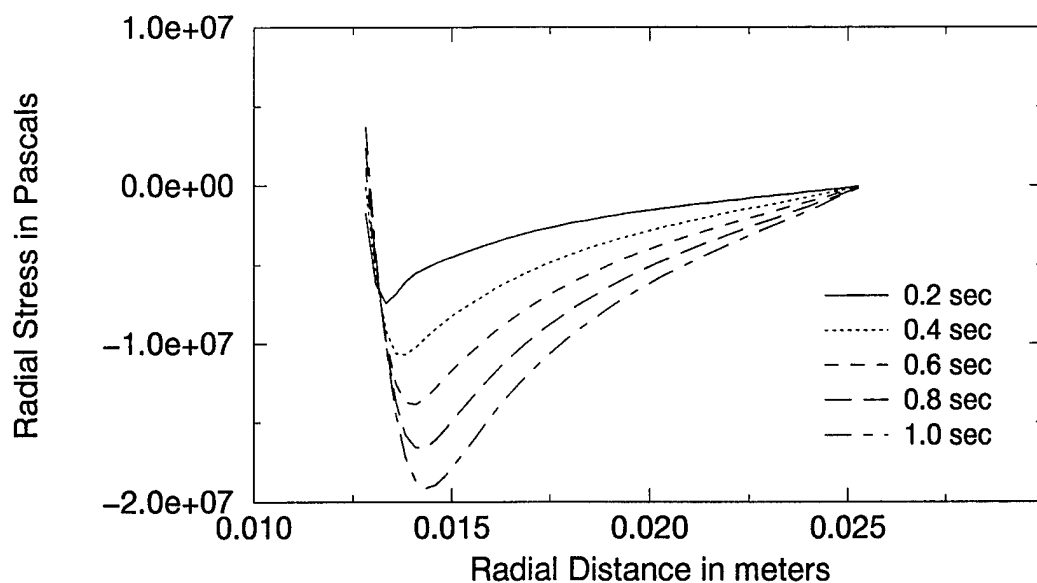
Figure 9. Distribution of radial stresses along the radius of a functionally gradient $ZrO_2/Ti-6Al-V$ cylinder with cubic metal volume fraction, $vf = \bar{r}^{3.00}$ $(0 \leq \bar{r} \leq 1)$, with temperature dependent material properties, for a time period of 1s.
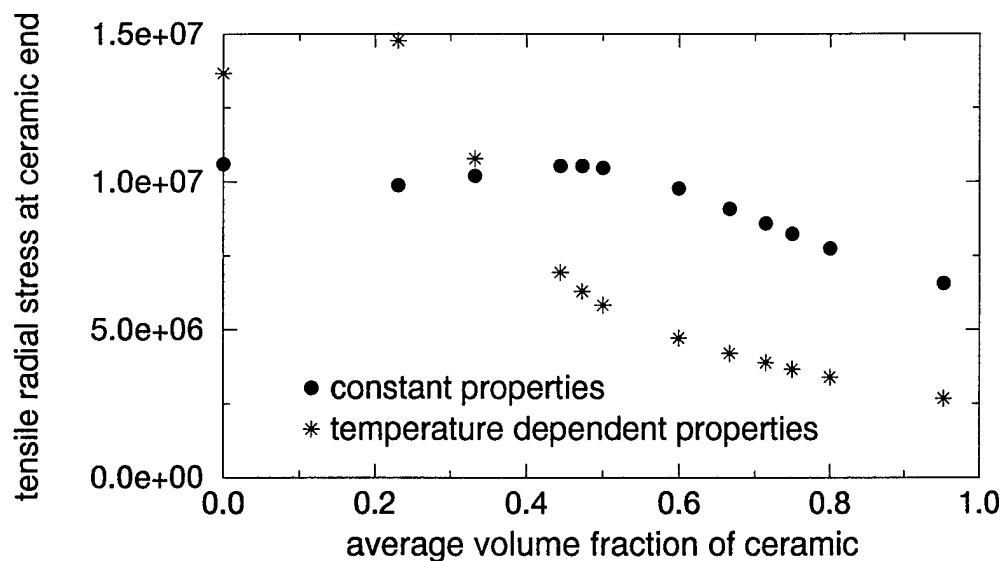

Figure 10. Comparison of the maximum radial tensile stress at the ceramic rich end, for a functionally gradient $ZrO_2/Ti - 6Al - V$ cylinder, with varying average volume fraction of ceramic, with temperature dependent material properties and constant properties, for a time period of 1s.

32

Figure 11. Comparison of the maximum radial compressive stress for a functionally gradient $ZrO_2/Ti - 6Al - V$ cylinder, with varying average volume fraction of ceramic, with temperature dependent material properties and constant properties, for a time period of 1s.
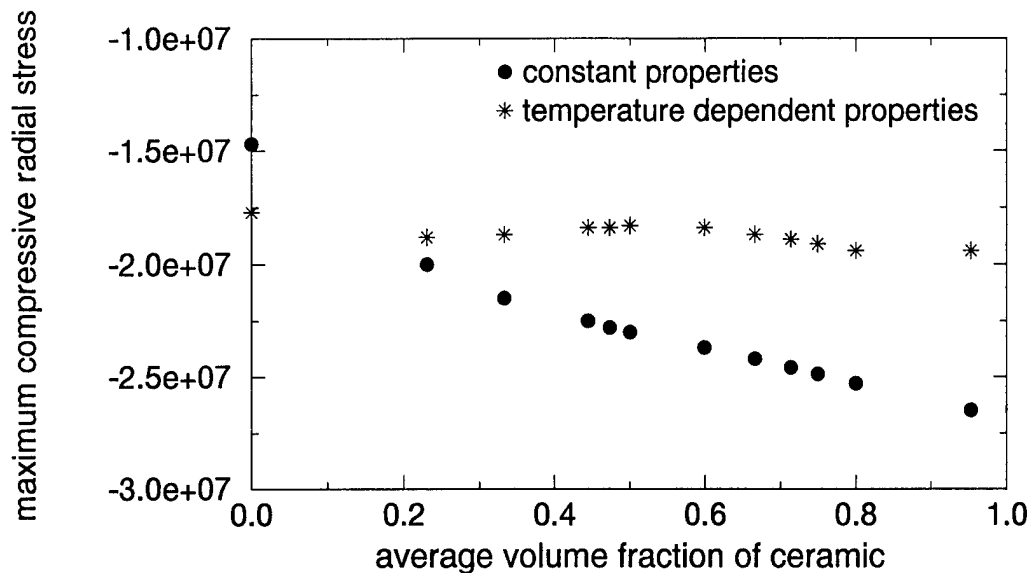

Figure 12. Distribution of hoop stresses along the radius of a functionally gradient $ZrO_2/Ti-6Al - V$ cylinder with metal volume fraction, $vf = \bar{r}^{0.30}$ $(0 \leq \bar{r} \leq 1)$, with temperature dependent material properties, for a time period of 1s.

Figure 13. Distribution of hoop stresses along the radius of a functionally gradient $ZrO_2/Ti - 6Al - V$ cylinder with linear metal volume fraction, $vf = \bar{r}^{1.00}$ $(0 \leq \bar{r} \leq 1)$, with temperature dependent material properties, for a time period of 1s.

Figure 14. Distribution of hoop stresses along the radius of a functionally gradient $ZrO_2/Ti-6Al-V$ cylinder with cubic metal volume fraction, $vf = \bar{r}^{3.00}$ $(0 \leq \bar{r} \leq 1)$, with temperature dependent material properties, for a time period of 1s.

34

Figure 15. Comparison of the maximum compressive hoop stress for a functionally gradient $ZrO_2/Ti - 6Al - V$ cylinder, with varying average volume fraction of ceramic, with temperature dependent material properties and constant properties, for a time period of 1s.
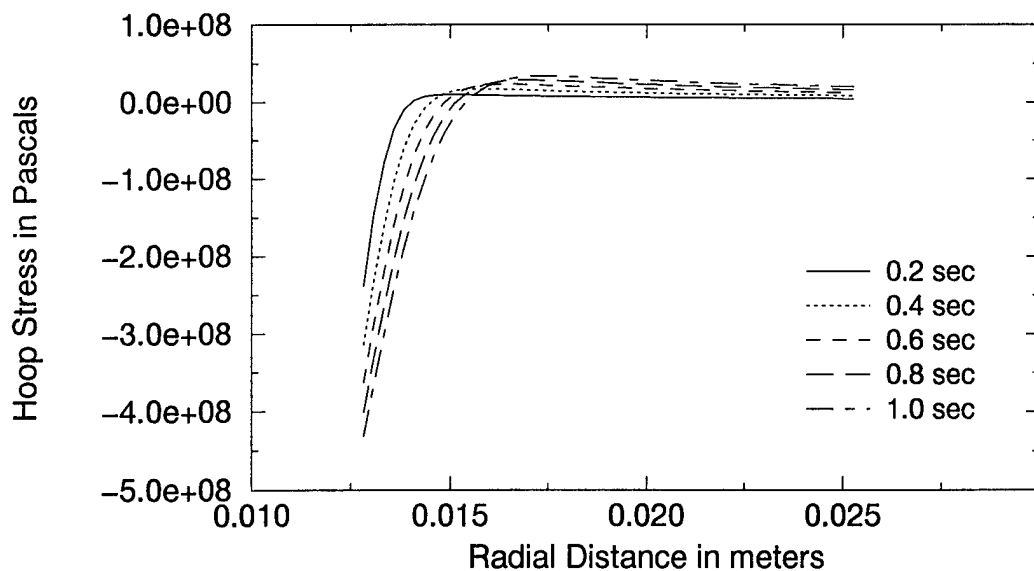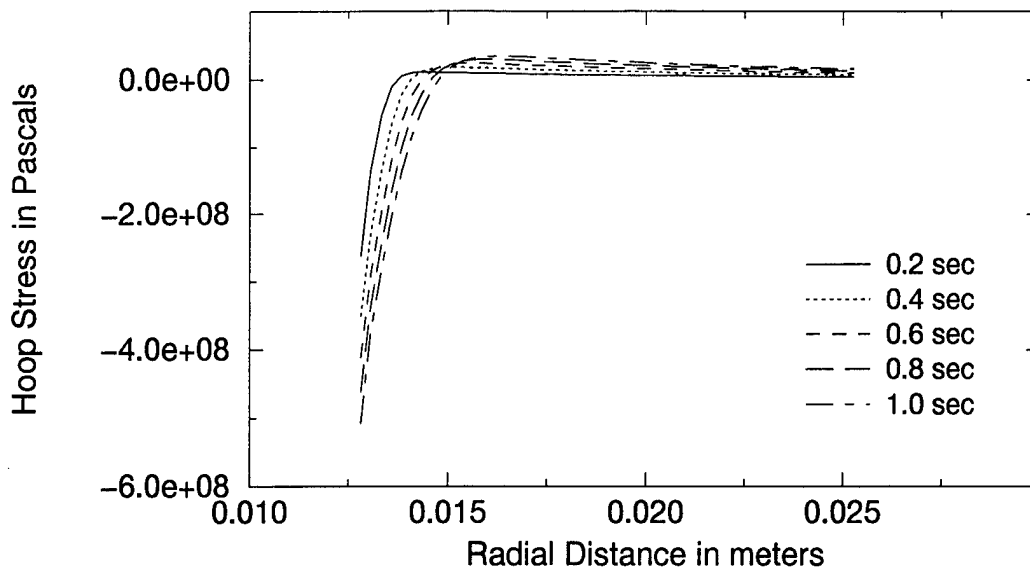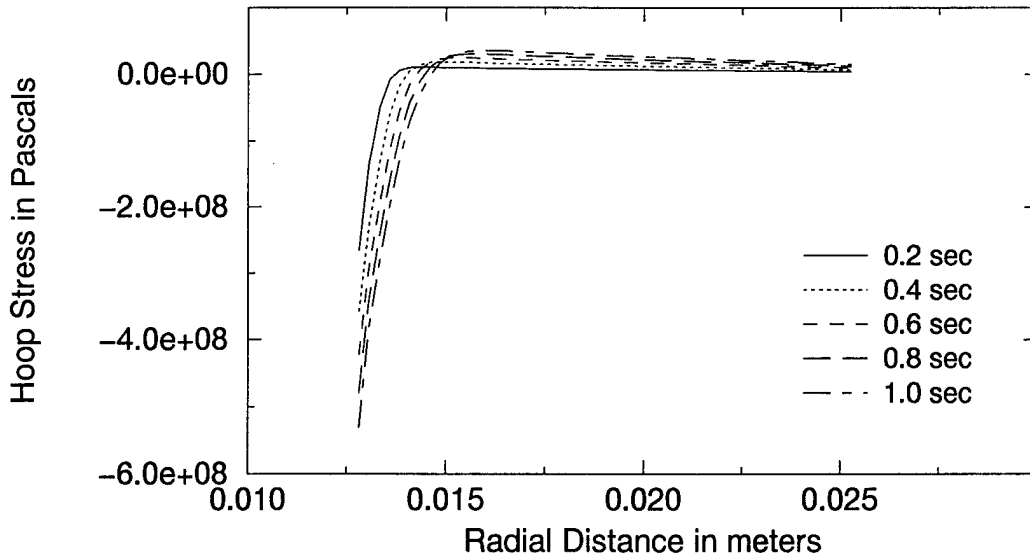

Figure 16. Distribution of temperature along the radius of a functionally gradient $ZrO_2/Ti - 6Al - V$ cylinder with linear metal volume fraction, $vf = \bar{r}^{1.00}$ $(0 \leq \bar{r} \leq 1)$, with constant material properties (at 298.15 K), over a time period of 15s.

35

Figure 17. Distribution of temperature along the radius of a functionally gradient $ZrO_2/Ti-6Al-V$ cylinder with linear metal volume fraction, $vf = \bar{r}^{1.00}$ $(0 \leq \bar{r} \leq 1)$, with temperature dependent material properties, over a time period of 15s.
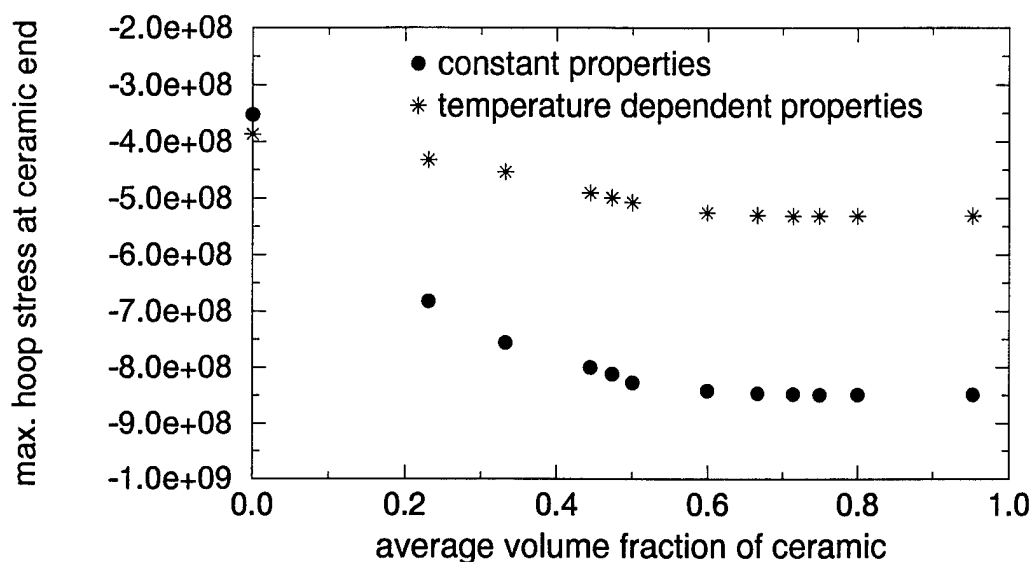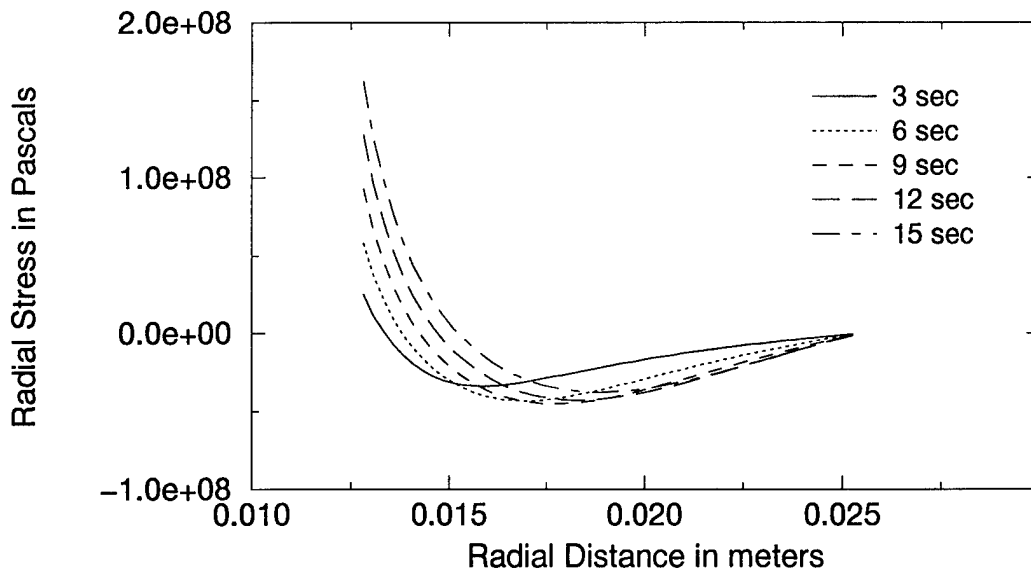

Figure 18. Distribution of radial stresses along the radius of a functionally gradient $ZrO_2/Ti - 6Al - V$ cylinder with linear metal volume fraction, $vf = \bar{r}^{1.00}$ $(0 \leq \bar{r} \leq 1)$, with temperature dependent material properties, over a time period of 15s.
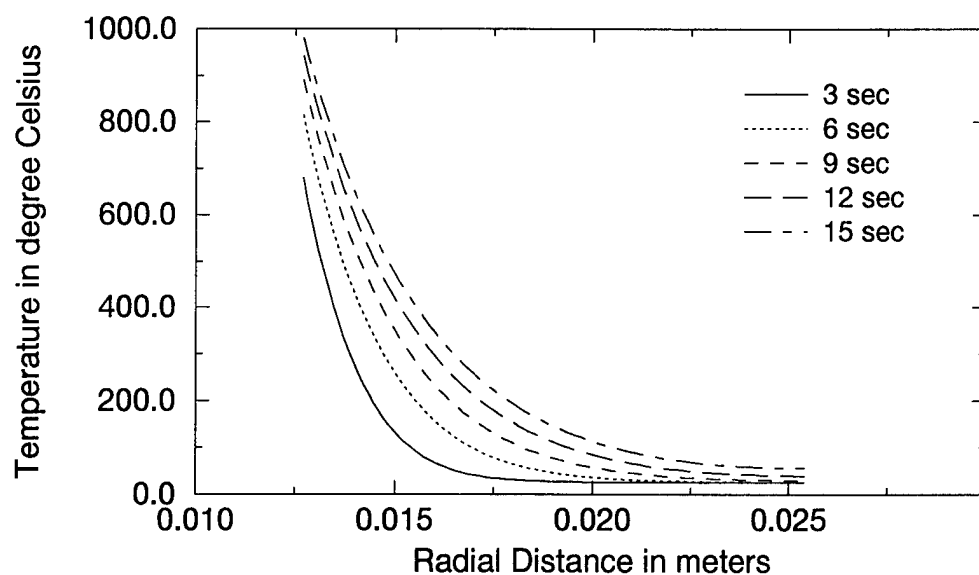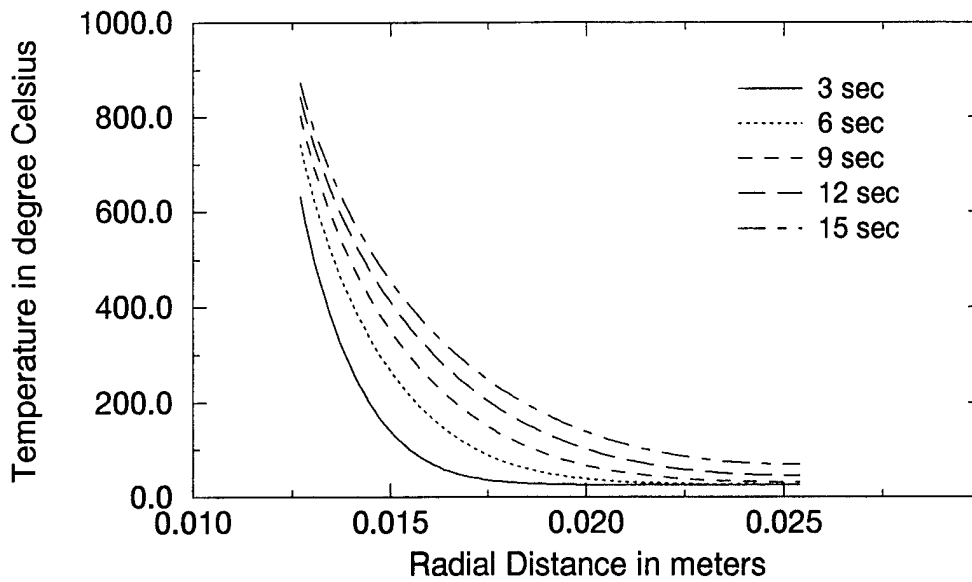
36
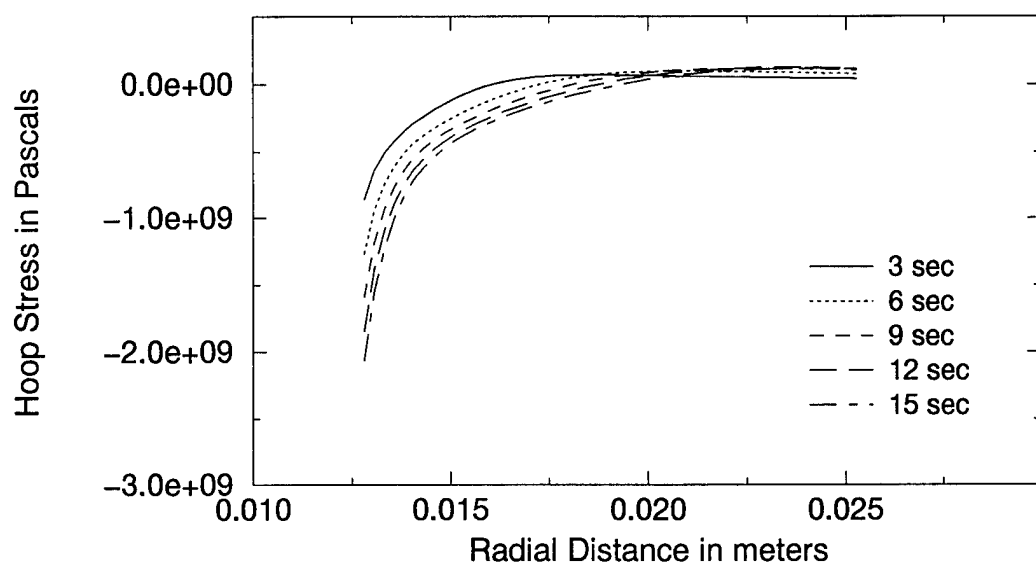
Figure 19. Distribution of hoop stresses along the radius of a functionally gradient $ZrO_2/Ti - 6Al - V$ cylinder with linear metal volume fraction, $vf = \bar{r}^{1.00}$ $(0 \leq \bar{r} \leq 1)$, with temperature dependent material properties, over a time period of 15s.

Table 1: Density of Ceramics and Metals

Material	density $\rho \ kg/m^3$
Zirconia	5700
Aluminum Oxide	3750
Silicon Carbide	3200
Silicon Nitride	2370
Ti-6Al-4V	4429
Stainless Steel	8166
Titanium	4500

Table 2: Thermal Conductivity in W/mK, $(k = c_o \left(c_{-1}T^{-1} + 1 + c_1T + c_2T^2 + c_3T^3\right))$

Material	c_o	c_{-1}	c_1	c_2	c_3
Zirconia	1.700	0	0.0001276	$0.66485 \ 10^{-5}$	0
Aluminum Oxide	-14.087	-1123.6	0.00044	0	0
Silicon Carbide	323.1355	0	0.0001	$0.025 \ 10^{-5}$	0
Silicon Nitride	13.72306	0	0.00103	$.546525 \ 10^{-6}$	$-0.07876 \ 10^{-9}$
Ti-6Al-4V	1.20947	0	0.0139375	0	0
Stainless Steel	15.378958	0	-0.001264	$0.20923 \ 10^{-5}$	$-0.0722 \ 10^{-8}$
Titanium	18.861972	64.977	-0.0003	$0.3134 \ 10^{-6}$	0

Table 3: Coefficient of Thermal Expansion, α /K, $(\alpha = c_o (c_{-1}T^{-1} + 1 + c_1 T + c_2 T^2 + c_3 T^3))$

Material	c_o	c_{-1}	c_1	c_2	c_3
Zirconia	$12.7657\ 10^{-6}$	0	-0.00149	$0.1\ 10^{-5}$	$-0.6775\ 10^{-11}$
Aluminum Oxide	$6.827\ 10^{-5}$	0	0.00018	0	0
Silicon Carbide	$5.0855\ 10^{-6}$	0	0.000116	0	0
Silicon Nitride	$5.8723\ 10^{-6}$	0	0.0009	0	0
Ti-6Al-4V	$7.57876\ 10^{-6}$	0	0.00065	$0.31467\ 10^{-6}$	0
Stainless Steel	$12.33\ 10^{-6}$	0	0.00080	0	0
Titanium[a]	$6.2204\ 10^{-6}$	0	0.00073	0	0
Titanium[b]	$7.3064\ 10^{-6}$	0	0.00044	0	0

[a]$300K \leq T \leq 1155K$

[b]$1155K \leq T$

Table 4: Possion Ratio, $(\nu = c_o (c_{-1}T^{-1} + 1 + c_1 T + c_2 T^2 + c_3 T^3))$

Material	c_o	c_{-1}	c_1	c_2	c_3
Zirconia	0.2882	0	$1.13345\ 10^{-4}$	0	0
Aluminum Oxide	0.26	0	0	0	0
Silicon Carbide	0.14	0	0	0	0
Silicon Nitride	0.24	0	0	0	0
Ti-6Al-4V	0.28838235	0	$1.12136\ 10^{-4}$	0	0
Stainless Steel	0.32622351	0	$-2.001822\ 10^{-4}$	$3.7973578\ 10^{-7}$	0
Titanium	0.36	0	0	0	0

Table 5: Specific Heat, J/kg K, $(C_v = c_o(c_{-1}T^{-1} + 1 + c_1 T + c_2 T^2 + c_3 T^3))$

Material	c_o	c_{-1}	c_1	c_2	c_3
Zirconia	487.34279	0	$3.04908\ 10^{-4}$	$-6.037232\ 10^{-8}$	0
Aluminum Oxide	1471.966	-138.8692	$-2.24063\ 10^{-5}$	0	0
Silicon Carbide	1493.5752	-155.1097	$-1.030263\ 10^{-4}$	$6.39324\ 10^{-8}$	0
Silicon Nitride	555.11365	0	$1.0155187\ 10^{-3}$	$2.919726\ 10^{-7}$	$-1.670176\ 10^{-10}$
Ti-6Al-4V	625.29692	0	$-4.2238757\ 10^{-4}$	$7.1786536\ 10^{-7}$	0
Stainless Steel	496.56409	0	$-1.15099\ 10^{-3}$	$1.63566\ 10^{-6}$	$-5.863285\ 10^{-10}$
Titanium [a]	460.83869	0	$4.53065\ 10^{-4}$	0	0
Titanium [b]	376.803	0	$5.55555\ 10^{-4}$	0	0

[a] $for\ 300K \leq T \leq 1155K$

[b] $for\ 1155K \leq T$

Table 6: Modulus of Elasticity, Pa, $(E = c_o(c_{-1}T^{-1} + 1 + c_1 T + c_2 T^2 + c_3 T^3))$

Material	c_o	c_{-1}	c_1	c_2	c_3
Zirconia	$244.26596\ 10^9$	0	$-1.3707\ 10^{-3}$	$1.21393\ 10^{-6}$	$-3.681378\ 10^{-10}$
Aluminum Oxide	$349.54865\ 10^9$	0	$-3.853206\ 10^{-4}$	$4.026993\ 10^{-7}$	$-1.67343\ 10^{-10}$
Silicon Carbide	$402.88748\ 10^9$	0	$-1.633110\ 10^{-4}$	$9.91273097\ 10^{-8}$	$-3.7755358\ 10^{-11}$
Silicon Nitride	$348.4323\ 10^9$	0	$-3.0697386\ 10^{-4}$	$2.160186\ 10^{-7}$	$-8.946165\ 10^{-11}$
Ti-6Al-4V	$122.55676\ 10^9$	0	$-4.58635\ 10^{-4}$	0	0
Stainless Steel	$201.03547\ 10^9$	0	$3.079296\ 10^{-4}$	$-6.533971\ 10^{-7}$	0
Titanium	$127.715\ 10^9$	0	$-4.933567\ 10^{-4}$	$8.069026\ 10^{-9}$	0

Table 7: Average volume fraction of metal and ceramic

exponent	$\bar{v}_{metal}$	$\bar{v}_{ceramic}$
0.0000	1.0000	0.0000
0.3000	0.7690	0.2307
0.5000	0.6666	0.3333
0.8000	0.5555	0.4445
0.9000	0.5263	0.4737
1.0000	0.5000	0.5000
1.5000	0.4000	0.6000
2.0000	0.3333	0.6666
2.5000	0.2857	0.7143
3.0000	0.2500	0.7500
4.0000	0.2000	0.8000
20.000	0.0476	0.9524

Table 8: Comparison of radial stresses for the cases of constant material properties (cmp) and temperature dependent properties (tdp)

$\bar{v}_{ceramic} \geq 0.5$	$\bar{v}_{ceramic} \leq 0.5$
$\left(\sigma_{max}^{t}\right)_{tdp} \leq \left(\sigma_{max}^{t}\right)_{cmp}$	$\left(\sigma_{max}^{t}\right)_{tdp} \geq \left(\sigma_{max}^{c}\right)_{cmp}$
$\left(\sigma_{max}^{c}\right)_{tdp} \leq \left(\sigma_{max}^{t}\right)_{cmp}$	$\left(\sigma_{max}^{c}\right)_{tdp} \leq \left(\sigma_{max}^{t}\right)_{cmp}$
-	$\left(\sigma_{max}^{t}\right)_{cmp}$ constant
-	$\left(\sigma_{max}^{c}\right)_{tdp}$ constant

3 Nonlinear Transient Thermomechanical Response of Functionally Graded Ceramic-Metal Plates

3.1 Introduction

Composites are materials with microstructures so tailored as to achieve desired response characteristics. In the case of laminated composite plates, tailoring is achieved commonly by varying the ply thickness, ply material and the stacking sequence. A new class of materials known as "functionally graded materials" (FGMs) has emerged, in which the material properties are continuously graded but continuous. By grading properties in a continuous manner, the disadvantages of interfaces in composites can be mitigated. These materials are microscopically heterogeneous and are typically made from isotropic components, such as metals and ceramics. FGMs are primarily used in situations where large temperature gradients are encountered. FGMs have also found applications in the semiconductor industry.

Thin walled members, i.e., plates and shells, used in reactor vessels, turbines and other machine parts are susceptible to failure from buckling, large amplitude deflections, or excessive stresses induced by thermal or combined thermomechanical loading. Investigations dealing with static and dynamic behavior of isotropic and anisotropic thermoelastic plates have been discussed in detail by Tauchert (1986,1987). In the present paper, attention is focussed on the thermomechanical response of thick plates, with a continuous variation of properties through the thickness. The temperature is assumed to vary only in the thickness direction. Thermal stresses in free plates under different one-dimensional temperature profiles have been investigated by Schneider (1955). Tang (1968) considered the response of free plates with temperature dependent properties. Bending in plates is generally accompanied by a stretching of the mid-surface when the material properties vary with temperature, but, bending-stretching coupling is shown to disappear in free plates when the temperature varies through the thickness only (Tauchert (1991)).

Das and Navaratna (1962) investigated the bending of rectangular plates, with two parallel edges simply supported, and exposed to a temperature distribution that is symmetric about the middle surface. De Leon and Paris (1987) developed boundary integral formulations based on the decomposition of the field equations into a pair of harmonic equations. Results were presented for a simply supported square plate under a temperature distribution which varied linearly through the thickness.

Thermoelastic analyses including transverse shear effects were performed by Das and Rath (1972) and Bapu Rao (1979). Das and Rath utilized Levy solutions to solve linear equations for thick rectangular plates with two parallel edges simply supported, and subjected to a temperature distribution which is antisymmetric about the mid plane.

Reddy and Hsu (1980) presented analytical closed-form solution for simply supported rectangular cross-ply laminated plates under sinusoidal mechanical loading. In this analysis, the temperature field was assumed to vary linearly through the thickness, consistent with the kinematics of the first order plate theory used. The governing equations solved in this paper were linear due to the assumption of small strains. Reddy and Chao (1981) studied the effects of reduced integration, mesh size, and element interpolation order on the accuracy of a finite element based on the first order shear deformation plate theory. They also developed exact

closed form solutions, in the linear case for the bending of cross-ply and antisymmetric angle-ply rectangular plates, that are simply-supported and subjected to sinusoidally distributed mechanical and thermal loads. Khdeir and Reddy (1991) presented exact analytical solutions for the Reddy third-order plate theory (1984,1987) for cross-ply rectangular plates. They used the state space approach in conjunction with the Lèvy method to solve the governing equations under various boundary conditions. Again, the temperature was assumed to vary linearly through the thickness.

All the aforementioned analyses refer to the small strain models. The von Kármán theory for large transverse deflection (of the order of the thickness of the plate) makes use of the non-linear strain displacement relations, in which the quadratic terms in the slopes of the deflection are retained while all other non-linear terms are neglected [see Reddy (1997)]. Several analyses for laminated composite plates and for homogeneous isotropic plates have been reported. For a more detailed review, the reader is referred to the classical review by Tauchert (1991). To the authors' knowledge, there exist no results for the dynamic thermomechanical analysis of functionally graded plates, in the literature. Functionally graded plates are multiphase material plates, constructed so that the interface effects are mitigated by providing a continuous variation in the material properties through the thickness. The property variations are so designed as to meet some functional requirement, typically, a lowering of the thermal stresses, the thermally induced deflections or vibration amplitudes.

Thermally induced vibration of a rectangular plate with one edge fixed and the other three edges simply supported was investigated by Jadeja and Loo (1974). Solutions for the case of surface heating were obtained using the Galerkin procedure. In the case of non-linear dynamic analysis, the von Kármán plate theory has been applied with the displacement field corresponding to the classical plate theory. Again, no results exist for the case of through-thickness material property varying plates using the von Kármán non-linearity in conjunction with the displacement field of the first order shear deformation plate theory. Most analyses corresponding to heterogeneous isotropic plates have been limited to plates with temperature sensitive material properties, and not spatially varying properties.

Finot and Suresh (1996) analyzed the response of multi-layered plates and fgm plates subjected to small and large deformation during temperature excursions. They examined general bilayer and trilayer plates with comparable layer thicknesses, with and without graded interfaces, all within the context of classical Kirchhoff theory for thin plates. They obtained closed-form solutions for stress-curvature relationships for the trilayer and graded isotropic elastic plates. They also analyzed plastic flow within these plates, as the temperature was varied.

Geometrically nonlinear transient analysis of isotropic and composite laminates have been reported in literature. To the authors' knowledge there are no previously reported results for the nonlinear, dynamic analysis of plates made of functionally graded materials, under thermal and mechanical loading. In this paper, we make use of the shear deformable element developed by Reddy (1984 a) for the von Kármán plate theory. Numerical results are presented to show the parametric effect of material properties, plate thickness, nonlinearity, boundary conditions, mechanical loading, and temperature fields on the transient analysis of fgm plates. These results are important from the point of view of the design of thermal barrier materials. Analyzing the transient response of graded materials will help in designing sensors and actuators to control vibrations. In the present paper, we examine the thermoelastostatic

and thermoelastodynamic response of plates subjected to pressure loading and thickness varying temperature fields. The thickness variation of the temperature field comes about due to the variation of the thermal properties.

3.2 Equations of motion and finite element model

The equations of motion used here are based on the combination of the first order plate theory and the von Kármán strains [see Reddy (1997)]. This theory predicts the global behavior accurately. The theory assumes that the transverse normal stress is negligible when compared to the other stress components, and normals to the plate midsurface before deformation remain straight but not necessarily normal to the midsurface after deformation.

The domain of the plate is such that the x and y coordinates are taken in the midplane of the plate and the displacements are assumed to be linear through the thickness - the z coordinate. Thus, the plate is modeled using an equivalent single layer theory. The displacement components are assumed to be of the following form [see Reddy (1994b,1997)]

$$
\begin{aligned}
u_1 &= u\left(x,y,t\right) + z\phi_x\left(x,y,t\right) \\
u_2 &= v\left(x,y,t\right) + z\phi_y\left(x,y,t\right) \\
u_3 &= w\left(x,y,t\right)
\end{aligned}
\tag{13}
$$

where t denotes time, u_1, u_2 and u_3 are the total displacements and (u,v,w) are the midplane displacements in the x, y and z directions respectively, and ϕ_x and ϕ_y are the rotations of the yz and xz planes due to bending. The von Kármán plate theory accounts for moderately large deflections and small strains. The strains according to this theory are (using standard vector notation)

$$
\begin{aligned}
\varepsilon_1 &= \frac{\partial u}{\partial x} + \frac{1}{2}\left(\frac{\partial w}{\partial x}\right)^2 + z\frac{\partial \phi_x}{\partial x} &\equiv \varepsilon_1^0 + z\varepsilon_1^1 \\
\varepsilon_2 &= \frac{\partial v}{\partial y} + \frac{1}{2}\left(\frac{\partial w}{\partial y}\right)^2 + z\frac{\partial \phi_y}{\partial y} &\equiv \varepsilon_2^0 + z\varepsilon_2^1 \\
\varepsilon_6 &= \frac{\partial u}{\partial y} + \frac{\partial v}{\partial x} + \frac{\partial w}{\partial x}\frac{\partial w}{\partial y} + z\left(\frac{\partial \phi_x}{\partial y} + \frac{\partial \phi_y}{\partial x}\right) &\equiv \varepsilon_6^0 + z\varepsilon_6^1 \\
\varepsilon_4 &= \phi_y + \frac{\partial w}{\partial y} \\
\varepsilon_5 &= \phi_x + \frac{\partial w}{\partial x}
\end{aligned}
\tag{14}
$$

wherein, the squares of the first partial derivatives of u, v, ϕ_x and ϕ_y are neglected. ε_i^0 are the in-plane strains and ε_i^1 are the curvatures due to bending. The strain ε_3 does not enter the constitutive equations, due to the plane stress assumption. The transverse shear strains ε_4 and ε_5 are constant through the thickness of the plate.

44

The governing equations of motion are derived from Hamilton's principle. In the absence of body moments, surface shearing forces, and thermal loading, the equations are given by

$$
\begin{aligned}
N_{xx,x} + N_{xy,y} &= I_0 u_{,tt} + I_1 \phi_{x,tt} \\
N_{xy,x} + N_{yy,y} &= I_0 v_{,tt} + I_1 \phi_{y,tt} \\
Q_{x,x} + Q_{y,y} &= I_0 w_{,tt} + q(x,y,t) + \bar{N}(w,N) \\
M_{xx,x} + M_{xy,y} - Q_1 &= I_2 \phi_{x,tt} + I_1 u_{,tt} \\
M_{xy,x} + M_{yy,y} - Q_2 &= I_2 \phi_{y,tt} + I_1 v_{,tt}
\end{aligned}
\tag{15}
$$

where I_0, I_1 and I_2 are the normal, coupled normal rotary, and rotary inertia coefficients, respectively, and a comma followed by a variable denotes differentiation with respect to that variable. Also, 'q' is the applied load on the plate top/bottom surface, and $N_{xx,yy,xy}$ and $M_{xx,yy,xy}$ are the force and moment resultants whose definitions are made precise later. $\bar{N}$ is a nonlinear force resultant that is dependent on the force resultants $N_{xx,yy,xy}$.

The fgm plate is considered to be a single layer plate of uniform thickness. The properties of the plate are assumed to vary through the thickness of the plate. The property variation is assumed to be in terms of a simple power law distribution given by

$$
P(z) = (P_c - P_m)\left(\frac{2z + h}{2h}\right)^n + P_m
\tag{16}
$$

where P_c and P_m are the corresponding properties of the ceramic and metal, and n is the volume fraction exponent which takes values greater than or equal to zero. The value of n equal to 0 represents a fully ceramic plate. The above power law assumption reflects a simple rule of mixtures used to obtain the effective properties of the ceramic-metal plate. The rule of mixtures applies only to the thickness direction. The density of the plate varies according to the power law, and the power law exponent may be varied to obtain different distributions of the component materials through the thickness of the plate. With the power-law variation in properties, the various inertias may be calculated as follows:

$$
(I_0, I_1, I_2) = \int_{-\frac{h}{2}}^{\frac{h}{2}} \left((\rho^c - \rho^m)\left(\frac{2z + h}{2h}\right)^n \left(1, z, z^2\right) + \rho^m \left(1, z, z^2\right) \right) dz
\tag{17}
$$

where quantities with superscripts, 'm' and 'c' correspond to the metal and ceramic respectively. The metal content in the plate increases as the value of n increases. The N, M s and Q s are the axial force, moment and shear force resultants, respectively. These are calculated from the following integral expressions:

$$
\begin{aligned}
(N_{\alpha\beta}, M_{\alpha\beta}) &= \int_{-\frac{h}{2}}^{\frac{h}{2}} (1, z)\,\sigma_{\alpha\beta}\ dz \\
(Q_x, Q_y) &= \int_{-\frac{h}{2}}^{\frac{h}{2}} (\sigma_{xz}, \sigma_{yz})\,dz
\end{aligned}
\tag{18}
$$

where α, β stand for x, y and $\bar{N}(w, N_{\alpha\beta})$ is the contribution due to the nonlinear terms,

45

$$\bar{N}\left(w, N_{\alpha\beta}\right) = \frac{\partial w}{\partial x}\left(\frac{\partial N_{xx}}{\partial x} + \frac{\partial N_{xy}}{\partial y}\right) + \frac{\partial w}{\partial y}\left(\frac{\partial N_{xy}}{\partial x} + \frac{\partial N_{yy}}{\partial y}\right) \tag{19}$$

If one plane of elastic symmetry parallel to the plane of the plate exists, the constitutive equations of the plate can be written in the form (purely mechanical loading)

$$\left\{\begin{array}{c} \{N\} \\ \{M\} \end{array}\right\} = \left[\begin{array}{cc} [A] & [B] \\ [B] & [D] \end{array}\right] \left\{\begin{array}{c} \{\varepsilon^o\} \\ \{\varepsilon^1\} \end{array}\right\} \tag{20}$$

In the case of thermal loading, the equations contain the thermal force resultants, $N_{\alpha\beta}^T$, and the thermal moment resultants, $M_{\alpha\beta}^T$, and are defined elsewhere in the paper. The form of the equations will be given here, with the details of the finite element implementation in the appendix.

$$\left\{\begin{array}{c} \{N + N^T\} \\ \{M + M^T\} \end{array}\right\} = \left[\begin{array}{cc} [A] & [B] \\ [B] & [D] \end{array}\right] \left\{\begin{array}{c} \{\varepsilon^o\} \\ \{\varepsilon_1\} \end{array}\right\} \tag{21}$$

$$\left\{\begin{array}{c} Q_y \\ Q_x \end{array}\right\} = \left[\begin{array}{cc} \bar{A}_{44} & \bar{A}_{45} \\ \bar{A}_{45} & \bar{A}_{55} \end{array}\right] \left\{\begin{array}{c} \varepsilon_4 \\ \varepsilon_5 \end{array}\right\} \tag{22}$$

where $[A]$, $[B]$, $[D]$ $(i, j = 1, 2, 6)$, and $\bar{A}_{ij}$ $(i, j = 4, 5)$ are the inplane, bending-stretching coupling, bending, and thickness-shear stiffnesses, respectively :

$$(A_{ij}, B_{ij}, D_{ij}) = \int_{-\frac{h}{2}}^{\frac{h}{2}} \left(\left(Q_{ij}^c - Q_{ij}^m\right)\left(\frac{2z+h}{2h}\right)^n \left(1, z, z^2\right) + Q_{ij}^m \left(1, z, z^2\right)\right) dz \tag{23}$$

$$\bar{A}_{ij} = \int_{-\frac{h}{2}}^{\frac{h}{2}} k_i k_j Q_{ij} dz \tag{24}$$

k_i are the shear correction coefficients and Q_{ij} are the material constants. For the plate in consideration, the bending-twisting coupling terms vanish and so the terms $A_{16}, A_{26}, B_{16}, B_{26}, D_{16}$, and D_{26} are identically zero. With the above stiffnesses vanishing, the non-linear force deflection relationships are

$$N_{xx} = A_{11}\left(\frac{\partial u}{\partial x} + \frac{1}{2}\left(\frac{\partial w}{\partial x}\right)^2\right) + A_{12}\left(\frac{\partial v}{\partial y} + \frac{1}{2}\left(\frac{\partial w}{\partial y}\right)^2\right) + B_{11}\frac{\partial \phi_x}{\partial x} + B_{12}\frac{\partial \phi_y}{\partial y} \tag{25}$$

$$N_{yy} = A_{12}\left(\frac{\partial u}{\partial x} + \frac{1}{2}\left(\frac{\partial w}{\partial x}\right)^2\right) + A_{22}\left(\frac{\partial v}{\partial y} + \frac{1}{2}\left(\frac{\partial w}{\partial y}\right)^2\right) + B_{12}\frac{\partial \phi_x}{\partial x} + B_{22}\frac{\partial \phi_y}{\partial y}$$

$$N_{xy} = A_{66}\left(\frac{\partial u}{\partial y} + \frac{\partial v}{\partial x} + \frac{\partial w}{\partial x}\frac{\partial w}{\partial y}\right) + B_{66}\left(\frac{\partial \phi_x}{\partial y} + \frac{\partial \phi_x}{\partial x}\right)$$

$$M_{xx} = B_{11}\left(\frac{\partial u}{\partial x} + \frac{1}{2}\left(\frac{\partial w}{\partial x}\right)^2\right) + B_{12}\left(\frac{\partial v}{\partial y} + \frac{1}{2}\left(\frac{\partial w}{\partial y}\right)^2\right) + D_{11}\frac{\partial \phi_x}{\partial x} + D_{12}\frac{\partial \phi_y}{\partial y}$$

$$M_{yy} = B_{12}\left(\frac{\partial u}{\partial x} + \frac{1}{2}\left(\frac{\partial w}{\partial x}\right)^2\right) + B_{22}\left(\frac{\partial v}{\partial y} + \frac{1}{2}\left(\frac{\partial w}{\partial y}\right)^2\right) + D_{12}\frac{\partial \phi_x}{\partial x} + D_{22}\frac{\partial \phi_y}{\partial y}$$

$$M_{xy} = B_{66}\left(\frac{\partial u}{\partial y} + \frac{\partial v}{\partial x} + \frac{\partial w}{\partial x}\frac{\partial w}{\partial y}\right) + D_{66}\left(\frac{\partial \phi_x}{\partial y} + \frac{\partial \phi_x}{\partial x}\right)$$

$$Q_x = A_{55}\left(\phi_x + \frac{\partial w}{\partial x}\right)$$

$$Q_y = A_{44}\left(\phi_y + \frac{\partial w}{\partial y}\right)$$

The finite element model of the above equations may be derived by substituting the element approximations of the generalized displacements $(u, v, w, \phi_x, \phi_y)$ into the appropriate weak forms of the five governing equations of motion. The element equations of motion are [see Reddy (1992, 1997)]

$$\sum_{\beta=1}^{5}\sum_{j=1}^{n(\beta)} K_{ij}^{\alpha\beta}\Delta_j^{\beta} + \sum_{\beta=1}^{5}\sum_{j=1}^{n(\beta)} M_{ij}^{\alpha\beta}\ddot{\Delta}_j^{\beta} = F_i^{\alpha} \tag{26}$$

The expressions for the individual finite element stiffness matrices are listed in the appendix.

3.2.1 Thermal analysis

The thermal analysis is conducted by imposing constant surface temperatures at the ceramic and metal rich surfaces. The variation of temperature is assumed to occur in the thickness direction only. The temperature is assumed to be constant in the plane of the plate. The thermal analysis is carried out by first solving a simple steady state heat transfer equation through the thickness of the plate. In this problem, all the quantities are non-dimensionalized, such that the non-dimensional temperature variable varied between 0 and 1 across the nondimensional domain of unit length. The problem is reduced to one with Dirichlet boundary conditions, with two independent parameters, namely the ratio of the thermal conductivity of the two materials, ρ_k, and the volume fraction index, n. The equation for the temperature through the thickness is as follows:

$$-\frac{d}{dz}\left(k\left(z\right)\frac{dT}{dz}\right) = 0 \tag{27}$$

where $T = T_c$ at $z = h/2$ and $T = T_m$ at $z = -h/2$.

In the present analysis, in addition to the uniform loading, the plate is subjected to a temperature field where the ceramic rich top surface is held at deg 300 C and the metal rich bottom surface is held at deg 20 C. A stress free temperature $T_0 = \deg 0$ C is assumed. The materials are assumed to be perfectly elastic throughout the deformation. The temperature field imposed on the fgm plate gives rise to additional terms due to the von Kármán nonlinearity. To see this, consider the statement of virtual work in the absence of external mechanical loading. The material is assumed to be isotropic and therefore, the matrix representation of the thermal conductivity tensor is diagonal. In view of this, and the plane

47

stress assumption, the temperature terms corresponding to ε_{11} and ε_{22} are the only remaining terms. To include the temperature terms, we define the thermal resultants, N_{xx}^T and M_{xx}^T (Note that the thermal resultants corresponding to the y direction are the same as those of x, because of isotropy and also, the resultant corresponding to the xy term is zero).

$$\int_{-\frac{h}{2}}^{\frac{h}{2}} \alpha C_{11} \left(1 + \nu\right) \left(T - T_0\right) \left(1, z\right) dz = \left(N^T, M^T\right) \tag{28}$$

With the above definitions, we have the following contribution to the thermal source terms of the standard finite element system of equations :

$$
\begin{aligned}
\int_V \sigma_{ij}^T \delta\varepsilon_{ij} dV &= \int_\Omega \left(N_{xx}^T \left[\frac{\partial \delta u}{\partial x} + \frac{\partial w}{\partial x}\frac{\partial \delta w}{\partial x} \right] + N_{yy}^T \left[\frac{\partial \delta v}{\partial y} + \frac{\partial w}{\partial y}\frac{\partial \delta w}{\partial y} \right] \right) \\
&\quad + \left(M_{xx}^T \left[\frac{\partial \delta \psi_x}{\partial x} \right] + M_{yy}^T \left[\frac{\partial \delta \psi_y}{\partial y} \right] \right) dA
\end{aligned}
\tag{29}
$$

$$\int_V \sigma_{ij}^T \delta\varepsilon_{ij} dV = \int_\Omega \left(N^T \left[\frac{\partial \delta u}{\partial x} + \frac{\partial \delta v}{\partial y} + \frac{\partial w}{\partial x}\frac{\partial \delta w}{\partial x} + \frac{\partial w}{\partial y}\frac{\partial \delta w}{\partial y} \right] + M^T \left[\frac{\partial \delta \psi_x}{\partial x} + \frac{\partial \delta \psi_y}{\partial y} \right] \right) dA \tag{30}$$

The temperature terms are included into the source terms of the element equations as follows:

$$
\begin{aligned}
\delta u \quad &: \quad \int_{\Omega_e} \left(N^T \right) \frac{\partial \psi_i}{\partial x} dx dy \\[2mm]
\delta v \quad &: \quad \int_{\Omega_e} \left(N^T \right) \frac{\partial \psi_i}{\partial y} dx dy \\[2mm]
\delta w \quad &: \quad \sum_{j=1}^n \int_{\Omega_e} \left(N^T \right) \left(\frac{\partial \psi_i}{\partial x}\frac{\partial \psi_j}{\partial x} + \frac{\partial \psi_i}{\partial y}\frac{\partial \psi_j}{\partial y} \right) w_j \ dx dy \\[2mm]
\delta \phi_x \quad &: \quad \int_{\Omega_e} \left(M^T \right) \frac{\partial \psi_i}{\partial x} dx dy \\[2mm]
\delta \phi_y \quad &: \quad \int_{\Omega_e} \left(M^T \right) \frac{\partial \psi_i}{\partial y} dx dy
\end{aligned}
\tag{31}
$$

The thermal source term corresponding to the deflection is non-linear. This non-linearity is significant at high temperatures and coupled with the various thermal properties of the materials, can lead to response of the graded plates that is not intermediate to that of the metal and ceramic. There are two ways in which one can include the thermal source terms. In the first method, the nodal values w_j, i.e., the deflection, can be treated as unknowns and the resulting force term is transferred to the left hand side of the standard finite element equations. Note that ψ_i and ψ_j that appear in the above equations are the finite element basis functions. Thus the term is included into the direct stiffness matrix. This does not require a recomputation of the tangent stiffness matrix. Alternatively, the nodal values w_j can be retained on the right hand side and evaluated using those corresponding to the previous iteration. Thus, the thermal force term corresponding to the deflection is nonlinear. This

48

in turn requires a recomputation of the tangent stiffness matrix corresponding to the third equilibrium equation. The two options discussed above were implemented in solving the thermoelastic problem for the fgm plate. At convergence, the difference between the results is found to be negligible, though, we may regard the first option as being more accurate and simpler to implement.

3.3 Numerical results

3.3.1 Static analysis

In the present study, the four noded rectangular isoparametric element was employed. The element has five degrees of freedom, three midplane displacements (u, v, w) and the two midplane rotations (ϕ_x, ϕ_y). Because the element accounts for the transverse shear strains, reduced integration is employed to evaluate the shear terms numerically. In the dynamic analysis, zero initial conditions are assumed and damping is neglected.

Figure 20 shows the geometry of the plate, the computational domain, and the boundary conditions used in the static problem. The static analysis was performed on a square plate of side, $('a')$ 0.2m and thickness $('h')$ 0.01m. A regular mesh of 8 by 8 linear elements was chosen after convergence studies. The boundary conditions corresponding to the quarter plate model are shown in figure 20. The value of the uniformly distributed loading chosen was equal to $0.01 \times 10^6 \text{N}/m^2$. The results were plotted after ten loadsteps. The analysis is performed for different values of the volume fraction exponent. The results are presented in terms of non-dimensionalized stress and deflection. The various non-dimensionalized parameters used are

$$center\ deflection\ (static)\ \ \bar{w}\ \ :\ \ \frac{w}{h}$$

$$load\ parameter\ \ P\ \ :\ \ \frac{q_0 a^4}{E_m h^4}$$

$$axial\ stress\ \ \bar{\sigma}_{xx}\ \ :\ \ \frac{\sigma_{xx} h^2}{|\ q_0\ |\ a^2}$$

$$thickness\ coordinate\ \ \bar{z}\ \ :\ \ \frac{z}{h}$$

where q is the applied mechanical load, a is the length of the plate, h is the plate thickness. The static analysis was conducted for two combinations of ceramic and metal. The first set of materials chosen were Aluminum and Zirconia. The second combination of materials consisted of Aluminum and Alumina. The Young's modulus, Poisson's ratio, density, conductivity and coefficient of thermal expansion, are for Aluminum : 70 GPa, 0.3, 2707 kg/m^3, 204 W/mK, 23.0×10^{-6}/deg C, for Alumina : 380 GPa, 0.3, 3800 kg/m^3, 10.4 W/mK, 7.4×10^{-6}/deg C, for Zirconia : 151 GPa, 0.3, 3000 kg/m^3, 2.09 W/mK, 10.0×10^{-6}/deg C, respectively. Note that the Poisson's ratio was chosen to be 0.3 for simplicity. The thermal conductivity ratio for the two different ceramic-metal pairs chosen is significantly different. The conductivity ratios are 19.6 and 97.6 respectively. Thus, the temperature variation across the thickness of the plates is vastly different for the two cases, even though the same

values of temperature were imposed on the top and bottom surfaces. The plate is assumed to be simply supported on all its edges, and the boundary conditions imposed on the edges are shown in figure 20. Note, that due to symmetry, only one quarter of the plate is used. There is no symmetry across the midplane, since the properties vary in a continuous manner through the thickness of the plate. In all cases, the lower surface of the plate is assumed to be metal rich and the top surface is assumed to be 100% ceramic. The ceramic surface is exposed to a temperature of deg 300 C and the lower metallic surface is exposed to a temperature of deg 20 C. A mechanical pressure loading q is also applied on the top surface of the plate.

Figure 21 shows the volume fraction of metallic phase, through the thickness. Note that the thickness coordinate has been non-dimensionalized. Figure 22 shows the variation of the temperature through the thickness of the Aluminum-Zirconia plates for various values of the volume fraction exponent, n. The temperature distribution was obtained by solving the one-dimensional heat conduction equation through the thickness, by assuming that the conductivity varies according to equation 4. The conduction equation was solved by imposing the temperature boundary conditions at the top and bottom surface of the plate. It is assumed that at any value of the thickness coordinate, the temperature is the same at all points in the plane. It is seen that the temperature in the plates with both ceramic and metal is always greater than that corresponding to a fully ceramic or fully metallic plate. Further, the temperature at any location through the thickness of the Alumina-Zirconia plates was found to be lesser than that in the Aluminum-Alumina plates.

Figure 23 shows the variation of the non-dimensional center deflection with load for the Aluminum-Zirconia plates. Analysis was also performed for Aluminum-Alumina plates. We will present only the significant results or differences in the response of plates with the different material combinations. This difference is expected to be mainly due to the large thermal expansion ratios. The applied pressure load is increased in each load step, and the solution is obtained by an iterative procedure. At any load step, the assumed solution at the beginning of the nonlinear iteration is taken to be the converged solution at the previous load step. This reduces the number of iterations required and also increases the accuracy, as compared to an arbitrary guess solution at each load step. In each case, the non-dimensionalization is carried out using the properties of the metal. In this case, the non-dimensional center deflection increases with pressure load. For the magnitude of the load chosen, the behavior was found to be linear. The effect of nonlinearity will be shown later. For both material pairs, the deflection of the metallic plate was found to be of the largest magnitude and that of the ceramic plate, of the smallest magnitude. All the plates with intermediate properties undergo corresponding intermediate values of center deflection. This is expected because the metallic plate is the one with the lowest stiffness and the ceramic plate is the one with the highest stiffness.

Figure 24 shows the variation of the center deflection with the mechanical load in the presence of the temperature field through the thickness of the Aluminum-Zirconia plate. Both the load and the center deflection are appropriately non-dimensionalized. It is important to observe that the through thickness temperature distribution for a fully ceramic plate coincides with that of a fully metal plate. This is because the plate for these two cases is fully homogeneous and the the solution to the equations for temperature do not depend on the thermal conductivity. In both these cases, the distribution is linear. Now, excursions

from this linear distribution are obtained by changing the volume fraction index. It is expected that the distribution will reach a minimum in terms of the average behavior, at some volume fraction index, and then turn back to the linear behavior. Thus, for a given pair of materials, there is a particular volume fraction that will minimize the deflection, under the same mechanical load. The non-dimensional deflection tends toward the negative side as the mechanical load increases. For the chosen temperature difference, the temperature effects on deflection reduce with increasing pressure loads. Note that the center deflection is reduced to zero for load parameter between -3 and -5 for the plates with different values of volume fraction exponent.

Note that the deflection of the plates under thermomechanical loading is positive. This is because, the thermal expansion at the top surface is higher due to the higher temperature, and this expansion results in an upward deflection of the plate. Note that the thermal strain in the ceramic rich portion may be comparable to that in the metal rich region (lower temperature) because of the ceramic has a lower coefficient of thermal expansion than the metal. The deflection therefore depends on the product of the temperature and the thermal expansion coefficient. Therefore, the response of the graded plates is not intermediate to the metal and ceramic plates. The purely mechanical load is applied downwards (negative). Also, note that the center deflection of both the metallic and the ceramic plates is higher in magnitude than the graded plates. The deflection of the fgm plate corresponding to $n = 0.5$ seems to be a minimum. Note that the temperature profiles for the various plates are close to each other, and this probably is the reason why the deflections under temperature field for the various graded plates are also close to each other.

Figures 25 and 26 show the comparison between the linear and non-linear analysis, under mechanical loading and under thermal loading. The linear analysis always overpredicts the deflection magnitude in the pressure loading case, and the difference increases as the plate becomes more and more metallic. The analysis was carried out at a load of $-10^5 N/m^2$, with 5 load steps. Any applied load greater in magnitude than this load, will result in an increased deviation from the linear behavior. The effect of nonlinearity does not seem to be very much pronounced when the temperature field is applied. At zero mechanical load, the metallic plate undergoes upward deflection with the largest magnitude and this reduces as the pressure load is applied.

Figures 27 and 28 represent the behavior of the non-dimensional center deflection with changing plate side to thickness ratio. The analysis was carried out with a load of $-1 \times 10^6 N/m^2$, with one loadstep. For all plates, the center deflection asymptotically reaches the same value for $\frac{a}{h} = 150$, when a purely mechanical loading is applied and this asymptotic behavior is reached for plates with $\frac{a}{h} = 75$, when the temperature field is also imposed.

Figures 29 and 30 contain the plots of the axial stress through the thickness of the plate under uniform loading applied on the top surface. Under the application of the pressure loading, the stresses are compressive at the top surface and tensile at the bottom surface. For the different volume fraction exponents chosen, the plate corresponding to $n = 2.0$ yielded the maximum compressive stress at the top surface. This is the ceramic rich surface. Note that ceramics are weaker in tension than in compression. The stress profiles under thermal loading are shown in figure 30. In this case, the nature of the profile changes drastically for the metallic plate, and the magnitude of the compressive stress increases for the fgm plates. Again, except for the ceramic plates, the stress profiles are close to each other, for the graded

plates. Note that the stresses in the latter case are again compressive, but with a higher magnitude, and this is because of the elastic strain which is the difference between the total strain and the thermal strain.

Figure 31 shows similar behavior to figure 29, except for the magnitudes. In both cases, the fgm plate corresponding to $n = 2.0$ experiences the maximum compressive stress at the top surface and the metallic and ceramic plates experience the maximum tensile stress at the bottom surface. For the case of Aluminum-Alumina (figure 32), the ratio of thermal conductivity is 19.6 and the temperatures are higher than in the case of Aluminum-Zirconia, and the compressive behavior in the whole domain is more pronounced as compared to Al-Z plates. The stress profiles are less clustered in Al-Z plates, even though the temperature profiles seem to be close to each other. The difference in stress patterns should be mainly due to the material properties. When no temperature field is applied, the plate with $n = 2.0$ experiences the maximum top surface compressive stress, but when the temperature field is also applied, the maximum is attained by the plate corresponding to $n = 0.2$. Figure 33 shows the non-dimensional axial stress in Aluminum-Alumina plate at higher value of the applied load ($-10 \times 10^4 N/m^2$, 20 th loadstep) under imposed temperature field. In the case where only the mechanical load was applied, the nondimensional stress was almost the same as the one corresponding to figure 31.

3.3.2 Dynamic Response : Simply supported boundary conditions

Next, numerical experiments were performed to characterize the dynamic response of the fgm plate to suddenly applied uniform pressure loading and also the case of suddenly applied load under an imposed temperature field. As mentioned earlier, the time derivatives in the semi-discrete model were approximated by using the Newmark direct integration method.

Since no estimate on the time step for the nonlinear analysis is available, the critical time step of a conditionally stable finite difference scheme was used as the starting time step, and a convergence study was conducted to select a time step that yielded a stable and accurate solution while keeping the computational time to a minimum. The estimate used in the present study is

$$\Delta t_1 \leq 0.25 \left(\rho h / D\right)^{\frac{1}{2}} \left(\Delta x\right)^2 \tag{32}$$

Here $D = \frac{Eh^3}{12(1-\nu^2)}$, and Δx is the minimum distance between the element node points. This estimate is due to Leech (1965), and was derived for thin plates. The values of E and ρ used in the above estimates correspond to the smallest time step that could be obtained.

First, in order to prove the validity of the present formulation and the code developed, the results were obtained for isotropic plates and compared with those existing in literature. For this, the problem solved in the papers by Akay (1980) (using a mixed finite element) and Reddy (1983) (using the present formulation) was solved. The geometry of the plate and the various dimensions, boundary conditions are the same as in figure 20. for the case of the simply supported plates. For validating the code, a side length of 2.438m, thickness 0.00635m and a load of $4.882 \times 10^6 N/m^2$ were taken. The time steps used in the computations are indicated in the figure. For the analysis of the FGM plates, a side length of 0.2m, thickness of 0.01m and a load of $-10^6 N/m^2$ were considered. For all the cases, a timestep of 0.00001s

was used. The first set of values were used to verify the analysis due to Akay and Reddy. The second set of values were used to obtain the results presented in this paper.

A 2 x 2 uniform mesh of quadratic elements is used in the quarter plate with five degrees of freedom per node. The same mesh was used in the analyses by Akay and Reddy. The figure shows the geometry of the plate, along with the boundary conditions and the material properties used in the analysis. The load was applied after the first time step and held constant thereafter. After convergence studies, with linear and quadratic elements, a mesh of 8 by 8 bilinear elements was chosen for the results presented herein.

Figure 34 shows the response of the isotropic plate under suddenly applied uniform pressure loading. The results were generated during the present study in order to validate the code developed. Results of the present nonlinear analysis agree closely with the finite element results of Akay and those of Reddy. The plots of center deflection vs time for various loads are shown. The center deflection and time were nondimensionalized according to the following expressions :

$$center \quad deflection \quad W \quad : \quad \frac{wE_m h}{q_0 a^2}$$
$$time \quad \bar{t} \quad : \quad t\sqrt{\frac{E_m}{a^2 \rho_m}}$$

Figures 35 and 36 show the transient response of the Aluminum-Alumina plates, and figures 37 and 38 show the dynamic response of the Aluminum-Zirconia plates. The higher the bending rigidity, the lower the magnitude of deflection. The amplitude of vibration is the maximum for the metallic plate and a minimum for the ceramic plate. It is seen that the amplitude of vibration increases smoothly as the amount of metal in the plate increases. Also, it is clear that the frequency of vibration of the ceramic plates is much higher than that of the metallic plates. When the sudden load is applied under a temperature field through the thickness the deflection changes, from negative to positive. Since the analysis is nonlinear, we cannot define a single natural frequency. The frequency of vibration of the surface heated plates appears to be a superposition of multiple frequencies. In order to obtain the response of the fgm plates under an imposed temperature field, the initial conditions are obtained from static analysis. The temperature field causes an upward deflection of the plates, and the load causes a downward deflection. Thus, vibrations occur about an equilibrium position which is displaced in the positive direction. One of the main inferences from the analysis is that the response of fgm plates is not intermediate to that of the metal and ceramic plates. This is due to the difference in bending stiffnesses and the thermal strains experienced by the various plates. Also, note that the coefficient of thermal expansion increases as the metallic content increases, but the temperature for the graded plates is higher than that of the ceramic or the metal plate.

3.3.3   Dynamic Response : Clamped boundary conditions

The computational domain for the dynamic analysis with clamped boundary conditions is the same as that of figure 20, except for some additional boundary conditions. The additional

boundary conditions are as follows : on the top boundary, $u = 0, \phi_y = 0$ and, on the right edge, $v = 0, \phi_x = 0$. The analysis was performed for the same two material combinations. Since the effective stiffness of the clamped plates is higher than the simply supported plates, it is clearly seen that the deflections are much lower corresponding to the simply supported case. Also, the frequency of vibration is higher as compared to the simply supported plates. A timestep of 0.00001s was used in the computations. Figures 39 and 40 show the temporal response of the plates under suddenly applied mechanical loading of $-1.0 \times 10^6 N/m^2$.

3.4 Closure

The static and dynamic thermoelastic response of functionally graded material plates is studied. Nonlinearity has been restricted to the von Kármán type. The stress and deflection response of the plates have been analyzed under mechanical loading and thermal loading. The gradation of properties through the thickness is assumed to be of the power law type and comparisons have been made with homogeneous isotropic plates. Non-dimensional stresses and deflection are computed for plates with two different ceramic-metal mixtures. It is seen that the basic response of the plates that correspond to properties intermediate to that of the metal and the ceramic, does not necessarily lie in between that of the ceramic and metal. The non-dimensional deflection was found to reach a minimum at a volume fraction index that depends on the properties and the ratio of the properties of the constituents. In the absence of thermal loading, the dynamic response of the graded plates is intermediate to that of the metal and ceramic plates. This is not the case when both thermal and mechanical loads are applied. This behavior is found to be true irrespective of boundary conditions. Thus, the gradients in material properties play an important role in determining the response of the fgm plates.

3.5 References

1. Akay, H. U.,(1980). "Dynamic Large deflection Analysis of Plates Using Mixed Finite Elements", *Computers and Structures*, Vol. 11, pp. 1-11.

2. Bapu Rao, M. N., (1979). "Thermal Bending of Thick Rectangular Plates", *Nuclear Engineering Design*, **54**, pp. 115-118.

3. Boley, B. A., and Weiner, J. H., (1960). *Theory of Thermal Stresses*, Wiley, New York.

4. Das, Y. C. and Navaratna, D. R., (1962) . "Thermal Bending of Rectangular Plate", *Journal of Aerospace Sciences*, **29**, pp. 1397-1399.

5. Das, Y. C., and Rath, B. K., (1972). "Thermal Bending of Moderately Thick Rectangular Plates ", *AIAA Journal*, **10**, pp. 1349-1351.

6. De Leon S and Paris, F. (1987). "Analysis of Thermal Stresses in Plates with Boundary Element Method", *Engineering Analysis*, **4**, pp. 199-203.

7. Finot. M. and Suresh, S., (1996). "Small and large deformation of thick and thin-film multilayers: effects of layer geometry, plasticity and compositional gradients", *Journal of Mechanics and Physics of Solids*, Vol. 44, (**5**), pp. 683-721.

8. Jadeja, N. D., and Loo, T. C., (1974). "Heat Induced Vibration of a Rectangular Plate", *Journal of Engineering Industry*, **96**, pp. 1015-1021.

9. Khdeir, A. A., and Reddy, J. N., (1991). "Thermal Stresses and Deflections of Cross-Ply Laminated Plates Using Refined Plate Theories", *Journal of Thermal Stresses*, V14, (**4**), pp. 419-438.

10. Khdeir, A. A., Ragab, M, D., and Reddy, J. N., (1992). "Thermal Effects on the Response of Cross-Ply Laminated Shallow Shells", *International Journal of Solids and Structures*, V29, (**5**), pp. 653-667 .

11. Reddy, J. N., (1984a). " Geometrically Nonlinear Transient Analysis of Laminated Composite Plates" *AIAA Journal*, Vol. 21, **4**, pp. 621-629.

12. Reddy, J. N., (1984b). *Energy and Variational Methods in Applied Mechanics*, Wiley Interscience, New York.

13. Reddy, J. N., (1992). *Introduction to the Finite Element Method- Second Edition*, McGraw-Hill, New York.

14. Reddy, J. N., (1997). *Mechanics of Laminated Composite Plates : Theory and Analysis*, CRC Press, Boca Raton, FL.

15. Reddy, J. N., and Hsu., Y. S., (1980). "Effects of Shear Deformation and Anisotropy on the Thermal Bending of Layered Composite Plates", *Journal of Thermal Stresses*, Vol. 3, pp. 475-493.

16. Reddy, J. N., and Chao., W. C., (1981). "A Comparison of Closed-Form and Finite Element Solutions of Thick, Laminated, Anisotropic Rectangular Plates", *Nuclear Engineering and Design*, Vol. 64, pp. 153-167.

17. Reddy, J. N., Bert., C. W., and Hsu., Y. S., (1981). " Thermoelasticity of Circular Cylindrical Shells Laminated of Bimodulus Composite Materials", *Journal of Thermal Stresses*, Vol. 4, pp. 155-177.

18. Schneider, P. J., (1955). "Variation of Maximum Thermal stress in Free Plates", *Journal of Aeronautical Sciences*, **22**, pp. 872-873.

19. Tang, S. , (1968). "Thermal Stresses in Temperature Dependent Isotropic Plates ", *J Spacecraft*, **5**, pp. 987-990.

20. Tauchert, T. R., (1986).," Thermal Stresses in Plates - Statical Problems", *Thermal Stresses - Vol I*, Ed. Hetnarski, R. B., pp. 23-137, North Holland, New York.

21. Tauchert, T. R., (1986). "Thermal Stresses in Plates - Dynamical Problems", *Thermal Stresses - Vol II*, Ed. Hetnarski, R. B., pp. 23-137, North Holland, New York.

22. Tauchert, T. R., (1991). "Thermally Induced Flexure, Buckling and Vibration of Plates", *Applied Mechanics Reviews*, Vol. 44, **8**, pp. 347-360.

23. Tsui, T. Y., and Ping Tong, (1971). "Stability of Transient Solution of Moderately Thick Plate by Finite Difference Method", *AIAA Journal*, Vol. 9, pp. 2062-2063.

Appendix : Finite element matrices

The individual matrices appearing in the finite element model are as follows:

$$K_{ij}^{1\alpha} = \int_{\Omega^e} \left(\frac{\partial \psi_i}{\partial x} N_{1j}^{\alpha} + \frac{\partial \psi_i}{\partial y} N_{6j}^{\alpha} \right) dxdy \tag{33}$$

$$K_{ij}^{2\alpha} = \int_{\Omega^e} \left(\frac{\partial \psi_i}{\partial x} N_{6j}^{\alpha} + \frac{\partial \psi_i}{\partial y} N_{2j}^{\alpha} \right) dxdy$$

$$K_{ij}^{3\alpha} = \int_{\Omega^e} \left[\frac{\partial \psi_i}{\partial x} Q_{1j}^{\alpha} + \frac{\partial \psi_i}{\partial y} Q_{2j}^{\alpha} + \frac{\partial \psi_i}{\partial x} \left(N_{1j}^{\alpha} \frac{\partial w}{\partial x} + N_{6j}^{\alpha} \frac{\partial w}{\partial y} \right) + \frac{\partial \psi_i}{\partial y} \left(N_{6j}^{\alpha} \frac{\partial w}{\partial x} + N_{2j}^{\alpha} \frac{\partial w}{\partial y} \right) \right] dxdy$$

$$K_{ij}^{4\alpha} = \int_{\Omega^e} \left(\frac{\partial \psi_i}{\partial x} M_{1j}^{\alpha} + \frac{\partial \psi_i}{\partial y} M_{6j}^{\alpha} \right) dxdy + \int_{\Omega^e} Q_{1j}^{\alpha} \psi_i dxdy$$

$$K_{ij}^{5\alpha} = \int_{\Omega^e} \left(\frac{\partial \psi_i}{\partial x} M_{6j}^{\beta} + \frac{\partial \psi_i}{\partial y} M_{2j}^{\beta} \right) dxdy + \int_{\Omega^e} Q_{2j}^{\alpha} \psi_i dxdy$$

where, we have

$$
\begin{array}{llll}
N_{1j}^1 = A_{11} \frac{\partial \psi_j}{\partial x} & N_{1j}^2 = A_{12} \frac{\partial \psi_j}{\partial y} & N_{1j}^3 = \frac{A_{11}}{2} \frac{\partial w}{\partial x} \frac{\partial \psi_j}{\partial x} + \frac{A_{12}}{2} \frac{\partial w}{\partial y} \frac{\partial \psi_j}{\partial y} & (34) \\[2mm]
N_{2j}^1 = A_{12} \frac{\partial \psi_j}{\partial x} & N_{2j}^2 = A_{22} \frac{\partial \psi_j}{\partial y} & N_{2j}^3 = \frac{A_{12}}{2} \frac{\partial w}{\partial x} \frac{\partial \psi_j}{\partial x} + \frac{A_{22}}{2} \frac{\partial w}{\partial y} \frac{\partial \psi_j}{\partial y} & \\[2mm]
N_{6j}^1 = A_{66} \frac{\partial \psi_j}{\partial y} & N_{6j}^2 = A_{66} \frac{\partial \psi_j}{\partial x} & N_{6j}^3 = \frac{A_{66}}{2} \frac{\partial w}{\partial x} \frac{\partial \psi_j}{\partial y} + \frac{A_{66}}{2} \frac{\partial w}{\partial y} \frac{\partial \psi_j}{\partial x} & \\[2mm]
M_{1j}^1 = B_{11} \frac{\partial \psi_j}{\partial x} & M_{1j}^2 = B_{12} \frac{\partial \psi_j}{\partial y} & M_{1j}^3 = \frac{B_{11}}{2} \frac{\partial w}{\partial x} \frac{\partial \psi_j}{\partial x} + \frac{B_{12}}{2} \frac{\partial w}{\partial y} \frac{\partial \psi_j}{\partial y} & \\[2mm]
M_{2j}^1 = B_{12} \frac{\partial \psi_j}{\partial x} & M_{2j}^2 = B_{22} \frac{\partial \psi_j}{\partial y} & M_{2j}^3 = \frac{B_{12}}{2} \frac{\partial w}{\partial x} \frac{\partial \psi_j}{\partial x} + \frac{B_{22}}{2} \frac{\partial w}{\partial y} \frac{\partial \psi_j}{\partial y} & \\[2mm]
M_{6j}^1 = B_{66} \frac{\partial \psi_j}{\partial y} & M_{6j}^2 = B_{66} \frac{\partial \psi_j}{\partial x} & M_{6j}^3 = \frac{B_{66}}{2} \frac{\partial w}{\partial x} \frac{\partial \psi_j}{\partial y} + \frac{B_{66}}{2} \frac{\partial w}{\partial y} \frac{\partial \psi_j}{\partial x} & \\[2mm]
Q_{1j}^1 = 0 & Q_{1j}^2 = 0 & Q_{1j}^3 = A_{55} \frac{\partial \psi_j}{\partial x} & \\[2mm]
Q_{2j}^1 = 0 & Q_{2j}^2 = 0 & Q_{2j}^3 = A_{44} \frac{\partial \psi_j}{\partial y} &
\end{array}
$$

$$N_{1j}^4 = B_{11}\frac{\partial \psi_j}{\partial x} \quad N_{1j}^5 = B_{12}\frac{\partial \psi_j}{\partial y} \qquad N_{2j}^4 = B_{12}\frac{\partial \psi_j}{\partial x} \quad N_{2j}^5 = B_{22}\frac{\partial \psi_j}{\partial y} \qquad (35)$$

$$N_{6j}^4 = B_{66}\frac{\partial \psi_j}{\partial y} \quad N_{6j}^5 = B_{66}\frac{\partial \psi_j}{\partial x} \qquad M_{1j}^4 = D_{11}\frac{\partial \psi_j}{\partial x} \quad M_{1j}^5 = D_{12}\frac{\partial \psi_j}{\partial y}$$

$$M_{2j}^4 = D_{12}\frac{\partial \psi_j}{\partial x} \quad M_{2j}^5 = D_{22}\frac{\partial \psi_j}{\partial y} \qquad M_{6j}^4 = D_{66}\frac{\partial \psi_j}{\partial y} \quad M_{6j}^5 = D_{66}\frac{\partial \psi_j}{\partial x}$$

$$Q_{1j}^4 = A_{55}\psi_j \quad Q_{1j}^5 = 0 \qquad Q_{2j}^5 = A_{44}\psi_j \quad Q_{2j}^4 = 0$$

In the expressions above, ψ_i and ψ_j are the finite element interpolation functions in the expansion

$$(u, v, w, \phi_x, \phi_y) = \sum_{j=1}^{n} \left(u_j(t), v_j(t), w_j(t), \phi_{x_j}(t), \phi_{y_j}(t) \right) \psi_j \qquad (36)$$

Note that for the sake of simplicity, the same interpolation function has been used for each of the generalized midplane displacements. The finite element equations are nonlinear. To complete the discretization, the time derivatives appearing in the semidiscrete form are approximated by the use of the Newmark direct integration method, with $\alpha = 0.5$ and $\beta = 0.25$ (corresponding to the constant average acceleration method). The scheme, although unconditionally stable for linear problems, is not proven stable for all nonlinear problems. The nonlinear element equations are then solved using the Newton-Raphson method. This involves the derivation of the tangent stiffness matrix. For the sake of brevity, the elements of the tangent stiffness matrix have been omitted.

The expressions for the plate stiffnesses are given below :

$$A_{ij} = \left(Q_{ij}^c - Q_{ij}^m \right) \left(\frac{h}{n+1} \right) + Q_{ij}^m h$$

$$B_{ij} = \left(Q_{ij}^c - Q_{ij}^m \right) \left(\frac{nh^2}{2(n+1)(n+2)} \right)$$

$$D_{ij} = \left(Q_{ij}^c - Q_{ij}^m \right) \left(\frac{(2+n+n^2)h^3}{4(n+1)(n+2)(n+3)} \right) + Q_{ij}^m \frac{h^3}{24}$$

The expression for the various inertias I_0, I_1, I_2, may be obtained by replacing the Q s in the above equations by the corresponding densities.
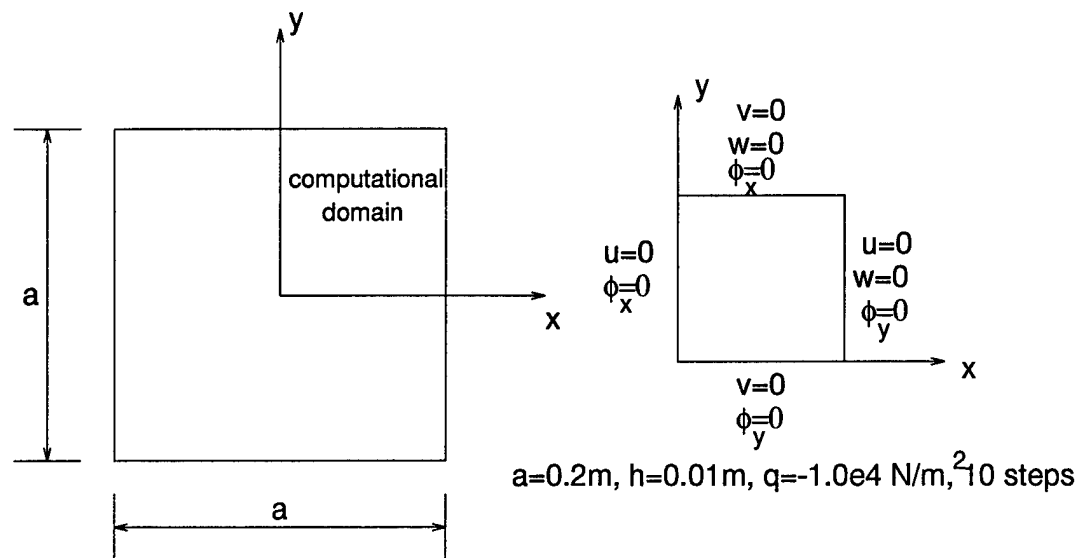
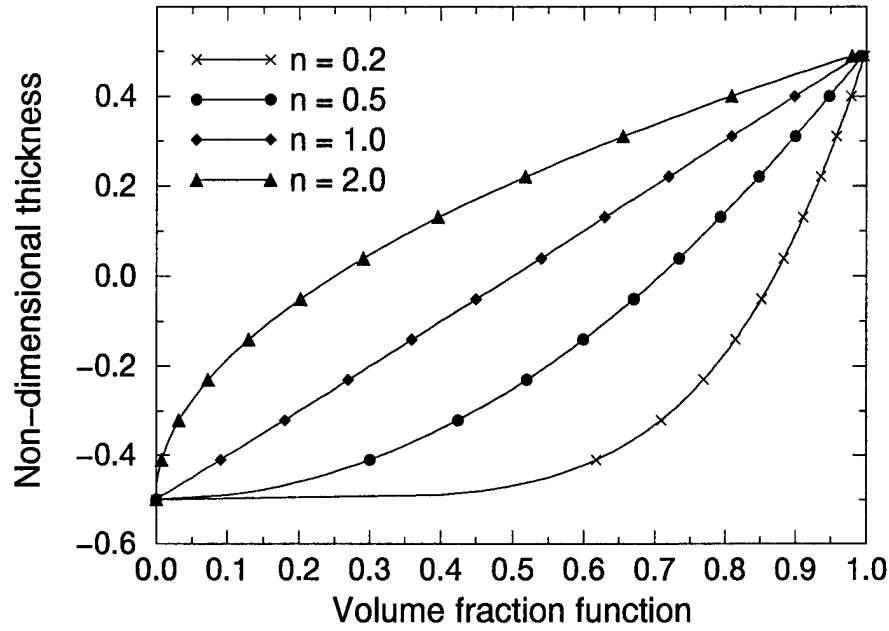Figure 20: A simply supported square plate with a quadrant as the computational domain

Figure 21: Variation of the volume fraction function $((2z + h)/2h)^n$ through the non-dimensionalized thickness.
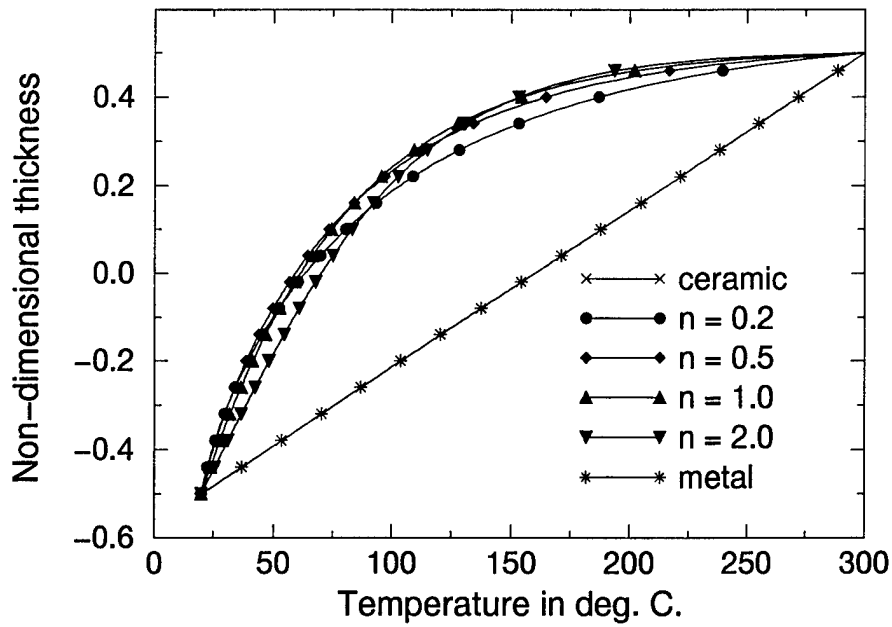

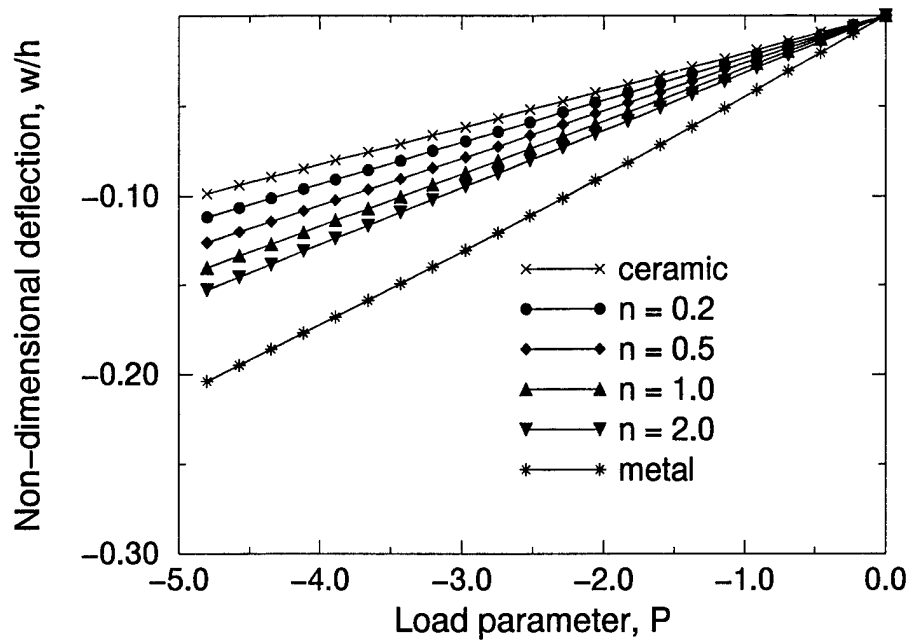Figure 22: Temperature field through the thickness of the fgm plate (Aluminum-Zirconia).

59

Figure 23: Nondimensionalized center deflection with load parameter for fgm plate, for various values of volume fraction exponent (Aluminum-Zirconia).
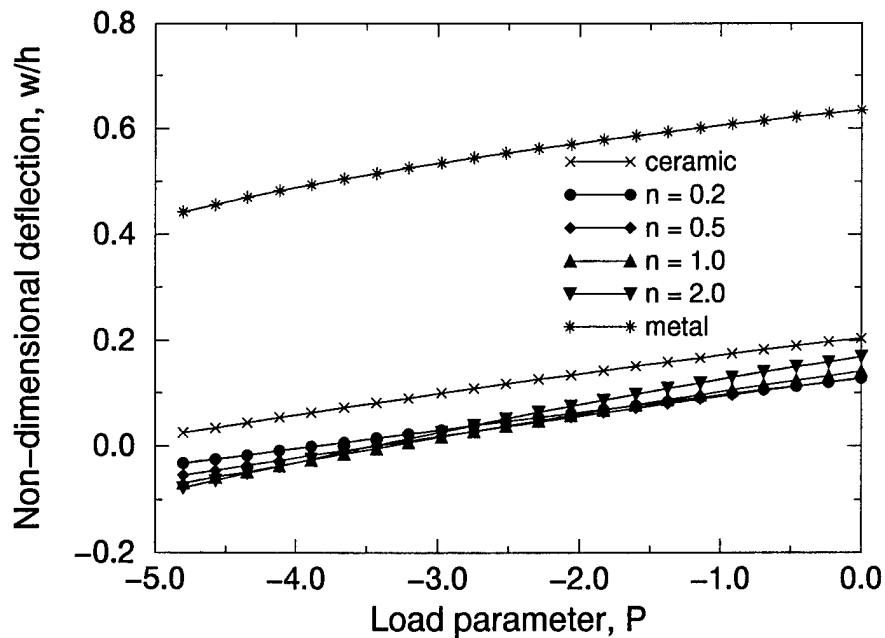

Figure 24: Center deflection of simply supported fgm plate under uniform load and temperature field (Aluminum-Zirconia).
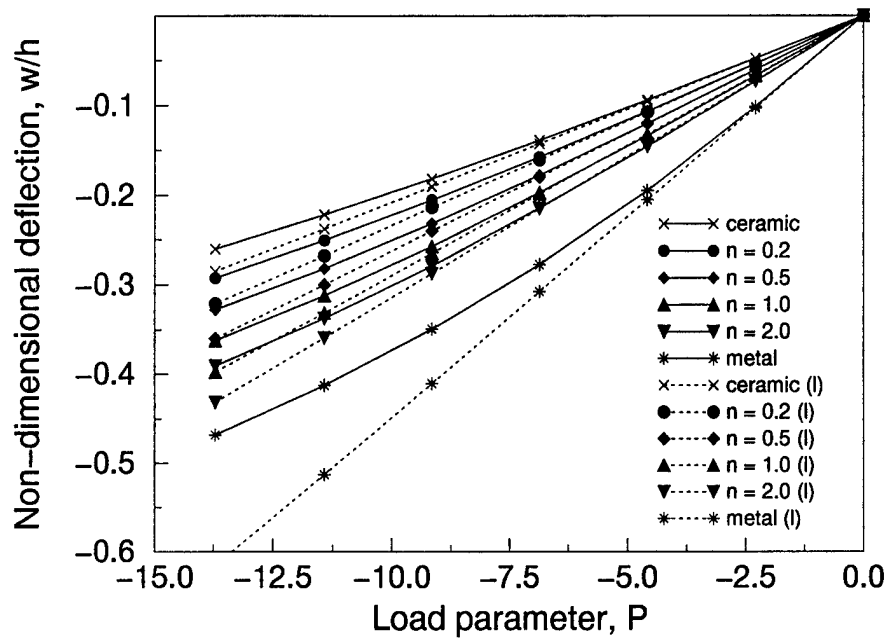
Figure 25: Non-dimensional center deflection with load parameter for fgm plate under uniform loading - linear/nonlinear analysis (Aluminum-Zirconia).
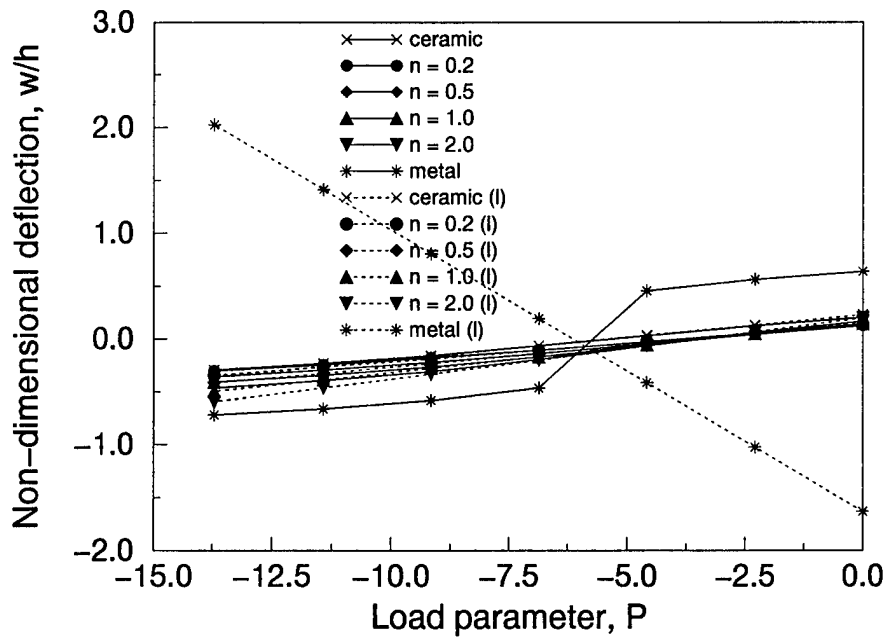
Figure 26: Non-dimensional center deflection with load parameter for fgm plate under uniform loading and temperature field - linear/nonlinear analysis (Aluminum-Zirconia).

61
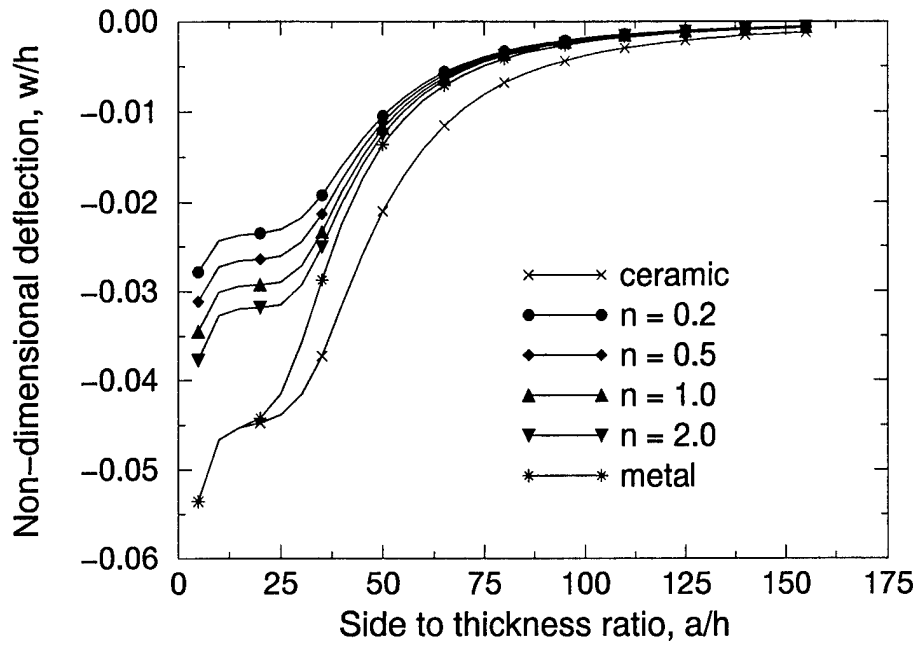
Figure 27: Non-dimensional center deflection with side to thickness ratio for fgm plate under uniform loading (Aluminum-Zirconia).
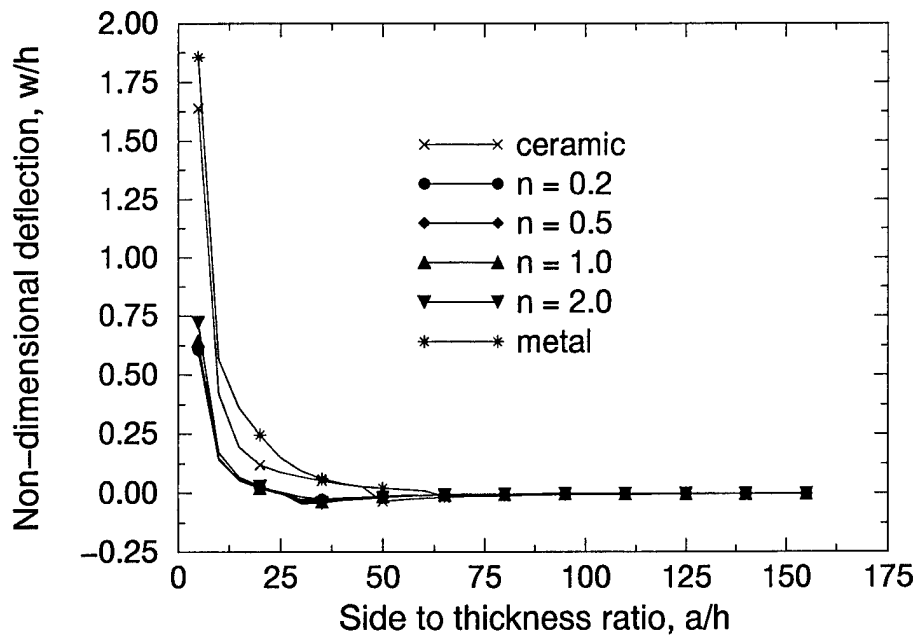
Figure 28: Non-dimensional center deflection with side to thickness ratio for fgm plate under uniform loading and temperature field (Aluminum-Zirconia).
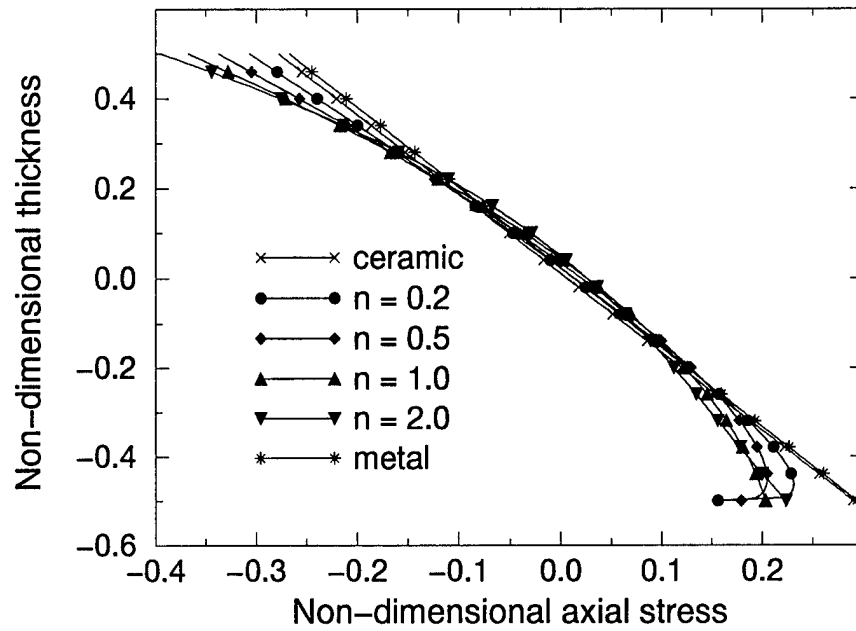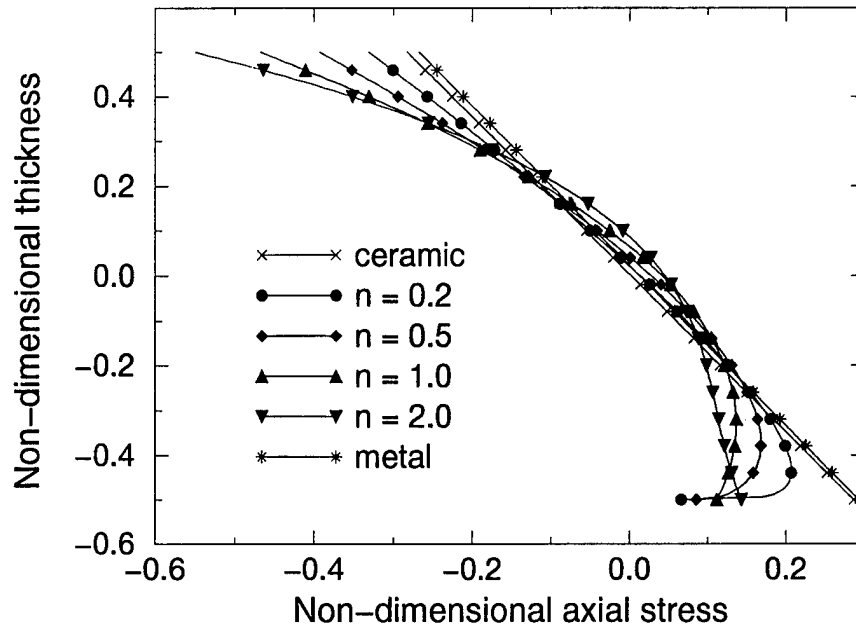
Figure 29: Non-dimensional axial stresses in a simply supported square fgm plate under uniform loading of -1x10^{4}N/m^2, 10 loadsteps (Aluminum-Zirconia).
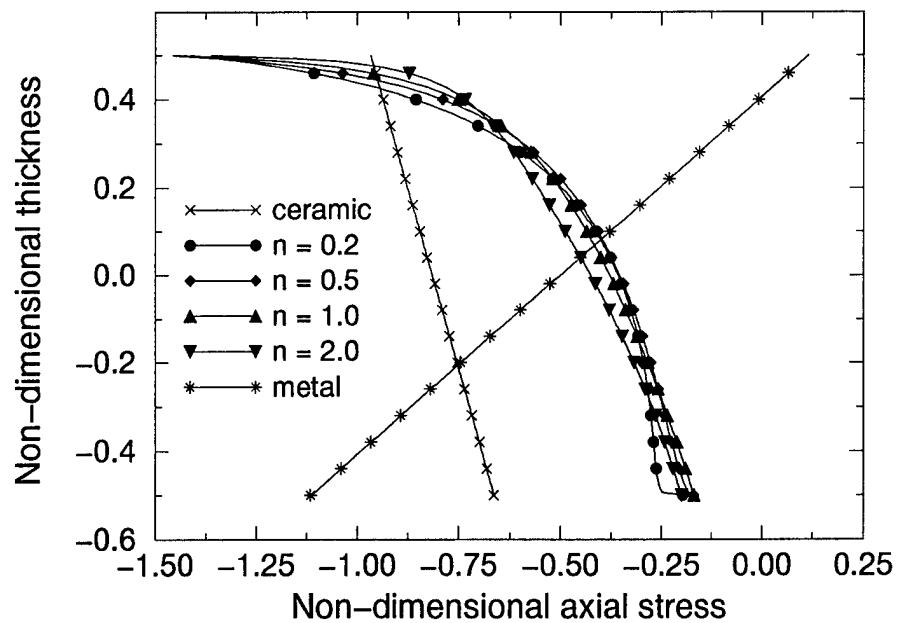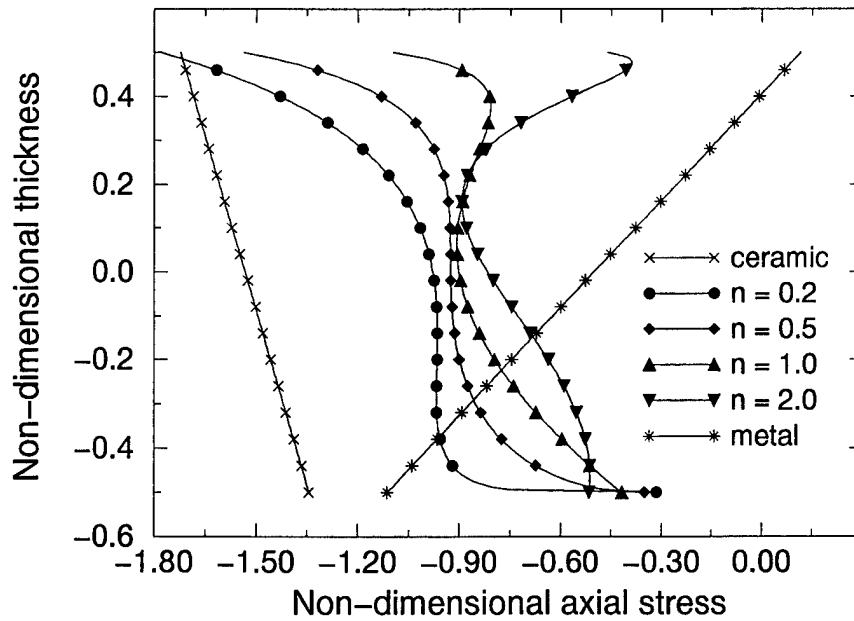

Figure 30: Non-dimensional axial stresses in a simply supported square fgm plate under uniform loading of -1x10^{4}N/m^2, 10 loadsteps and temperature field. (Aluminum-Zirconia).

Figure 31: Non-dimensional axial stresses in a simply supported square fgm plate under uniform loading of $-1\text{x}10^4 N/m^2$, 10 loadsteps (Aluminum-Alumina).

Figure 32: Non-dimensional axial stresses in a simply supported square fgm plate under uniform loading of $-1\text{x}10^4 N/m^2$, 10 loadsteps and temperature field (Aluminum-Alumina).
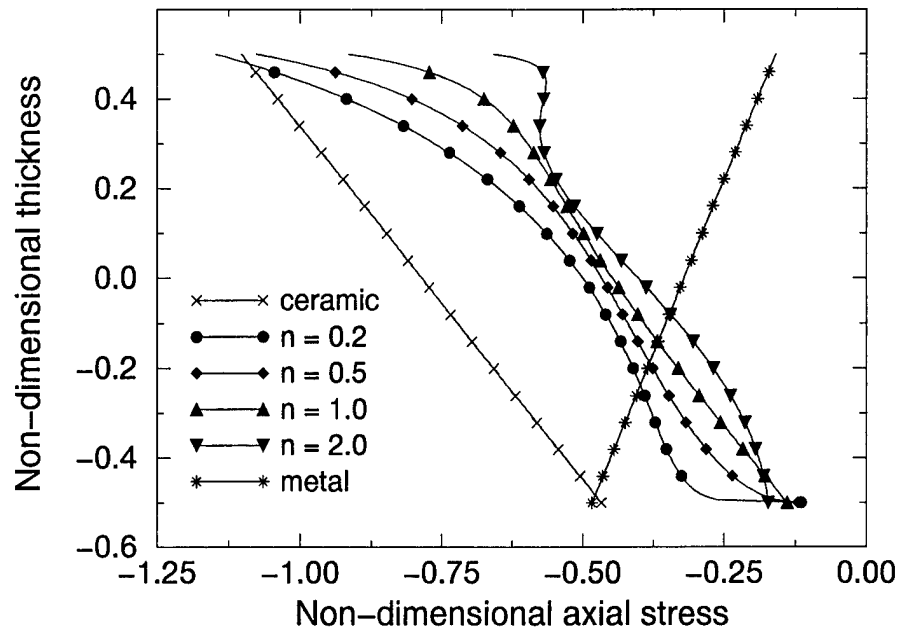
Figure 33: Non-dimensional axial stresses in a simply supported square fgm plate under uniform loading of $-10 \times 10^4 N/m^2$, 20 loadsteps and temperature field (Aluminum-Alumina).
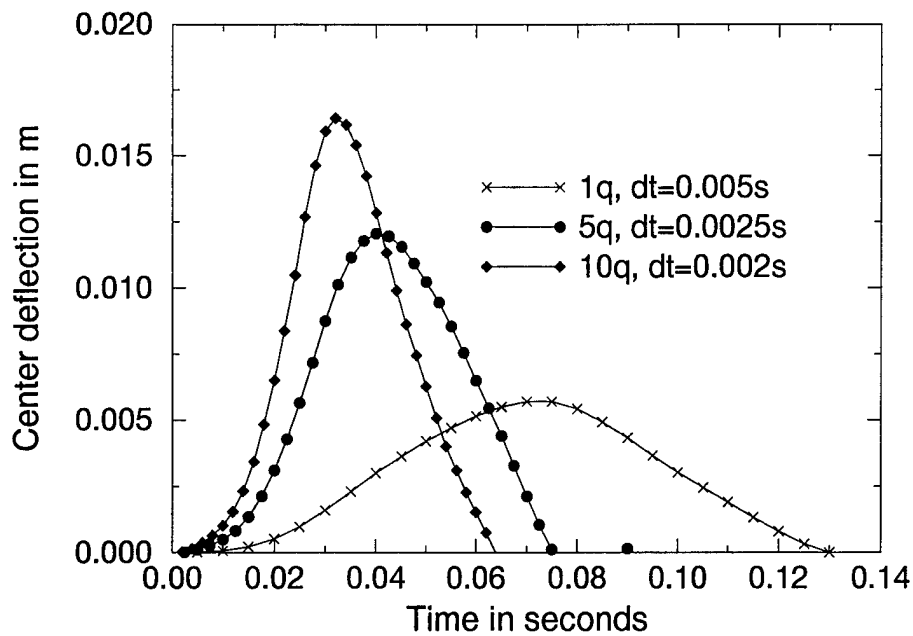

Figure 34: Vibrations of simply supported isotropic plate under suddenly applied uniform loading - Results of analysis by Akay and Reddy.
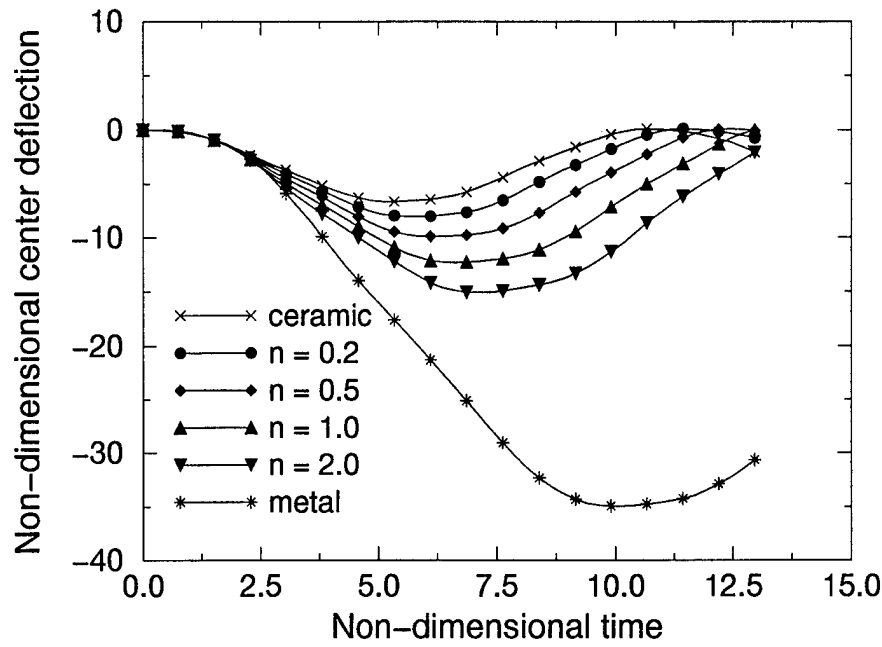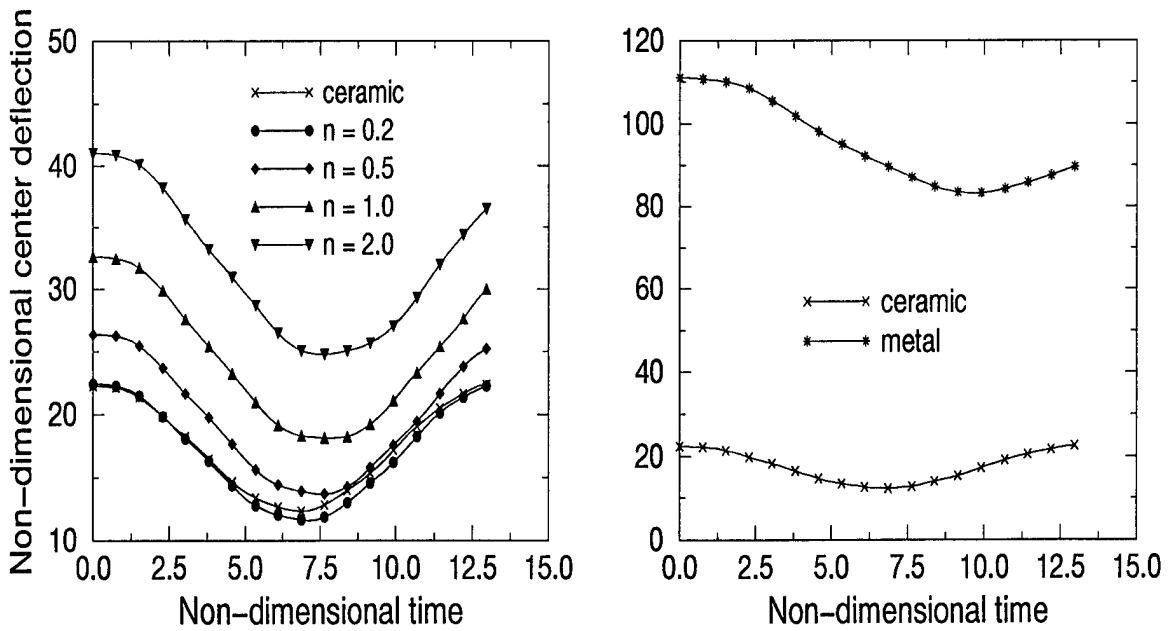
Figure 35: Temporal evolution of center deflection of simply supported fgm plate under suddenly applied uniform loading of $-1.0 \times 10^6 N/m^2$(Aluminum-Alumina).

Figure 36: Temporal evolution of center deflection of simply supported fgm plate under suddenly applied uniform loading of $-1.0 \times 10^6 N/m^2$ and temperature field (Aluminum-Alumina).
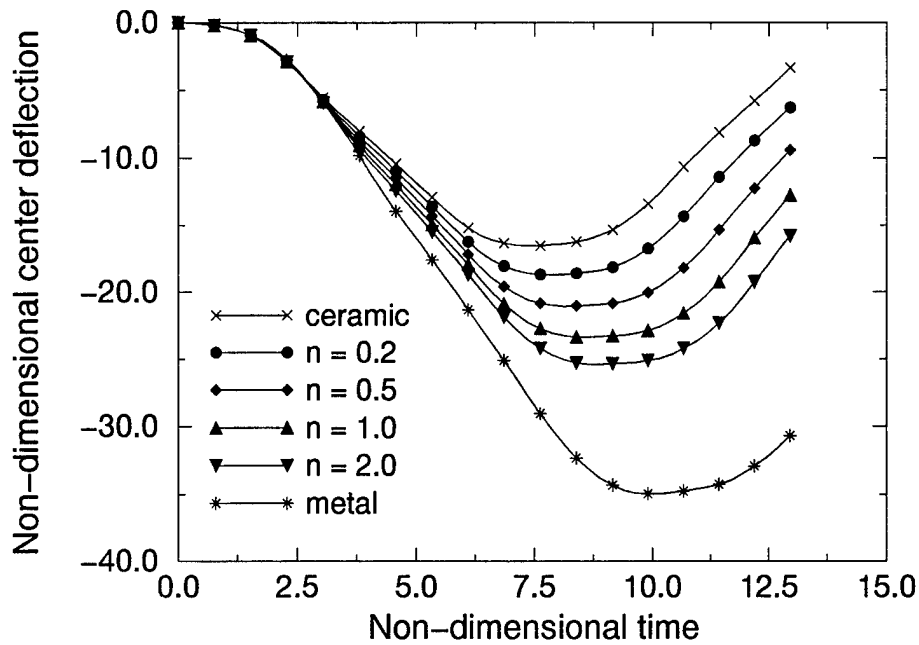
66

Figure 37: Temporal evolution of center deflection of simply supported fgm plate under suddenly applied uniform loading of $-1.0\mathrm{x}10^6 N/m^2$ (Aluminum-Zirconia).
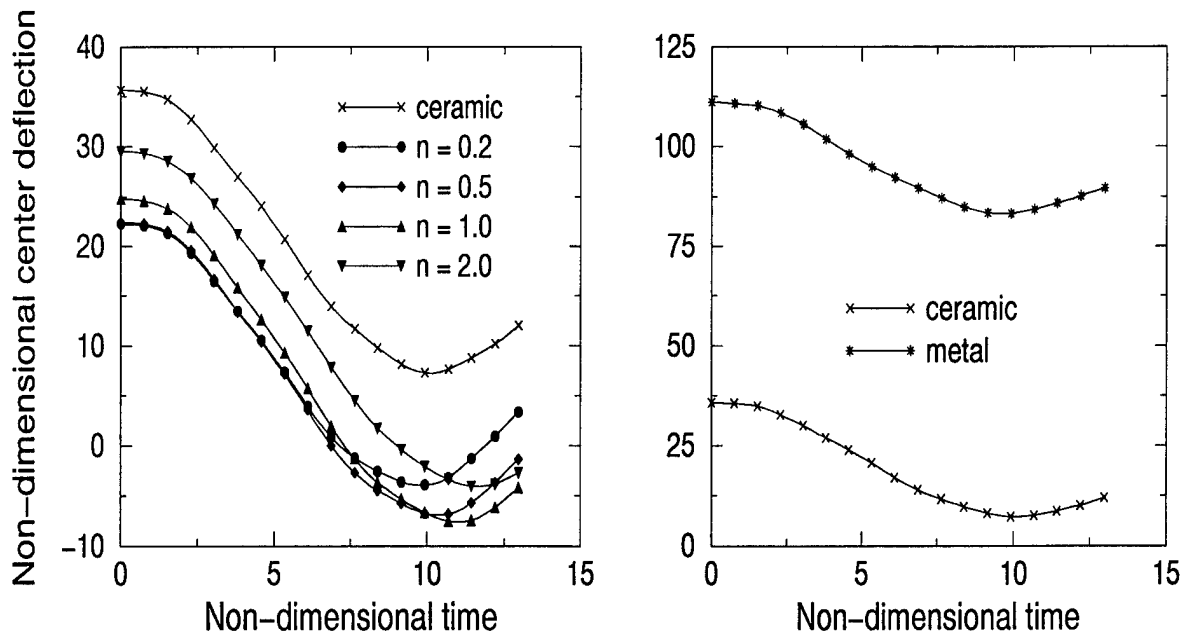

Figure 38: Temporal evolution of center deflection of simply supported fgm plate under suddenly applied uniform loading of $-1.0\mathrm{x}10^6 N/m^2$ and temperature field (Aluminum-Zirconia).

Figure 39: Temporal evolution of center deflection of clamped fgm plate under suddenly applied uniform loading of $-1.0 \times 10^6 N/m^2$ (Aluminum-Zirconia).
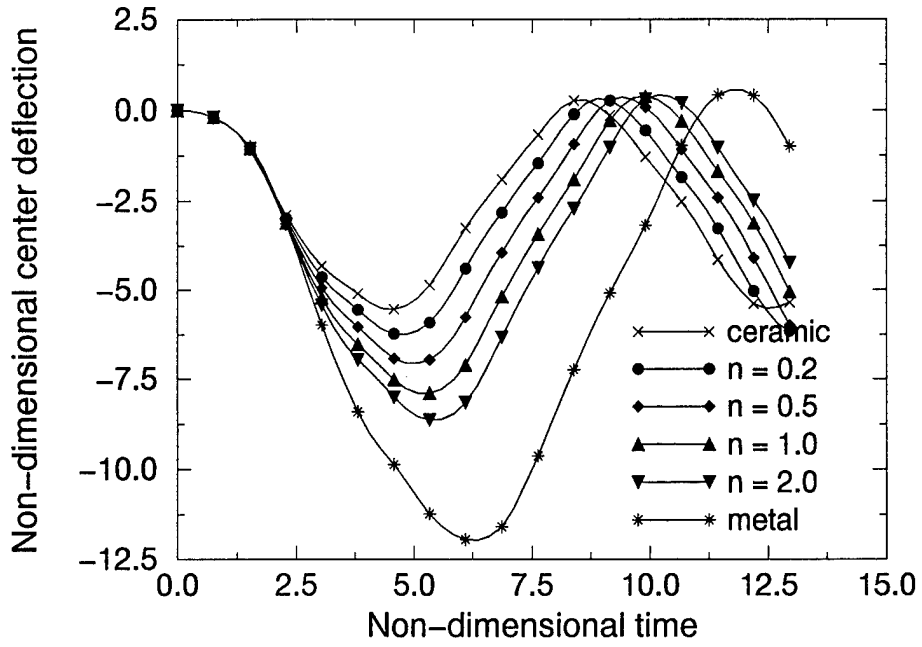

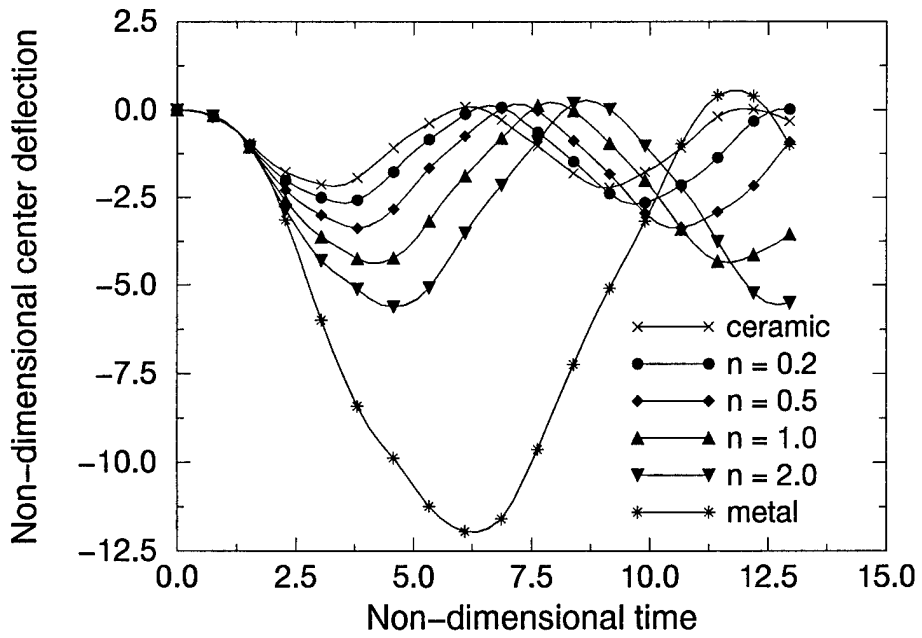Figure 40: Temporal evolution of center deflection of clamped fgm plate under suddenly applied uniform loading of $-1.0 \times 10^6 N/m^2$ (Aluminum-Alumina).

4 Analysis of the Effective Yield Behavior of Brittle-Ductile Mixtures

4.1 Introduction

Most monolithic materials exhibit desirable properties in certain ranges of temperature and mechanical loading. This also depends on the microstructure of the material. Metals, for instance, are very good load bearing components and are used for reinforcements in structural applications like concrete and so on. They possess high ductility which enables them to be drawn into wires. Also, they undergo yielding and this relaxes the stresses and reduces stress concentration. Ceramics on the other hand, are mostly brittle. They are unforgiving in situations where the tensile loads are very high, and they fail by instantaneous cracking. However, they are very good in thermal shock resistance and in situations where we have large temperature gradients. Ceramic metal mixtures offer excellent resistance to heat and also, have very good load bearing capacity. Intermetallics and solid-solutions are materials with such properties. Another class of mixtures, namely the functionally graded materials, are now being manufactured by various techniques like CVD, PVD, etc, and are being used in environments with severe thermal gradients and high loads. The gradation in material properties is designed by optimizing the performance of these materials.

In using mixtures of ceramics and metals, a central issue is one of effective properties. There are several models to compute effective properties of composites, including, the self-consistent models, micromechanical models, models based on energy equivalence and so on. In this work, we will look at the yielding behavior of ceramic-metal mixtures. Results based on mixture theory approach as well as discrete finite element approach will be compared. A one-dimensional model will also be presented.

4.2 Problem Statement and Assumptions

The aim of the present work is to compute the yield stress in ceramic - metal mixtures, as a function of the volume fraction of either component. The dependence of yield stress on the stiffness of either phase will be studied. In the analysis, we will make the following assumptions. Assumptions that are specific to models discussed below, will be explicity stated in the respective sections. The restrictions and assumptions common to the different models are:

1. The analysis will be restricted to *linearized isotropic elasticity*. Linearized elasticity is not frame invariant, however, the error in the solutions is on the order of ϵ^2, where $\| \epsilon \|_{tr} = \epsilon \ll 1$ and is the standard trace norm of the linearized Green Lagrange strain tensor.

2. Yielding will be considered as an event in the linearized elastic response of the mixture. In particuar, the mixture is assumed to have yielded, if the partial stress in the metallic component satisfies the classical J_2 criterion.

4.3 One-dimensional Model

4.3.1 Features

- An idealized representation contiguous microstructure is assumed such that the material consists of three parallel ligaments, (see Figure 41) the first being metal, the second being ceramic, the third being a series connection between ceramic and metal. All ligaments heights being equal.

- The relative volume fraction of the metal and ceramic within the monolithic ligaments is controlled by varying their cross-sectional area and within, the composite ligament, by varying their relative lengths. The cross sectional area of the third ligament is arbitrary, and will be chosen appropriately.

- The yield load of the composite model is the load at which either metallic component yields.

- The columns undergo the same extension.

The computed expressions for the yield load, in terms of the volume fractions of the metal and ceramic are as follows:

$$\sigma_y = \sigma_y^1 \left(\frac{v_1}{1 + v_1} + \frac{E_2}{E_1} \frac{v_2}{1 + v_1} + \frac{1}{(1 + v_1)\left(1 + \frac{v_2 E_1}{v_1 E_2}\right)} \right)$$

$$\sigma_y = \sigma_y^1 \left(\frac{v_1}{1 + v_2} + \frac{E_2}{E_1} \frac{v_2}{1 + v_2} + \frac{v_2}{v_1 (1 + v_2)\left(1 + \frac{v_2 E_1}{v_1 E_2}\right)} \right)$$

where, v_1 and v_2 are volume fractiosn of the metal and ceramic respectively. The cross-sectional area of the third column is arbitrary. In this analysis, this cross-sectional area was assumed to be equal to that of either column 1 or column 2 and the above two results were obtained for both these cases. The results so obtained are close to each other. The results of the analysis are compared to that obtained by mixture theory. The graphs show that the predictions of the one dimensional model are very close to that due to the mixture theory model.

4.3.2 Mixture Theory Model

A two-dimensional analysis was performed using the equations of linearized elasticity derived with recourse to mixture theory Rajagopal, 1996 applied to two elastic solids. The central assumptions are :

- Every continuum point is co-occupied by the metallic and ceramic phases.

- Each component of the mixture undergoes identical deformation.

• Each component is distributed uniformly within the mixture. Note that, we can analyse graded mixtures in a rather simple manner, by simply assuming a spatially varying volume fraction distribution.

The equations as a result of the standard balance laws are well known and the reader is referred to the works by Chadwick, 1976 and by Rajagopal, 1996. In using the mixture theory we note that the effective density ρ and the Helmholtz free energy A is computed from

$$
\begin{aligned}
v_c + v_m &= 1 \\
\rho &= \rho_c v_c + \rho_m v_m \\
\rho A &= \rho_c v_c A_c + \rho_m v_m A_m
\end{aligned}
$$

The resulting expression for the Cauchy stress tensor is obtained as $\sigma = \mathbf{v_c}\sigma_\mathbf{c} + \mathbf{v_m}\sigma_\mathbf{m}$
The equations for which the finite element model is obtained, are listed as under :

$$
\begin{aligned}
\frac{\partial \sigma_{xx}}{\partial x} + \frac{\partial \sigma_{xy}}{\partial y} &= 0 \\
\frac{\partial \sigma_{xy}}{\partial x} + \frac{\partial \sigma_{yy}}{\partial y} &= 0 \\
\epsilon_x &= \frac{\partial u}{\partial x} \\
\epsilon_y &= \frac{\partial v}{\partial y} \\
\epsilon_{xy} &= \frac{1}{2}\left(\frac{\partial u}{\partial y} + \frac{\partial v}{\partial x}\right)
\end{aligned}
$$

$$
\left\{\begin{array}{c} \sigma_{xx} \\ \sigma_{yy} \\ \sigma_{xy} \end{array}\right\} = \left[\begin{array}{ccc} C_{11} & C_{12} & 0 \\ C_{12} & C_{22} & 0 \\ 0 & 0 & C_{66} \end{array}\right] \left\{\begin{array}{c} \epsilon_{xx} \\ \epsilon_{yy} \\ 2\epsilon_{xy} \end{array}\right\} \tag{37}
$$

Plane stress constitutive equations were used in the analysis. The finite element model may be derived from the weak form (see Reddy, 1994) and the element stiffness matrices are as follows :

$$
\begin{aligned}
[K^e]\{\Delta^e\} &= \{F^e\} \\
K_{ij}^{11} &= \int_{\Omega^e} h\left(C_{11}\frac{\partial \psi_x}{\partial x}\frac{\partial \psi_j}{\partial x} + C_{66}\frac{\partial \psi_i}{\partial y}\frac{\partial \psi_j}{\partial y}\right) dxdy \\
K_{ij}^{12} &= \int_{\Omega^e} h\left(C_{12}\frac{\partial \psi_x}{\partial x}\frac{\partial \psi_j}{\partial y} + C_{66}\frac{\partial \psi_i}{\partial y}\frac{\partial \psi_j}{\partial x}\right) dxdy \\
K_{ij}^{s2} &= \int_{\Omega^e} h\left(C_{66}\frac{\partial \psi_x}{\partial x}\frac{\partial \psi_j}{\partial y} + C_{22}\frac{\partial \psi_i}{\partial y}\frac{\partial \psi_j}{\partial x}\right) dxdy
\end{aligned}
$$

71

where the C s are the material stiffness coefficients (Reddy 1992). The integrals are evaluated using gauss quadrature, and also, note that the material coefficients are obtained using a rule of mixtures. The specimens are assumed to have a constant volume fraction and the yield analysis is performed on these specimens. The geometry of the computational domain corresponds to a bar. This bar is subjected to an axial load, P. Note that the yield condition is checked on the stress tensor $\sigma_\mathbf{m}$ and not on $v_m\sigma_\mathbf{m}$. The methodology consists in applying a load P, and checking the yield condition. If the material is still elastic, the load is incremented and the condition again checked. In the example probelm worked, we make use of the fact that $J_2 \propto P^2$ and this may be used to compute the load corresponding to the critical value of J_2. Note that, the stress state that is used to correct the load corresponds to the metallic point that is closest to yielding. The analysis is stopped when yielding is satisfied to within a numerical tolerance. Figure 42 shows the variation of effective yield stress of the mixture of Nickel and Alumina. Alumina is much stiffer than nickel and therefore, the mixture has a higher yield stress than nickel, corresponding to all volume fractions of Alumina. If we mix nickel with a more compliant ceramic, the yield stress would have been lesser than that corresponding to the pure metal. The yield criterion for the mixture of brittle ceramic and ductile metal, as stated before, may be expressed as follows:

$$J_2\left(\sigma_{metal}\right) = J_{2,critical}$$

where, the stresses in the above computation correspond to the partial stresses in the metallic component of the mixture. It is to be noted that the partial stresses are not the stresses multiplied by the volume fraction of the metal.

In performing inelastic analysis on a graded material, the yield stress at any point in the material can be obtained by assuming that the material point is part of a continuum with a uniform volume fraction as that at the point in the graded specimen. The yield check can be performed using the classical J_2 criterion, the critical value of which varied at each point. Since, yield check is often performed at the quadrature points or the Barlow points, the critical value of the second invariant of the stress deviator, has to be computed at these points.

4.3.3 Effect of failure of the brittle phase

In brittle-ductile mixtures where the brittle phase is stiffer, the stresses in the brittle phase are much higher than the stresses in the ductile phase. Brittle failure is assumed to occur in the ceramic when the stresses satisfy the maximum normal stress criterion. When brittle failure occurs, if we set the stiffness of the ceramic component to zero, as a first approximation, then, the load is transferred to the metallic component, and therefore, the stress in the ductile phase increases and this brings the state of stress within that phase, closer to yielding. Thus, it is expected that the overall yield stress of such a specimen is much lower than that corresponding to a specimen where we ignore the failure of the brittle phase. The material is expected to show a piecewise linear behavior between the stress and strain, until yielding occurs within the metallic phase. The yield stress of the mixture increases as the volume fraction of the metal increases. It is noted however, that the yield stress with brittle failure is much lower than the yield stress without brittle failure in the ceramic. This can be

seen from Figure 43. Note that, higher the volume fraction of the brittle phase, greater the load transfer to the ductile phase due to failure by cracking in the brittle phase. Therefore, the yield stress corresponding to the high volume fraction of the brittle phase is very low, when brittle failure is considered. On the other hand, it is seen that, when the brittle phase is intact, the yield stress of the mixture is very high, at higher volume fractions of the stiffer, brittle ceramic phase.

4.4 Closure

- Predictions of the yield stress due to the one-dimensional model is fairly close to that obtained using the mixture theory.

- When a ductile phase is combined with a stiffer brittle phase, the yield stress of the mixture increases. This is because, the stresses in the ductile phase is much lower as compared to the case of pure ductile phase. Consequently, a higher value of external load is required to induce yielding in the ductile phase.

- When the brittle phase fails by cracking before the ductile phase yields, the effective yield stress is much lower than that corresponding to the pure metal. Mixture theory and the finite element model predict the same qualitative trends.

4.5 References

1. Reddy, J. N., *Introduction to the finite element method*, Second Edition, Mc Graw Hill Company, New York, 1992.

2. Ragagopal, K. R., and Tao, L., "Mechanics of Mixtures", 1996.

3. Chadwick, P., 'Continuum Mechanics - Concise Theory and Problems", Halsted Book Press, John Wiley and Sons, 1976.
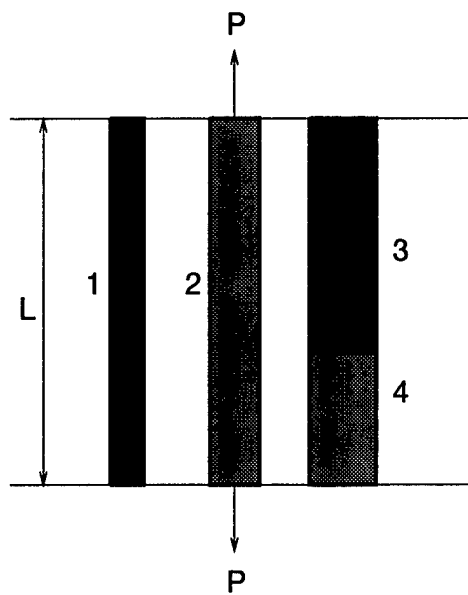
4. Louyi Tao, Personal communication, 1997-98.

Figure 41: A simple one-dimensional model of discrete component model of ceramic - metal miture.
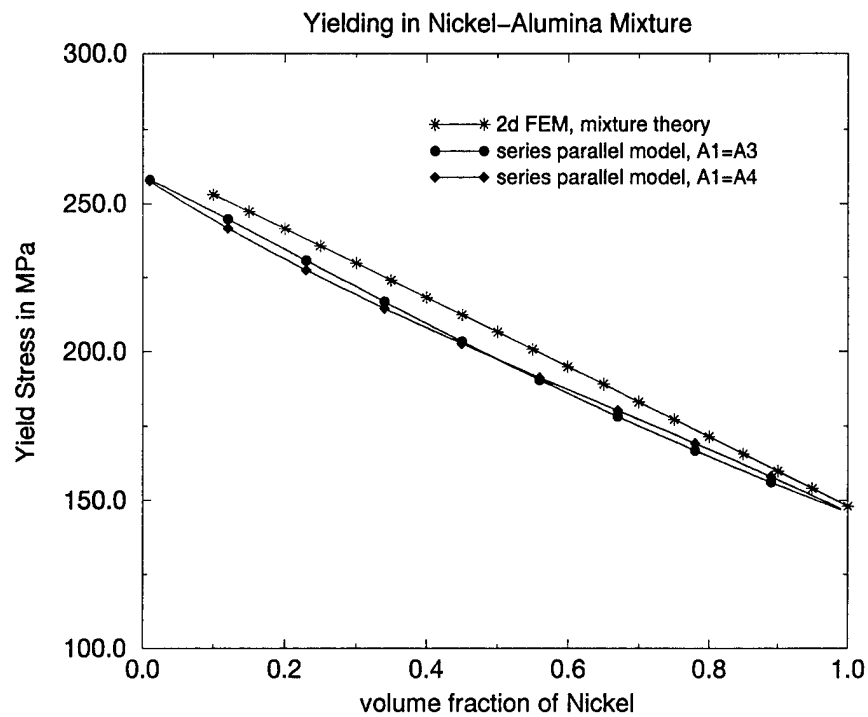
Figure 42: Comparison of yield stress of Nickel-Alumina mixture - One-dimensional model and the mixture theory model
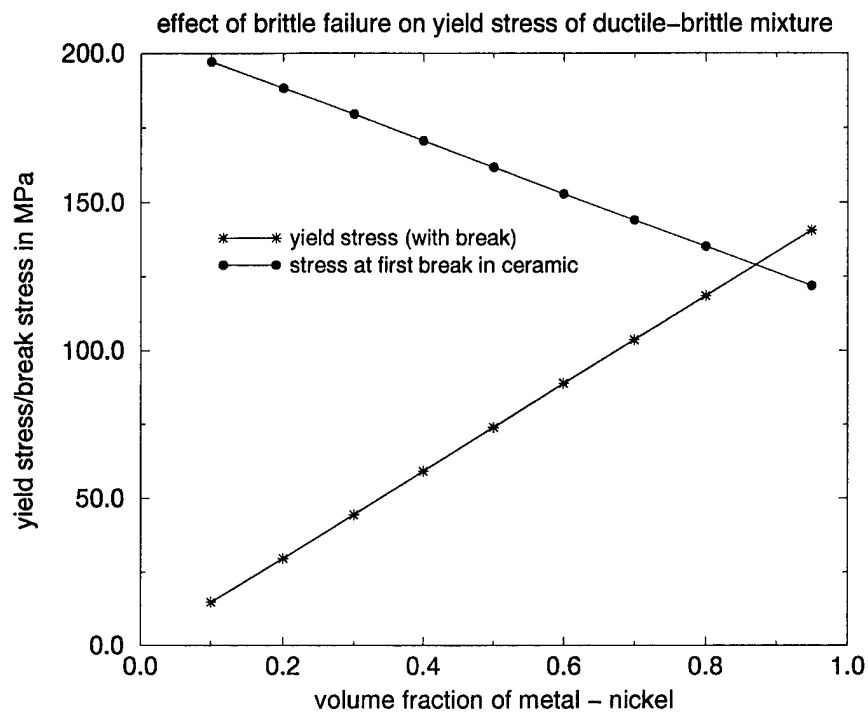
Figure 43: Comparison of yield stress of Nickel-Alumina mixture - One-dimensional model and the mixture theory model

5 Conclusions

The research work outlined in this report contains an indepth study into the mechanics formulations of functionally graded materials. A detailed literature survey was presented and the relevance of the present work in the light of the existing literature was highlighted. Important mechanics formulations were outlined and specific problems solved were discussed in detail in the present report and previous reports. Nonlinear finite element programs with Picard and Newton-Raphson procedures were developed, and also algorithms for transient analysis were implemented. Geometric, material and thermal coupling nonlinearities were both included.

The response of functionally gradient ceramic-metal plates was investigated using a finite element that accounts for the transverse shear strains, rotary inertia and large rotations in the von Kármán sense. The static and dynamic response of the functionally gradient material (fgm) plates were investigated by varying the volume fraction of the ceramic and metal using a simple power law distribution. Numerical results for the deflection and stresses were presented. The effect of the temperature field imposed on the fgm plate has been discussed. It is demonstrated that the response of the plates with material properties between that of the ceramic and metal is not intermediate to that of the ceramic and metal plates. The effect of the thermal nonlinearity leading to non-intermediate response of the graded plates, as compared to that of the metal and ceramic plates was also discussed. Results were obtained for both static and dynamic analyses. Two different material combinations were chosen, to study the effect of the material properties and the structural response. Studies of the variation of the center deflection, with plate aspect ratios were also performed. The analysis of temporal response of thermally loaded plates with simply supported edges and clamped edges was conducted. In the above studies, the heat conduction equation and the equilibrium equations were not coupled. The heat conduction equation was solved separately and the temperature field was imposed as a thermal loading term in the equilibrium equations. Also, the material properties were taken to be independent of temperature. In the subsequent analysis, a three dimensional heat conduction equation was solved and the effect of the thermomechanical coupling was considered.

The dynamic thermoelastic response of functionally gradient cylinders and plates was studied. Thermomechanical coupling is significant in these materials when they are used in high temperature applications, and hence, the coupling wass included in the formulation. The heat conduction and the thermoelastic equations were solved for a functionally graded axisymmetric cylinder subjected to thermal loading. In addition, a thermoelastic boundary value problem using first-order shear deformation plate theory (FSDT) that accounts for the transverse shear strains and the rotations, coupled with a three dimensional heat conduction equation was formulated for a functionally graded plate. Both problems were studied by varying the volume fraction of a ceramic and a metal using a power law distribution. Nonlinearities due to temperature and spatial dependence of material properties of the constituents were considered in the numerical studies. Parametric studies with respect to volume fraction of the ceramic and combinations of different constituents of the functionally gradient material were conducted using the finite element method. Issues related to optimization of the composition of functionally gradient cylinder were also discussed. More details are available in earlier reports.

Predictions of the yield stress of brittle-ductile mixtures were obtained from the one dimensional models and two dimensional mixture theory models. The effects of the relative elastic stiffness of the ductile and brittle phases have been discussed. The effects of brittle failure on the effective yielding behavior of the mixture was also addressed. The present research adds significantly to the vast body of knowledge in key issues involved in the area of functionally graded materials.